A Thesis for the Degree of Doctor of Philosophy in Engineering

Hydrogen Permeation with Flat Sheet Pd/Ag Membrane for Compact Methanol Steam Reformer

January 2014

Graduate School of Science and Technology
Keio University

Mohd Faizal Bin Hasan

Acknowledgement

Praise be to Allah S.W.T. for giving me a chance to have a meaningful life until today. Alhamdulillah…

Firstly, I would like to express my highest gratitude to my supervisor, Professor Toshihisa Ueda for all the valuable advices and guidance in every aspect since before I started my Ph.D. study at Keio University. There were a lot of things I learnt from Professor throughout my study, especially on how to manage the research until completion. I really appreciate his knowledge and experience sharing on how to be a good researcher.

My deepest appreciation also goes to my co-supervisor, Associate Professor Takeshi Yokomori for his advices throughout my study, especially on numerical simulation and during evaluation of my thesis.

I would also like to highlight my deepest appreciation to the other members of examination committee, Professor Koichi Hishida and Associate Professor Kuniyasu Ogawa for their constructive advices and careful reviews during my thesis evaluation.

This research was supported in part by a Grant-in-Aid for the Global Center of Excellence Program for the “Center for Education and Research of Symbiotic, Safe and Secure System Design” from the Ministry of Education, Culture, Sport, and Technology in Japan.

I also would like to take this opportunity to express my high gratitude to Ministry of Higher Education Malaysia and Universiti Teknologi Malaysia for valuable financial supports for my Ph.D. study and my life in Japan with my family.

To all members of Reformer Group, especially Ryo Kizu, Masato Kuwabara, Yuki Kawasaki, Yuta Kawamura, and Jun Ohtani, thank a lot for your helps in carrying out the

experiments. Indeed, I learnt a lot through our team work. To Mohd Rosdzimin Bin Abdul Rahman, thank you very much for your guidance about FLUENT software. And thank you to all members of Ueda Laboratory and Yokomori Laboratory for kind helps.

To my beloved parents, Hasan bin Aluwi and Hasnah Binti Hashim, and my brother, Mohd Farouk Bin Hasan, thank you very much for meaningful prayers and strong moral support even though we are far apart.

To my best friend, my motivator, my dear wife, Norlida Binti Mohammad, thank you very much for all that you have endured with me for these past three years. Your word of wisdom, your encouragement, and your strong mental support has carried me through the challenges. For all your sacrifices and care for our family, and kids Naufal Farhan and Naurah Atiqah, I love you and thank you.

Abstract

The characteristics of hydrogen permeation with flat sheet Pd/Ag purification membrane for compact methanol steam reformer were investigated experimentally, theoretically and numerically.

The performance of high purity hydrogen production from methanol for a compact steam reformer was investigated experimentally. A 77wt.% Pd/23wt.%Ag membrane with 25μm thickness and $CuO/ZnO/Al_2O_3$ catalyst were used. Heating was performed by a Bunsen type burner using City Gas 13A. The methanol reforming and purification of H_2 were investigated at different reference catalyst zone temperatures (589-689K), pressures at the upstream side (0.20-0.50MPa), steam to methanol(S/C) ratios (0.8-1.6) and reactant flow rates (1.7×10^{-4} to 4.4×10^{-4} mol/s). The results show that at high reference temperature, high pressure and certain points of the reactant flow rate, the maximum hydrogen permeation rate is obtained when the S/C ratio is around 1. In addition, it is shown that the compact methanol steam reformer with a Pd/Ag membrane is able to produce high purity hydrogen with very low CO concentration, which fulfills the Polymer Electrolyte Fuel Cell (PEFC) requirement (<10ppm). It was found that the H_2 permeation rate obtained from the experiment could not be well predicted by Sieverts' equation, therefore a more fundamental study is necessary to clarify the reason why such significant difference occurs.

The fundamental study on the effect of feed flow rate of hydrogen mixture on the H_2 permeation for flat sheet Pd/Ag membrane was performed experimentally. H_2:N_2 mixture was used to neglect the surface adsorption effect of non-H_2 species. For hydrogen purification, a same type of Pd/Ag membrane with 25μm thickness and 0.02m diameter was used. No metal support was set with the membrane to prevent any possible influence

from it. The permeation rate of H_2 was investigated under various feed flow rates (1.49×10^{-5}-2.98×10^{-4}mol/s), for pressures of 0.20-0.30MPa, reference membrane temperatures of 523-723K and inlet hydrogen mole fraction of 0.75-0.80. The downstream (permeated) side pressure was set constant at 0.10MPa. The results demonstrated that when the feed flow rate is decreased, the H_2 permeation rate decreases. In this case, the prediction by the Sieverts' equation is still not going well with the experimental results, both qualitatively and quantitatively. Thus, it is confirmed that the phenomenon of decrease in hydrogen concentration at the membrane surface occurs, which is supposed due to the effect of H_2 permeation itself. It is suggested that a new prediction method which can well estimate the H_2 permeation rate with such trend is needed.

Then, a theoretical equation to estimate H_2 permeation mole flux was proposed, which considers the decrease in hydrogen concentration at the membrane surface due to effect of H_2 permeation itself. When the proposed equation that takes into account the effect of H_2 permeation is used, the H_2 permeation mole flux can be predicted quantitatively by using the concentration of H_2 of the feed mixture. This shows that the diffusive transport effect plays an important role as well as the convective transport effect when determining H_2 concentration at the membrane surface. In addition, the normalization of the theoretical results shows that the trend of the decrease in the H_2 permeation mole flux with respect to the mean mole flux follows the first order lag function, regardless of the inlet H_2 partial pressures and inlet H_2 mole fractions.

Finally, the H_2 concentration distribution during permeation for a flat sheet Pd/Ag membrane was investigated numerically. The geometry considered in the present investigation was similar with those of the experimental study to imitate the real hydrogen purification process. In addition to the various feed flow rates, the inlet H_2 mole fraction

was varied from 0.70 to 0.80 and different species besides N_2 (CO_2, Ar and He) were considered for binary H_2 mixture to understand the behaviour of H_2 permeation in a wider range. The numerical result for the case of H_2:N_2 mixture was validated experimentally, and is found quantitatively fit with the estimation by the proposed analytical method. For the cases with different inlet H_2 mole fraction and species in H_2 mixture, the numerical results show very good agreement with the analytical results except for the case of H_2:He mixture. Generally, for various operating conditions, the numerical results demonstrate the decrease in H_2 mole fraction towards the membrane surface, which makes clear the concentration polarization phenomena near the surface. It was found that the concentration polarization is strengthened when hydrogen mixture with low mean mole flux, high upstream pressure and high binary diffusivity is used. Overall, it can be said that the molecular diffusion, that is concentration polarization plays a significant role for permeation with flat sheet Pd/Ag membrane.

Nomenclature

A : effective membrane surface area, m^2

C : mole concentration, $mol.m^{-3}$

c_1 : hydrogen concentration of hydrogen atoms on the metal surface, mol/m^3

d : membrane thickness, m

D : mass diffusivity, $m^2. s^{-1}$

F : estimated hydrogen permeation rate, mol/s

F_{per} : hydrogen permeation rate, mol/s

$F_{all,off-gas}$: total flow rate of off-gas, mol/s

$F_{H_2,off-gas}$: flow rate of hydrogen in off-gas, mol/s

F_{in} : feed flow rate, mol/s

F_{in,H_2} : feed flow rate of hydrogen, mol/s

F_r : radial external force, N

F_{reac} : reactant flow rate, mol/s

$F_{unreacted}$: total flow rate of unreacted methanol and steam, mol/s

F_z : axial external force, N

f : hydrogen permeation mole flux, $mol.s^{-1}m^{-2}$

f_{mass} : hydrogen mass flux, $kg\ m^{-2}\ s^{-1}$

f_{massd} : mass flux of hydrogen which comes out from membrane at downstream side , $kg.s^{-1}.m^{-2}$

$f_{mass,u}$: mass flux of hydrogen towards membrane surface at upstream side, $kg.s^{-1}.m^{-2}$

$f_{mean,o}$: mean mole flux for normalization, $mol.s^{-1}.m^{-2}$

f_{mean} : mean mole flux, $mol.s^{-1}.m^{-2}$

f_{mean,H_2} : hydrogen mean mole flux, $mol.s^{-1}.m^{-2}$

f_{net-in,H_2} : net inlet hydrogen mass flux , $kg.s^{-1}.m^{-2}$

z : vertical distance from center of membrane surface, m

z_{inlet} : vertical distance between membrane surface and inlet, m

K : Sieverts' constant or solubility, $mol.m^{-3}.Pa^{-0.5}$

M : molecular weight, $kg.mol^{-1}$

P_0 : total pressure at upstream side, Pa

P_1 : total pressure at membrane surface of upstream side, Pa

P_2 : total pressure at membrane surface of downstream side, Pa

P_{H_2} : hydrogen partial pressure, Pa

$P_{H_2,in}$: hydrogen partial pressure at inlet, Pa

$P_{H_2,1}$: hydrogen partial pressure at membrane surface of upstream side, Pa

$P_{H_2,1(ref)}$: reference hydrogen partial pressure at membrane surface of upstream side, Pa

$P_{H_2,2}$:hydrogen partial pressure at membrane surface of downstream side, Pa

P_{in} : total pressure at the inlet, Pa

P_0 : total pressure at upstream side, Pa

P_1 : total pressure at membrane surface of upstream side, Pa

p : static pressure, Pa

q : hydrogen permeance coefficient, $mol.m^{-1}.s^{-1}.Pa^{-0.5}$

r : radial distance on membrane surface, m

r_{max} : maximum radial distance (membrane radius), m

T : temperature, K

T_{mem} : membrane temperature, K

$T_{mem(ref)}$: reference membrane temperature, K

$T_{cat(ref)}$: reference catalyst zone temperature, K

v : velocity, $m.s^{-1}$

v_b : velocity towards membrane surface at very close to membrane, $m.s^{-1}$

v_{inlet} :velocity at the inlet, $m.s^{-1}$

$v_{z,in}$: inlet velocity, $m.s^{-1}$

X : mole fraction , -

$X_{H_2,in}$: inlet mole fraction of hydrogen, -

$X_{H_2,1}$: H_2 mole fraction at membrane surface of upstream side, -

$X_{N_2,in}$: inlet mole fraction of nitrogen, -

$X_{H_2,off-gas}$: mole fraction of hydrogen in off-gas, -

Y : mass fraction, -

Greek letters and Symbols

α : steam to methanol (S/C) ratio

δ : normalized permeation mole flux, -

ε : normalized mean mole flux, -

μ : viscosity, Pa.s

ρ : mixture density, $kg.m^{-3}$

ρ_{H_2} : mass concentration of hydrogen, $kg.m^{-3}$

ρ_{N_2} : mass concentration of nitrogen, $kg.m^{-3}$

σ : collision diameter, $\mathring{A}$

Ω : collision integral

Subscripts

i	: species i
j	: species j
r	: radial direction
z	: axial direction

Table of Contents

Chapter 1

Introduction

1.1 Background

The interest on hydrogen technologies is, in recent years, growing due to capability in producing energy in a clean way, without harmful influence on environment. For instance, Polymer Electrolyte Fuel Cell (PEFC) converts directly chemical energy, that is hydrogen to electrical energy while having only water and heat as by-products.

Even though hydrogen is the most abundant chemical element on our earth, it is primarily in a form of water and hydrocarbons, which needs suitable extraction processes in order to obtain hydrogen molecules. In industrial scale, the extraction is mainly performed by reforming of hydrocarbons (Dicks 1996), such as catalytic steam reforming, catalytic partial oxidation and autothermal reforming (the combination of catalytic steam reforming and catalytic partial oxidation). However, the reforming processes simultaneously produce undesirable impurities for fuel cell systems especially CO which could damage the fuel cell when the amount becomes sufficiently high. Therefore, purification is necessary to separate these impurities, in which membrane is the best choice for the small to medium scale industries due to low energy expenditure (Vadrucci *et al.* 2013). Membrane for hydrogen purification can be classified into two categories, namely as polymeric membrane and inorganic membrane. Then, the inorganic membrane can be divided into porous membrane and nonporous(dense) membrane. The present study focuses mainly on the dense membrane, that is Pd based purification membrane.

The phenomenon of hydrogen diffusion through heated palladium (Pd) has been firstly observed by Thomas Graham in 1866 and a breakthrough in researches on Pd based

membrane occurs in 1960s when the Palladium(Pd)/Silver(Ag) alloy membrane was discovered which could prevent embrittlement problem faced by Pd membrane (Grashoff *et al.* 1983). In recent years, there has been considerable interest on the use of Pd based membrane such as Pd/Ag and Pd/Cu membrane to separate hydrogen (H_2) from gaseous mixtures in industrial sectors due to its high permeability and permselectivity. The Pd based membrane was very useful to produce on-site hydrogen by methanol reforming for electronic industry and for fuel cells. In line with the increase in applications of Pd based membrane, the phenomenon of hydrogen permeation through this type of membrane has attracted many researchers to understand the permeation behavior under various operating conditions. It was found that there is still a lack in theoretical study to predict hydrogen permeation through the Pd based membrane for the case of hydrogen mixture.

Therefore, in this dissertation, a prediction method of hydrogen permeation through Pd based membrane, that is Pd/Ag membrane for the case of hydrogen mixture is introduced, in which the method is validated experimentally. Numerical investigation is performed to understand the characteristics of hydrogen concentration distribution during permeation, for various operating conditions. The hydrogen permeation characteristics of the membrane are described at first using our compact methanol steam reformer.

1.1.1 Compact Methanol Steam Reformer with Pd Based Membrane

The compact reformer in connection with Polymer Electrolyte Fuel Cell (PEFC) is an attractive option for supplying hydrogen for light-duty vehicles and portable electronic devices such as cellular phones, tablet computers and laptop computers. The development of compact reformers started more than a decade ago, with the aim of setting a reformer,

catalytic burner and hydrogen purification device in a single package for vehicle application (Emonts *et al.* 1998). The integrated compact reformer is supposed to be a reliable solution compared to complex, high price and bulky designed reformer systems consisting of separated units (Gepert *et al.* 2006). Due to the difficulty in transporting and storing hydrogen, the compact reformer which utilizes alcohols as fuel seems to be more practical (Liwei *et al.* 2011). Methanol is suitable for steam reforming because of the high H/C ratio, high reactivity and moderate reforming temperature (Fujimoto *et al.* 1987, Gepert *et al.* 2006). Compared to the other liquid fuels such as liquid hydrogen and ammonia, the cost of hydrogen generation from methanol is still relatively low (Sato *et al.* 1998, Saika *et al.* 2006,).

Based on the reaction formula, the endothermic steam reforming process is more preferable than exothermic partial oxidation due to the higher hydrogen production from one mole methanol. The reaction model of methanol steam reforming is shown by Eq. 1.1 as follows:

$$CH_3OH + H_2O \longrightarrow 3H_2 + CO_2 \text{ -49.5 kJ/mol} \quad (1.1)$$

For methanol steam reforming, the commercial catalyst $CuO/ZnO/Al_2O_3$ was widely used at moderate temperature ranges from about 423K to 623K because a high conversion rate was obtained (Agrell *et al.* 2002, Basile *et al.* 2006,). Previous studies demonstrated that geometry, steam to carbon (S/C) ratio, temperature and flow pattern are the key performance of the catalytic reforming reactor (Davieau and Erickson 2007, Yoon *et al.* 2007, Chein *et al.* 2012).

Through methanol steam reforming, gas species other than H_2 such as CO_2 and CO are

also produced. Previous studies showed that CO causes a decrease in the reactive surface area of the electrode fuel cell for H_2 dissociation (Narusawa *et al.* 2003) while both CO and CO_2 cause a decline in H_2 partial pressure (Narusawa *et al.* 2003[ii], Jae-Young *et al.* 2010), which affects the fuel cell performance. It was shown that CO damages the PEFC if it is more than 10ppm (Katsuki 2005). Therefore, it is necessary to purify hydrogen produced by methanol steam reforming before it is sent to the PEFC. There are several potential methods available for the hydrogen purification, such as selective CO methanation, selective CO oxidation and purification by Pd based membrane. The first two methods only can give very low CO concentration (<10ppm) at very low temperature of around 100 to 200^{o}C. Due to this, purification by Pd based membrane is the most suitable method, that is the membrane is well-known for its high permeability and permselectivity characteristics (Hohlein *et al.* 1996).

Experimental and theoretical studies related to methanol steam reformer integrated with a purification membrane were conducted under various operating conditions and different configurations (Arstad *et al.* 2006, Basile *et al.* 2006, Iulianelli *et al.* 2008, S. Damle 2009, H. Israni and P. Harold 2011) with the aim to obtain high methanol conversion and high H_2 permeation. In previous studies, two types of membrane were used; tubular type (Iulianelli *et al.* 2008, H. Israni and P. Harold 2011) and flat sheet or foil type (Arstad *et al.* 2006, Basile *et al.* 2006, S. Damle 2009). Generally, the flat sheet type membrane is widely used and is more suitable for commercial applications because the simpler process to produce it and compability with various experimental conditions and geometries. Besides, less thickness of flat sheet type membrane is sufficient for structural stability, which results in the less cost (S. Damle 2009). Meanwhile, the available tubular type membrane is already fixed with its holder, which makes it difficult to be modified for various reformer designs

and experimental conditions. As mentioned by Tong *et al.* (2008), there were efforts to increase the hydrogen permeation flux through tubular type membrane, such as depositing Pd-based film with thickness 0.8-5μm on a metal porous substrate by sputtering technique. In 2008, a tubular type membrane was produced by a new electroless plating process which seems to be commercially useful. However, as asserted by S. Damle (2009), the flat sheet type membrane is still less expensive than the existing tubular type membrane.

A Pd or Pd/Ag alloy membrane was adopted in many hydrogen purification studies due to its ability to provide high fluxes and high permselectivity. Alloying Pd with Ag or Cu is necessary to prevent embrittlement when the membrane is exposed to hydrogen at temperatures below 573K (critical temperature), and at pressures below 2MPa (critical pressure) (Gepert *et al.* 2006). In addition, previous researchers have demonstrated that the addition of Ag to a Pd membrane could improve the hydrogen permeability, reaching maximum when the Ag content is around 23 wt.% (Uemiya *et al.* 1991[(ii)]). This is a main reason why Pd 77wt.%/Ag 23.wt% membrane is widely used nowadays for hydrogen purification.

Nevertheless, for application in gas mixture, hydrogen permeation through Pd based membrane deteriorates, which is caused by the competitive adsorption and resistance by other gas species such as CO, CO_2, excessive methanol and steam (Hara *et al.* 1999, Amandusson *et al.* 2000). The experimental and simulation studies that were conducted at moderate temperature (498-573K) and pressure (0.3-0.5MPa) ranges revealed that the decrease in transmembrane H_2 flux through the Pd/Ag membrane is mainly caused by the competitive adsorption of CO, followed by CH_3OH, CO_2 and H_2O (Israni and Harold 2010). The study also demonstrated that the surface adsorption effect due to all species, except CH_3OH, weakened with an increase in membrane temperature. Based on several

previous studies, it seems to be necessary to keep the membrane temperature of 553K and above when using the Pd or Pd alloy membrane to reduce the disturbance effect of these non-hydrogen species and to obtain higher hydrogen permeation flux (Hara *et al.* 1999, Israni and Harold 2010).

For compact reformer, the S/C ratio, the reactant flow rate, and the pressure are supposed to be important parameters to be considered as well as the temperature. In summary, it can be said that there are many issues to be made clear to design efficient compact methanol steam reformer.

1.1.2 Transport Mechanism of Hydrogen Permeation through Pd Based Membrane

Generally, hydrogen purification membrane can be classified into two categories: (i)organic(polymer) and (ii) inorganic membrane (Adhikari and Fernando 2006). For the inorganic membrane, in the view point of membrane structure categorization, it is then can be subdivided into ceramic and metal membrane. Meanwhile, in the view point of the separation mechanism, it is also can be divided into porous and nonporous (dense) membrane (Adhikari and Fernando 2006, Baker 2012). In general, porous membranes are typically made of ceramic, while nonporous (dense) membranes are typically made of polycrystalline ceramic or metal.

Among these types of membranes, inorganic dense membranes have attracted the interests of many researchers due to their capability to separate completely hydrogen from gaseous mixtures (Basile et al. 2011). Here, the dense Pd based membrane is widely used because of its high permeability and permselectivity (Uemiya *et al.* 1991, Lin 2001, Basile

et al. 2011). Hydrogen permeation through the Pd based membrane follows solution-diffusion transport mechanism as schematically illustrated by Fig. 1.1, which is mainly based on two main processes; i) adsorption and dissociation of hydrogen molecule at the membrane surface of upstream side, while recombination and desorption of hydrogen molecule at the downstream side, and ii) diffusion of hydrogen atom in metallic lattice (Baker 2012, L. Holleck 1970, L. Ward and Dao 1999). L. Ward and Dao (1999) considered the additional elementary processes for better understanding of hydrogen permeation; (iii) molecular hydrogen transportation from (to) the bulk gas phase to (from) the gas layer adjacent to the surface at the upstream (downstream) side, and (iv) transition of atomic hydrogen from the surface (bulk metal) into the bulk metal (surface) at the high (low) pressure side .

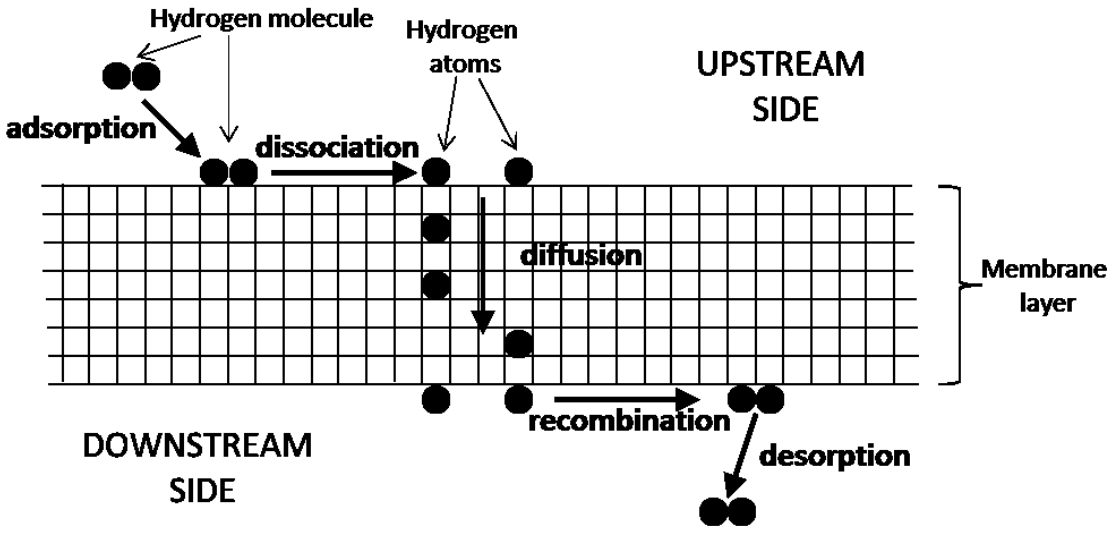

Fig. 1.1 Solution-Diffusion Transport Mechanism (L. Holleck 1970, L. Ward and Dao 1999, Baker 2012)

If the adsorption and dissociation is a very rapid process, then the hydrogen atoms on the

membrane surface are considered in equilibrium with the gas phase. In this case, the hydrogen concentration of hydrogen atoms on the metal surface, c_1, is given by Sieverts' Law (Sieverts and Zapf 1935, Baker 2012):

$$c_1 = KP_{H_2}^{0.5} \tag{1.2}$$

where K is Sieverts' constant or solubility and P_{H_2} is the hydrogen partial pressure in the gas phase. Then, it can be quantified with Fick's First Law as follows (Uemiya *et al.* 1991[(ii)]): (see Appendix A)

$$f = \frac{q}{d}\left(\sqrt{P_{H_2,1}} - \sqrt{P_{H_2,2}}\right) \tag{1.3}$$

where f: hydrogen permeation mole flux, q: hydrogen permeance coefficient, d: membrane thickness, $P_{H_2,1}$: hydrogen partial pressure at membrane surface of upstream side and $P_{H_2,2}$: hydrogen partial pressure at membrane surface of downstream side.

When the temperature is sufficiently high, the adsorption and dissociation are very fast, thus the diffusion of atomic hydrogen through the metallic lattice becomes the rate-controlling step (Baker 2012). Therefore, Sieverts' Law is obeyed, in which H_2 mole flux is linear with respect to difference in square root of hydrogen partial pressures between upstream and downstream side. Ma (2008) mentioned that for the case of Pd/Cu membrane, the Sieverts' Law is followed when only the temperature is kept above 573K , while Israni and Harold (2010) observed that the permeation through Pd/Ag membrane still follows Sieverts' Law even the temperature was set lower than 500K. However, at sufficiently low temperature, the adsorption and dissociation becomes the rate-controlling

step, and the permeation characteristics deviate from Sieverts' Law.

In addition to temperature, the thickness of the membrane also plays an important role which can affect the compliance with Sieverts' Law. As the Pd based membrane becomes thinner, diffusion in metallic lattice becomes rapid enough that the other processes could begin to affect the permeation, which is supposed to be caused by various factors such as surface processes (Collins and Ways 1993), surface poisoning (Antoniazzi *et al.* 1989) and grain boundaries (Yan *et al.* 1994). In this case, several studies have put different limitation of thickness, but generally it can be said that the thickness should be higher than 10μm (L Ward and Dao 1999, Federico *et al.* 2006) in order to ensure Sieverts' Law is followed. Meanwhile, several researchers have concluded that diffusion-limited permeation, that is Sieverts' Law still can be extended to thicknesses less than 10μm (Uemiya *et al.* 1991, Israni and Harold 2010). Regarding to this contrary conclusion, when the difficulty in controlling and quantifying factors such as aforementioned membrane surface and grain boundary condition is considered, it can be acceptable that there is no exact agreement about the limitation of membrane thickness.

1.1.3 Permeation with High H_2 Permeation Ratio

H_2 permeation ratio is defined as the fraction of H_2 feed flow rate which permeates membrane (Chen *et al.* 2011). When the feed flow rate of hydrogen is sufficiently high to cause the rate of permeated hydrogen becomes relatively very small in comparison to the feed flow rate, the Sieverts' equation as shown by Eq.(1.3) could be applied directly to predict the H_2 permeation rate through Pd based membrane for both pure H_2 and H_2 mixture (Catalano *et al.* 2009, Chen *et al.* 2011). For the case of H_2 mixture, the value of

hydrogen partial pressure at membrane surface of upstream side ($P_{H_2,1}$) in Eq.(1.3) can be determined by using the hydrogen mole fraction of the bulk flow. That is to say, it is assumed that the hydrogen partial pressure at membrane surface and bulk flow of upstream side are uniform.

The recent technical breakthrough in membrane technology since about 20th century has changed the scenery of hydrogen purification, in which the performance of membrane has substantially improved due to the rapid development of membrane materials, membrane modification and fabrication (He *et al.* 1999). However, in line with the progress of membrane technology, it is unavoidable that the H_2 permeation ratio increases to certain extent, in which the fraction of H_2 feed rate which permeates membrane becomes sufficiently high. In this case, the direct prediction by Sieverts' equation causes deviation from the actual permeation rate when H_2 mixture is used as a feed gas (Chen *et al.* 2008, Catalano *et al.* 2009), implies that the use of feed hydrogen concentration cannot give the correct $P_{H_2,1}$ in Sieverts' equation. Chen *et al.*(2011) mentioned that the H_2 permeation ratio must be less than or equal to 30% in order to use directly the Sieverts' equation for the case of tubular type Pd based membrane with H_2 mixture cross-flow.

Number of researchers (Catalano *et al.* 2009, Chen *et al.* 2011,Chen *et al.* 2012) asserted that the H_2 permeation rate becomes significantly important for the case of high H_2 permeation ratio, in which the permeation rate starts to affect the flow condition near the membrane surface. This situation could trigger the phenomenon of concentration polarization, which could be clearly observed when a long tubular type membrane was used (Caravella *et al.* 2009, Catalano *et al.* 2009, Chen *et al.* 2011, Chen *et al.* 2012). The concentration polarization is described as an accumulation of the less permeable species and a depletion of the more permeable species in the boundary layer adjacent to the

membrane, which causes the build up of concentration gradient in the boundary layer (Gaohong et al. 1999). In such situation, H_2 permeation rate becomes dominant, that is the concentration polarization becomes more pronounced for higher H_2 permeation ratio. In addition, Morgues and Sanchez (2005) mentioned that the concentration polarization also becomes more serious when the operating pressure is increased and the membrane selectivity is enhanced. Contrary to the pressure and selectivity, they expected that the concentration polarization is abated when the feed velocity is increased because the boundary layer where hydrogen concentration gradient is built up becomes thinner. This statement was then supported by Chen *et al.* (2011) who performed 2-D simulation to observe the concentration polarization of hydrogen permeation for Pd based membrane tube with the H_2 mixture cross flow.

The phenomenon of concentration polarization in the case of high H_2 permeation ratio has attracted many researchers recently to introduce the prediction method of H_2 permeation rate under such case. Catalano *et al.*(2009) considers the concentration polarization as a resistance which causes the hydrogen concentration decrease towards the membrane surface. They introduced an external mass transport coefficient for such phenomenon to relate the value of hydrogen concentration at the bulk gas phase and at the membrane surface. Because of the major contribution of diffusion due to H_2 permeation, the mass transport coefficient has been introduced which takes into account such contribution. Semi-empirical equations have been proposed for prediction of H_2 permeation rate, in which some experimental data are necessary in order to use it.

Meanwhile, Caravella *et al.* (2009) created the concentration polarization maps to evaluate the phenomenon quantitatively when the inlet and outlet conditions are specified. They have adopted the concentration polarization coefficient to create the map which takes

into account the permeation elementary steps, including adsorption of hydrogen molecule at the membrane surface, diffusion through the Pd-based membrane and desorption of H_2 molecule from the membrane surface. The proposed manual map is very useful to reduce the uncertainties when designing hydrogen purification equipment.

Then, an analytical method to predict H_2 permeation rate for a flat sheet Pd/Ag membrane with H_2 mixture stagnating flow has been introduced (Faizal *et al.* 2012, Faizal *et al.* 2013), with the assumption that both diffusive and convective transport around the membrane plays an important role to determine the permeation rate. Similar concept has been applied by Xie *et al.* (2013) to obtain the potential maximum hydrogen permeation rate for ideal tubular type Pd membrane.

1.1.4 Inhibiting Characteristics of Non-H_2 Species on Pd Based Membrane

For permeation through Pd based membrane with H_2 mixture, besides the decrease in bulk H_2 partial pressure difference across the two sides of the membrane due to dilution by the existence of other species, the decline in H_2 permeation flux still could be observed because of two main factors (Hou and Hughes 2002). First factor is the decrease in H_2 partial pressure at the membrane surface due to external mass transfer resistance, that is concentration polarization which has been described in the Section 1.1.3. The other factor is competitive adsorption and possible poisonous or coking of non-H_2 species on the surface of Pd based membrane. For the latter case, the non-H_2 species in hydrogen mixture can be classified into three categories, namely as inert gas (N_2, Ar etc.), inhibitors (CO, H_2O etc.) and poisonous gases (H_2S etc.) (Barbieri *et al.* 2008). In many experiments, due

to negligible competitive adsorption of N_2 on the surface of Pd based membrane, the binary H_2:N_2 mixture is widely used as a benchmark when evaluating the effect of inhibitors and poisonous gases on H_2 permeation through Pd based membrane (Hou and Hughes 2002). In the present study, the poisonous gases are not included into our discussion because the attention is mainly paid to the products and excessive reactants of methanol stream reforming (CO, CO_2, excessive CH_3OH and excessive H_2O). These gases are considered as inhibitors (Hou and Hughes 2002, Israni and Harold 2010), which are closely related to the interaction between the gases and the surface of membrane.

The competitive adsorption of non-H_2 species could decrease the hydrogen permeation by occupying the hydrogen dissociative sites, thus reducing the amount of adsorbed H_2 (Amandusson *et al.* 2000, Hou and Hughes 2002, Catalano *et al.* 2010). Several researchers found in their experiment that the adsorption effect by CO is very strong if compared to that by other non-H_2 species which causes dramatic reduction in H_2 permeation when it is added to feed pure H_2 or H_2 mixture (Amandusson *et al.* 2000, Barbieri *et al.* 2008, Nguyen *et al*. 2009). This is the reason why most of the experimental work (Hara *et al.* 1999, Amandusson *et al.* 2000, Li *et al.* 2000) focused on CO behavior rather than the other species, with the aim to prevent or reduce the competition by CO. Generally, the capability of adsorption of non-H_2 species on Pd based membrane is in sequence of CO > CH_3OH > CO_2 > H_2O (Israni and Harold 2010).

Hou and Hughes (2002) mentioned that adsorption effect of aforementioned non-H_2 species except CH_3OH are temperature dependence, that is the effect becomes less when the temperature is increased because the species easily desorb from membrane surface at higher temperature. In addition, for thicker membrane, diffusion of atomic hydrogen through the metallic membrane would be the controlling step, thus the adsorption effect of

these species are less if compared to that for thinner membrane. Therefore, it can be concluded that higher temperature is needed to completely eliminate the adsorption effect of these species for thinner membrane. For instance, Amano *et al.* (1990) found that the CO starts to influence the permeation through 0.7mm (700μm) thickness Pd membrane when the operating temperature was below 523K while Li *et al.* (2000) could observe the CO inhibitive effect at temperatures up to 653K when using the same type of membrane with 10 μm thickness.

To predict H_2 permeation flux through Pd based membrane with the present of CO for the case of low H_2 permeation ratio, Barbieri *et al.* (2008) introduced a model which is a combination of Sieverts' equation and Langmuir isotherm to take into account both dilution and adsorption effects caused by CO. They revealed that hydrogen permeation flux decreases with an increase in partial pressure of inhibitors (in this case, CO). Then, Miguel *et al.* (2012) proposed a rearrangement of Sieverts'-Langmuir equation which is based on average partial pressure of inhibitors and the logarithm-mean-driving force to take into account the concentration gradients along the axial length of the tubular membrane. They concluded besides CO, the inhibition effect caused by CO_2 also must not be neglected.

For the case of H_2:CO mixture with high H_2 permeation ratio, the polarization map proposed by Caravella *et al.* (2010) which considers both inhibitive effect by CO and concentration polarization simultaneously can be used to predict the H_2 permeation mole flux through Pd based membrane. When the inlet and outlet conditions are specified, the map can be referred manually.

1.2 Objectives

Polymer Electrolyte Fuel Cell (PEFC) which converts directly chemical energy (hydrogen) to electrical energy is one of the attractive options to supply energy in a clean way, that is without any harmful effect on environment. This is because the PEFC only produces water and heat as by-products. Thus, the compact reformer in connection with PEFC is an attractive option for light duty vehicles, such as motorcycle and power assisted bicycle, and small electrical device applications such as cellular phones, tablets and laptop computers. The development of the compact reformer already started more than a decade, but most undergoing researches still investigated the best operating condition which could provide the high permeation of H_2. Based on the literature survey, it is revealed that the effect of key parameters such as temperature, pressure, steam to carbon (S/C) ratio and reactant feed flow rate on the performance of compact methanol steam reformer with purification membrane was less explored, although for the methanol steam reformer without membrane configuration, has been done. In addition, the mechanism how the key parameters affect the performance of compact reformer is still not clearly described.

Therefore, the first objective of the present study is to understand the performance of a compact methanol steam reformer with hydrogen purification Pd/Ag membrane, which is suitable for small electrical device application. The effect of aforementioned key parameters on the performance of methanol steam reforming reaction and hydrogen permeation are investigated for the compact methanol steam reformer.

Based on the results of experiment for compact methanol steam reformer, it was found that the well-known Sieverts' equation is not going well for estimation of H_2 permeation rate. In this case, a more fundamental study is necessary to confirm the reason why the

significant difference between the prediction by Sieverts' equation and experimental results occurs.

Therefore, the second objective is to understand the fundamental characteristics of hydrogen permeation through a flat sheet Pd/Ag membrane. In this case, experimental study is carried out without using any metal support. In addition, H_2:N_2 mixture was used in the experiment because nitrogen is non-inhibiting gas, thus the effect of competitive adsorption of non-H_2 species can be neglected.

Number of researchers asserted that for the case of high H_2 permeation ratio, H_2 flux becomes an important parameter in addition to pressure and feed flow rate which could affect the permeation. However, a theoretical equation which considers directly the effect of H_2 flux itself, has not been proposed yet. Therefore, the third objective of the present study is to propose a theoretical equation based on Sieverts' equation to estimate H_2 permeation mole flux for hydrogen mixture. The proposed analytical method considers the hydrogen concentration decrease at the membrane surface due to effect of H_2 permeation itself, with the assumption that both diffusive and convective transport around the membrane are taken into account. In this case, the proposed method is validated with the present experimental results.

The proposed theoretical equation, however, could not describe the H_2 concentration distribution near the membrane surface during permeation. In this case, two-dimensional numerical simulation is performed to understand the H_2 concentration distribution near the membrane surface for a flat sheet Pd/Ag membrane. The geometry and boundary conditions used in the simulation are similar with the membrane module of the present experimental study to imitate the real hydrogen permeation process.

1.3 Scheme of Dissertation

This dissertation consists of six chapters: Chapter 1 is an introduction of this thesis, and the following Chapter 2 refers to the experimental investigation on performance of compact methanol steam reformer with a flat sheet Pd/Ag membrane. Meanwhile, Chapter 3 is much more fundamental than Chapter 2, which regards to the experimental investigation on the effect of feed flow rate on H_2 permeation for a flat sheet Pd/Ag membrane, by using a membrane module. In Chapter 4, a theoretical equation is proposed, and it is used to discuss fundamentally the effect of feed flow rate. In addition to experimental and theoretical investigation, numerical simulation is performed in Chapter 5, to demonstrate clearly the H_2 concentration distribution near the membrane surface during permeation. Finally, the concluding remarks are presented in Chapter 6.

In Chapter 2, the performance of compact methanol steam reformer is evaluated experimentally for various reference temperatures, pressures, S/C ratios and reactant flow rates. The discussion is mainly focused on the characteristics of methanol steam reforming and permeation of H_2 for various aforementioned parameters. The best operating condition to obtain the maximum hydrogen permeation rate is finally concluded. In this part, the comparison between the estimation of H_2 permeation rate by original Sieverts' equation and experimental results is performed, which demonstrates the significant deviation between them. In this case, a much more fundamental study is necessary to understand the characteristics of H_2 permeation for flat sheet Pd/Ag membrane, which can confirm the reason why such significant difference occurs.

In Chapter 3, the effect of feed flow rate on H_2 permeation for a flat sheet Pd/Ag membrane is investigated experimentally, without considering resistance from metal

support and the adsorption effect of non-H_2 species. In this Chapter, the comparison between the estimation by the Sieverts' equation and experimental results are performed again.

Meanwhile, in Chapter 4, a theoretical equation which considers the hydrogen concentration decrease at membrane surface due to the effect of H_2 flux itself is proposed, and is validated with experimental results of Chapter 3. Then, the effect of feed flow rate on H_2 permeation for hydrogen mixture is discussed fundamentally by using this equation.

Finally, in Chapter 5, a two-dimensional numerical simulation is performed, to discuss the H_2 concentration distribution near the membrane surface for the case of high H_2 permeation ratio. In this numerical study, the geometry is similar with that of the present experimental study. The comparison between the numerical, theoretical and experimental results is performed initially in this part. Then, the hydrogen concentration profiles along the central axis of the membrane and along the radial distance of the membrane surface for various feed flow rates, pressures, inlet H_2 mole fractions and species in H_2 mixture are particularly discussed.

Chapter 2

Compact Methanol Steam Reformer with Hydrogen Purification Pd/Ag Membrane

2.1 Introduction

Experimental and theoretical studies related to methanol steam reformer integrated with a purification membrane have been conducted under various operating conditions and different configurations (Arstad *et al.* 2006, Basile *et al.* 2006, Iulianelli *et al.* 2008, S. Damle 2009, H. Israni and P. Harold 2011). Most of the researchers nowadays paid more attention on the best operating condition to obtain the reliable performance of the compact reformer. Iulianelli *et al.* (2008) investigated the optimum condition for methanol steam reforming in a Pd/Ag membrane reactor by determining the most suitable pressure, sweep factor and flow configuration without emphasizing on the effect of temperature and steam/methanol ratio. Meanwhile, the other studies (Arstad *et al.* 2006, H. Israni and P. Harold 2011) investigated the possibility to perform the methanol steam reforming in a Pd based membrane reactor, with the discussion on the effect of non-H_2 species on the membrane performance. Therefore, it is suggested that the performance evaluation of compact methanol steam reformer for various operating conditions and designs is being actively carried out, with the aim to obtain high methanol conversion and high H_2 permeation. However, the effect of key parameters especially steam/carbon (S/C) ratio and reactant flow rate on the performance is still less explored, and this is included in our present discussion.

Hydrogen permeates the Pd based membrane due to a solution-diffusion transport and then hydrogen permeation through the membrane can be estimated by applying Sieverts' equation with Fick's First Law (Catalano *et al.* 2009). The permeation is based on two main processes; i) adsorption (desorption) and dissociation (recombination) of hydrogen

molecule (atoms) at the upstream (downstream) membrane surface, and (ii) diffusion of hydrogen atoms in the metallic lattice (L. Holleck 1970, L. Ward and Dao 1999). Sieverts' law states that for a relatively thick membrane (thickness ≥ 10μm), this diffusion mechanism is a rate-limiting step for hydrogen permeation (L. Ward and Dao 1999, Federico *et al.* 2006). In this case, the Sieverts' type driving force exponent is 0.5, which is applicable for dense Pd-based membranes. L. Ward and Dao (1999) considered the additional elementary processes for better understanding of hydrogen permeation; (iii) molecular hydrogen transportation from (to) the bulk gas phase to (from) the gas layer adjacent to the surface at the upstream (downstream) side, and (iv) transition of atomic hydrogen from the surface (bulk metal) into the bulk metal (surface) at the high (low) pressure side.

In our study, the characteristics of methanol steam reforming reaction and hydrogen permeation through Pd/Ag membrane for compact methanol stream reformer were investigated under various operating conditions. Based on several previous studies (Hara *et al.* 1999, Israni and Harold 2010), it seems necessary to maintain the hydrogen purification at a temperature of 553K and above when using the Pd or Pd alloy membrane to reduce the disturbance effect of non-hydrogen species and to obtain higher hydrogen permeation flux. Additional power for pressurization of the upstream side was not necessary because the pressure was exerted by reformed gas instead of using a compressor. In addition, H_2 permeation rate obtained from the experiment was compared with the prediction by the original Sieverts' equation.

2.2 Reaction Model, Experimental and Estimation Method

2.2.1 Reaction Formula of Methanol Steam Reforming

The overall methanol steam reforming reaction model is shown in the following equation.

$$CH_3OH + H_2O \longrightarrow 3H_2 + CO_2 \text{ -49.5 kJ/mol} \quad (2.1)$$

In a real methanol steam reformer, a small amount of CO is formed. As we mentioned in Chapter 1, CO reduces H_2 permeation even though the concentration of CO is as low as the order of magnitude of 10ppm. In this paper, CO formation is modeled using the following two-step equations:

Methanol decomposition reaction: $CH_3OH \longrightarrow CO + 2H_2$ -90 kJ/mol (2.2)

Water-gas shift reaction : $CO + H_2O \longrightarrow CO_2 + H_2$ +40.5 kJ/mol (2.3)

2.2.2 Experimental Setup and Procedures

The experimental setup of the flow system and the compact reformer unit are shown in Figs. 2.1 and 2.2, respectively. For the reforming process, tablet type catalyst $CuO/ZnO/Al_2O_3$ (CuO 42 mass%, ZnO 47 mass% and Al_2O_3 10mass%) with diameter and height of 3.2mm, was arranged around the center of the reformer. To obtain high purity hydrogen, a 25μm thickness 77 wt.% Pd/23 wt.% Ag flat sheet membrane with diameter of

0.068m and effective surface area of $3.63\times10^{-3}m^2$ was hold by copper gasket and was set downstream of the catalyst zone. The purification membrane was supported by sintering porous stainless steel. For both measurement of reference catalyst zone and reference membrane temperature, K-type thermocouples (sheath diameter 1.6mm, material SUS316) were used. For measurement of reference catalyst zone temperature, a hole with diameter of 0.002m (2mm) and depth of 0.045m (45mm) was made to locate the thermocouple, as shown in Fig. 2.2. The position for the measurement of the reference catalyst zone temperature was set at horizontal distance of ~0.005m (~5mm) next to the wall of catalyst zone. Meanwhile, the position for the measurement of the reference membrane temperature was set at vertical distance of ~0.01m (~10mm) below the purification membrane. A thermocouple was placed at the one of the outlets of off-gas for measuring the reference membrane temperature. The whole reformer body was insulated with insulation materials (asahi light caster 10 with water addition 80 mass%, and glass wool) to prevent heat loss.

As shown in Fig. 2.1, the heating was performed by a Bunsen type burner using City Gas 13A while the reformer was first purged with nitrogen. The purging process was stopped when the measurement value became close to desired reference catalyst zone temperature. Then, methanol and water pressurized by nitrogen were supplied to the catalyst zone through the piping which was heated by ribbon heater. The flow rate of methanol and water were set by mass flow controllers (Horiba STEC, model: LV-410). After vaporization of methanol and water by heat from ribbon heater, hydrogen then was formed at the catalyst zone by steam reforming. To keep the reference catalyst zone temperature, the heat from the Bunsen type burner was controlled by adjusting City Gas 13A flow rate. In this case, the reference catalyst zone temperature and respective reference membrane temperature were almost stable for sufficiently long time period, due

to the high heat capacity of stainless steel and heat loss protection by the insulation materials.

After the reference catalyst zone temperature was stable, a needle valve was controlled to pressurize the reformed gas at the upstream side. When the pressure of the reformed gas was increased, hydrogen started to permeate the membrane. In this case, the pressure was adjusted parallel with the observation on the pressure reading. The flow rate of off-gas was measured by a high precision film flow meter (Horiba STEC, model: VP-4U) and its mole concentration was measured by a gas chromatograph (Shimazu, model: GC-2014ATE and C-R8A). The flow rate of the purified gas was measured by a soap-film flow meter (GL Sciences 50ml) and its mole concentration was measured by a gas chromatograph and a CO infrared instrument (Horiba, model VIA-510) with a range of 0ppm to 200ppm as well because CO concentration was usually lower than 200ppm.

In our study, the experiments were conducted under various experimental conditions as mentioned in Table 2.1.

Table 2.1 Experimental Conditions

No.	**Reference Catalyst Zone Temperature, $T_{cat(ref)}$ [K]**	**Upstream Pressure, P_0 [MPa]**	**S/C Ratio, α**	**Reactant Flow Rate, F_{reac} [mol/s]**
1	589-689	0.40	1	2.8×10^{-4}
2	637	0.20-0.50	1	2.8×10^{-4}
3	637	0.40	0.8-1.6	2.8×10^{-4}
4	637	0.40	1	$(1.7\text{-}4.4)\times10^{-4}$

The reference catalyst zone temperature ($T_{cat(ref)}$) was set from 589 to 689 K to obtain

maximum methanol conversion rate. The pressure range was set from 0.20 to 0.50MPa, to obtain high hydrogen flux and at the same time, to consider the mechanical strength of the membrane. In other words, the range of pressure difference between upstream side and downstream(permeated) side was 0.10MPa to 0.40MPa and the permeated pressure was atmospheric in all series of experiment. Meanwhile, the S/C ratio was varied between 0.8 to 1.6, which was commonly used for reducing CO in the reformed gas while maintaining high methanol conversion rate. The reactant flow rate was set from 1.7×10^{-4} to 4.4×10^{-4}mol/s to supply around 5.6×10^{-4} mol/s (2 mol/h) highly purified hydrogen to a PEFC.

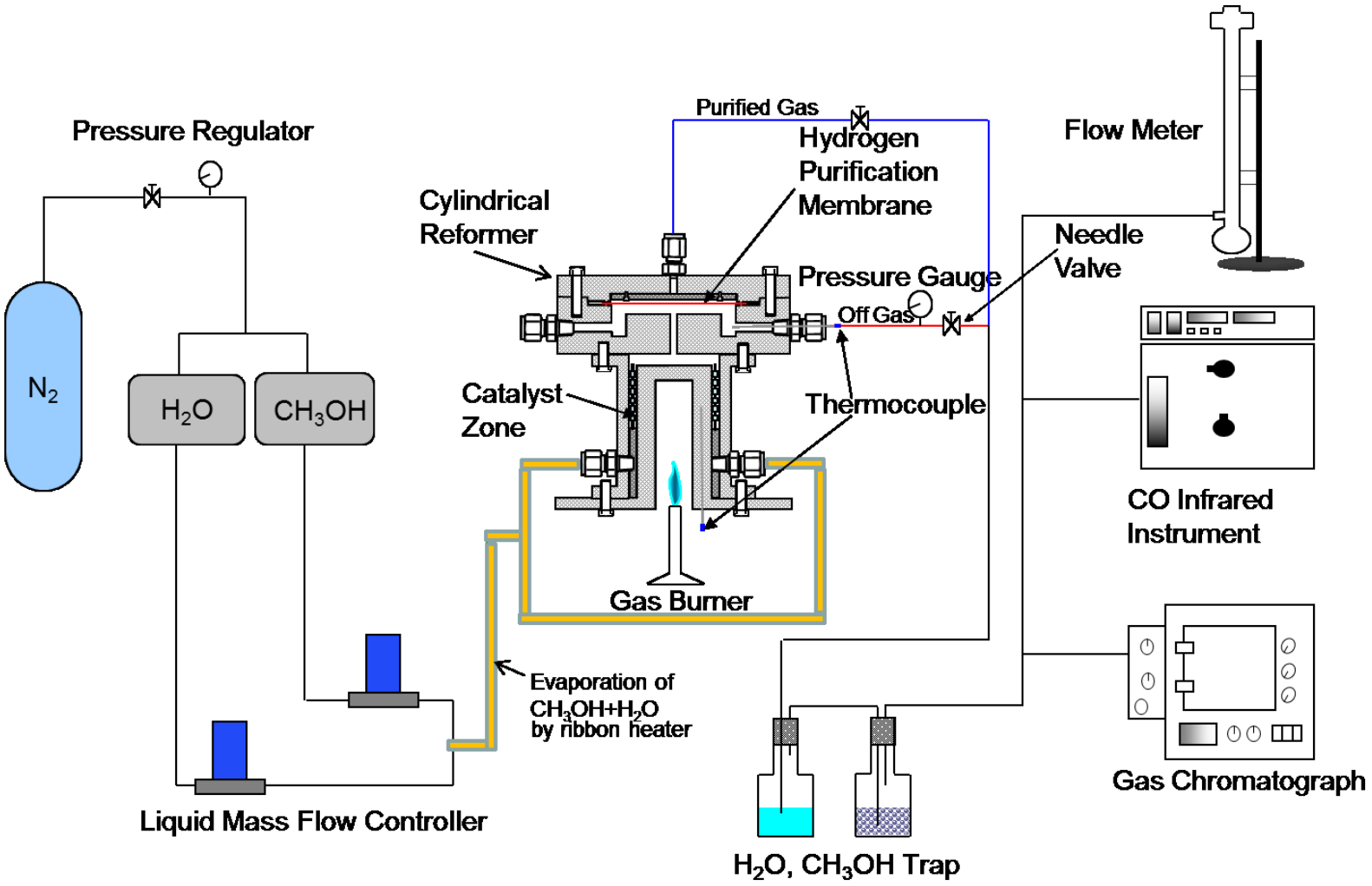

Fig. 2.1 Experimental Setup

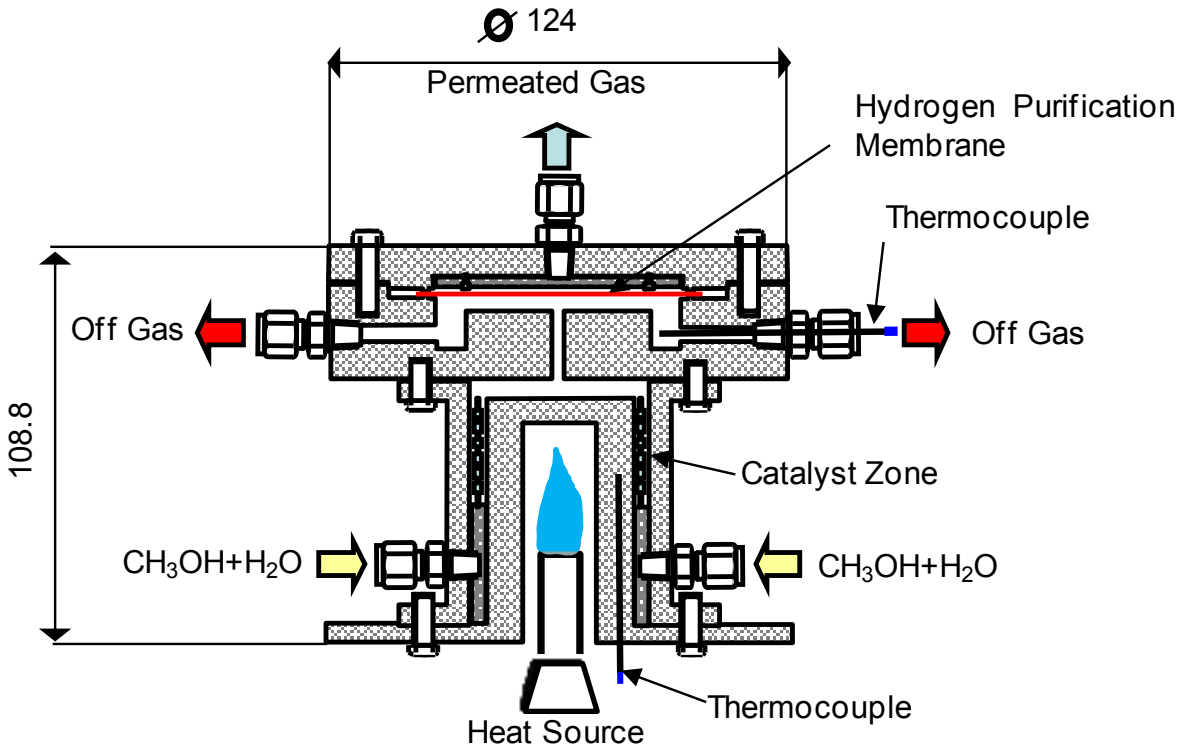

(a) Compact Methanol Steam Reformer

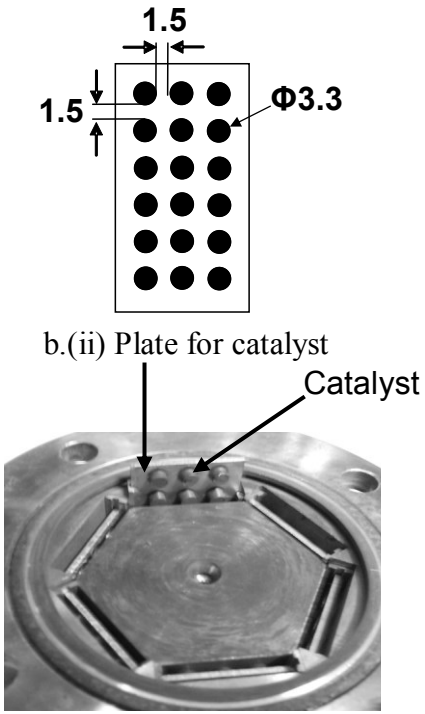

b.(ii) Plate for catalyst

b.(i) Catalyst arrangement

Fig. 2.2 Compact reformer for methanol steam reforming and catalyst arrangement

2.2.3 Structure of Compact Methanol Steam Reformer

It is important to consider what kind of design that can give the reliable performance, which fulfills the requirement for the small electrical devices. It is desirable to design the compact reformer with high hydrogen permeation rate, but at the same time, it is important to minimize the power input. In this case, high heat capacity of stainless steel is used as material for the reformer body and the insulation materials are used to prevent heat loss. As a result, the reference catalyst zone temperature and respective reference membrane temperature were almost stable for sufficiently long time period. In addition, due to the use of stainless steel and the location of the burner as shown by Fig.2.2, one burner is sufficient to heat both catalyst zone and hydrogen purification zone simultaneously. In this case, the burner is set inside the reformer, and the whole reformer is heated.

Then, as shown by Fig. 2.2(b), the catalysts are arranged around the center, and are hold by plates. In this case, a good gas circulation can be obtained which can give the reliable methanol conversion rate. The use of plates to hold the catalysts can prevent the possible waste caused by excessive catalysts.

Figure 2.2 also shows that there is a separation or partition between the hydrogen purification zone and catalyst zone. The separation is very important to protect the membrane from damage due to very reactive methanol steam reforming reaction.

A small tunnel which connects the catalyst zone and hydrogen purification zone is created. This tunnel is necessary to form a smooth flow around the membrane surface. Besides, due to the effect of feed flow rate on hydrogen permeation, such geometry is necessary to increase the hydrogen permeation rate by increasing the flow rate towards the membrane surface.

For hydrogen purification, a Pd/Ag membrane with 25μm thickness is used because to

obtain high hydrogen permeation rate while considering the mechanical strength of the membrane. Besides, this thickness is sufficient in order to ensure that the membrane follows Sieverts' Law. The compliance with Sieverts' Law enables us to predict the hydrogen permeation rate that can be obtained under certain operating conditions.

When we think the compact reformer for home devices application, safety aspect must be taken into account. Therefore, the use of stainless steel material is supposed to be practical to withstand with pressurization. Besides, we do not operate the compact reformer under high pressure for the safety reason.

Furthermore, there are several recommendations for compact methanol steam reformer in connection with Polymer Electrolyte Fuel Cell (PEFC):

i) The structure of the compact reformer should be as simple as possible for easier maintenance, thus the time allocated for the maintenance will become shorter. This includes the use of flat sheet type membrane for hydrogen purification and the simple structure of catalyst zone for methanol steam reforming reaction.

ii) Flat sheet Pd/Ag membrane should be used instead of tubular Pd/Ag membrane because simpler structure of the flat sheet membrane is less expensive than tubular type membrane.

iii) The use of flat sheet Pd/Ag membrane with sufficient thickness in compact methanol steam reformer allows us to estimate the maximum hydrogen permeation rate prior to designing the reformer. The estimation can be done by using our proposed analytical method based on Sieverts' equation with the consideration of permeation effect.

2.2.4 Theoretical Background

The hydrogen permeation rate of the hydrogen purification membrane is estimated by Sieverts' Law, which is quantified with Fick's First Law as mentioned in Eq. (2.4) (Uemiya *et al.* 1991[ii]):

$$F = \frac{qA}{d}\left(\sqrt{P_{H_2,1}} - \sqrt{P_{H_2,2}}\right) \tag{2.4}$$

The hydrogen permeance coefficient (q) for the Pd/Ag membrane is estimated using Fig. 2.3 as a function of membrane temperature.

Figure 2.3 shows that the hydrogen permeance coefficient is around $1.0\text{x}10^{-8}$ to $2.0\text{x}10^{-8}$ $\text{mol.H}_2\text{.m}^{-1}\text{.s}^{-1}\text{.Pa}^{-0.5}$ and increases with an increase in temperature. The values of the coefficient, however, are different quantitatively (Chabot *et al.* 1988, Nishimura *et al.* 2002). It is not clear the difference in the present study , but it can be supposed that the characteristics of the membrane is sensitive to the manufacturing process, the condition to be used and so on. Thus, we used two values in Fig. 2.3 in the analysis of the present study.

Figure 2.4 shows a schematic of the hydrogen partial pressure profile near the membrane surface. As shown in Fig. 2.4, the H_2 concentration variation close to the membrane is not taken into account . In this case, $P_{H_2,1}$ is estimated as follows,

$$P_{H_2,1} = \frac{F_{in,H_2}}{F_{in}} P_{in} \tag{2.5}$$

In this experiment, the mixture which is supplied to the upstream side of the membrane, is produced by steam reforming. Then, we use the actual reformed gas composition to

estimate the permeation rate through the membrane based on Sieverts' equation. In our experimental study, F_{in,H_2} and F_{in} are then determined as follows,

$$F_{in,H_2} = F_{per} + F_{H_2,off-gas} \tag{2.6}$$

where $F_{H_2,off-gas}$ is obtained by Eq. (2.7) below.

$$F_{H_2,off-gas} = X_{H_2,off-gas} \times F_{all,off-gas} \tag{2.7}$$

Then, inlet total gas flow rate F_{in} is determined from the Eq. (2.8), as shown below.

$$F_{in} = F_{per} + F_{all,off-gas} + F_{unreacted} \tag{2.8}$$

By substituting $P_{H_2,1}$ in Eq.(2.4) with Eq.(2.5), the following Eq.(2.9) is obtained.

$$F = \frac{qA}{d}\left(\sqrt{\frac{F_{in,H_2}}{F_{in}}P_{in}} - \sqrt{P_{H_2,2}}\right) \tag{2.9}$$

Then, Eq.(2.9) is used to estimate the H_2 permeation rate based on Sieverts' equation.

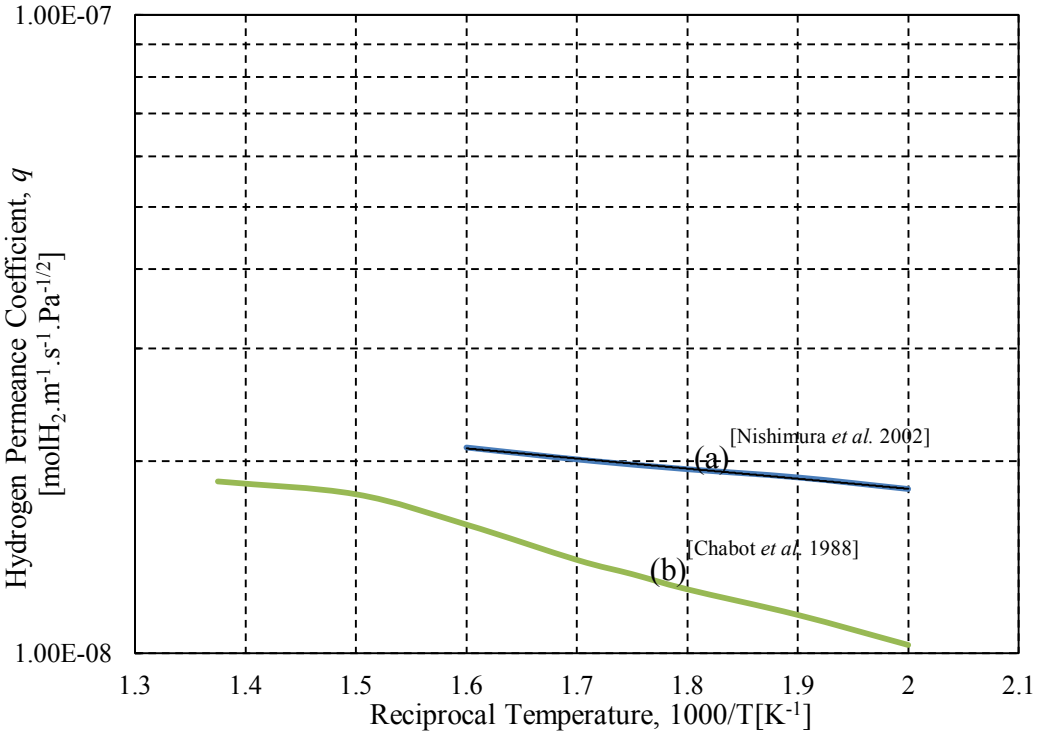

Fig. 2.3 Hydrogen permeance coefficient (q) of 77wt.% Pd/23wt.% Ag membrane

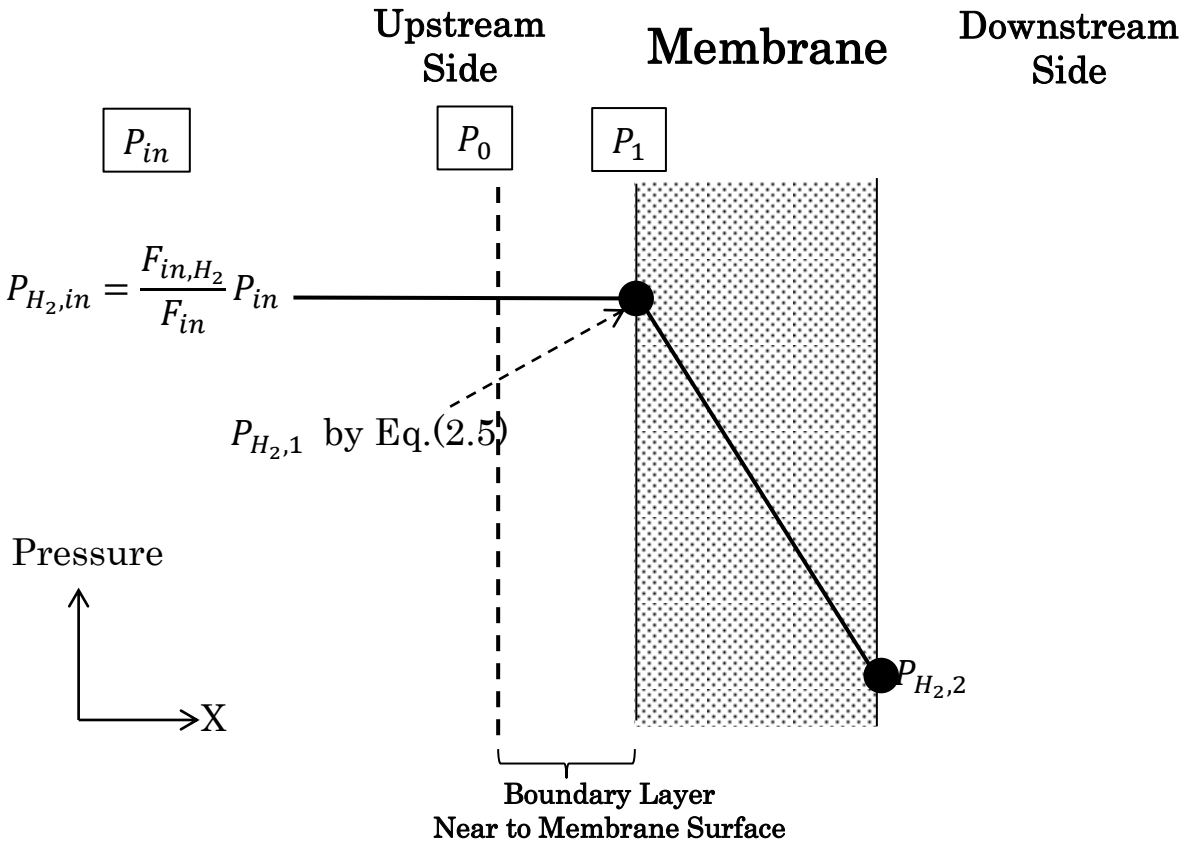

Fig. 2.4 Pressure profile of the permeation system

2.3 Results and Discussion

The performance of compact methanol steam reformer was investigated experimentally in terms of mole fraction of reformed gas, methanol conversion rate and H_2 purification.

2.3.1 Methanol Steam Reforming Process

In this section, the experimental results of the effect of reference catalyst zone temperatures, pressures at the upstream side, steam to methanol ratios (S/C ratio), and reactant flow rates on mole fraction of reformed gas and methanol conversion rate, are presented.

2.3.1.1 Temperature Dependence

Figure 2.5 shows the effect of reference catalyst zone temperature on the mole fraction of reformed gas and the methanol conversion rate. The figure shows that the mole fraction of reformed hydrogen is constant in the experimental temperature range, at almost 0.75, which is the theoretical mole fraction of H_2 estimated from Eq. (2.1). Meanwhile, the CO_2 decreases while CO increases with an increase in reference temperature. This is mainly caused by the formation of more CO and less CO_2 at higher reference temperature due to the suppression of the exothermic water-gas shift reaction, which is shown in Eq.(2.3). The figure shows that the methanol conversion rate reaches maximum at around 0.75, indicating that not all of the methanol is converted to hydrogen. In addition, the conversion rate decreases significantly when the reference catalyst zone temperature is decreased from 620K to 590K. This is mainly due to a decrease in the catalyst activity, when the reference catalyst zone temperature becomes lower than 620K.

2.3.1.2 Pressure Dependence

Figure 2.6 shows the mole fraction of reformed gas and the methanol conversion rate under various operating pressures. The figure shows that the mole fractions of reformed H_2, CO_2 and CO are 0.75, 0.20 and 0.05, respectively. The reformed H_2, CO_2 and CO remained constant, indicating that the methanol decomposition and water-gas shift reaction are little

influenced by the pressure. The methanol conversion rate is almost constant at about 0.75 once the pressure reaches 0.30MPa. Initially, when the pressure decreases to 0.20MPa, the conversion rate slightly decreases. Since the contact time between the reactants and catalyst decreases with a decrease in pressure, the amount of hydrogen produced also decreases.

2.3.1.3 Dependence on Steam/Methanol (S/C) Ratio

Figure 2.7 shows the effect of the S/C ratio on the mole fraction of reformed gas and the methanol conversion rate. The figure shows that the reformed hydrogen is almost constant at 0.75 though it decreases slightly when S/C ratio<1. When S/C ratio<1, there is insufficient steam to react with methanol, and as a result, the hydrogen mole fraction slightly decreases. The mole fraction of CO_2 increases while CO decreases with an increase in the S/C ratio. This is because more CO from methanol decomposition is converted to CO_2 by the water-gas shift reaction when the S/C ratio is increased. The figure shows that the conversion rate is almost constant for various S/C ratios though it shows a slight fluctuation.

2.3.1.4 Dependence on Reactant Flow Rate

Figure 2.8 shows the effect of reactant flow rate on the mole fraction of reformed gas and the methanol conversion rate. The figure shows that the mole fraction of H_2, CO_2 and CO tends to be constant at 0.75, 0.21 and 0.04, respectively. It is interesting to note that the methanol conversion rate dramatically decreases with an increase in the reactant flow rate. This is mainly caused by the decrease in the residence time of the reactants when the flow rate is increased. The decrease in the residence time causes fewer reactant molecules to contact the catalyst in a sufficient time for reforming. Consequently, fewer reactants were converted to hydrogen through the reforming process.

As a conclusion for the Section 2.3.1.1 to 2.3.1.4, the results show that when reference catalyst zone temperature is equal or higher than 620K, and pressure is equal or higher than 0.30MPa, the maximum methanol conversion rate is obtained when the reactant flow rate is low. The methanol conversion rate is insensitive to the S/C ratio within this experimental range. However, even when the reference temperature is increased or S/C ratio is decreased, the undesired CO also increases, which is mainly caused by the suppression of the

exothermic water-gas shift reaction. Besides, as reported by previous study (Huang *et al.* 2007), at certain point of high temperature, the performance of catalyst $CuO/ZnO/Al_2O_3$ starts to deteriorate, which may cause the decrease in methanol conversion rate. In addition, even higher conversion rate is obtained at lower reactant flow rate, less hydrogen is produced.

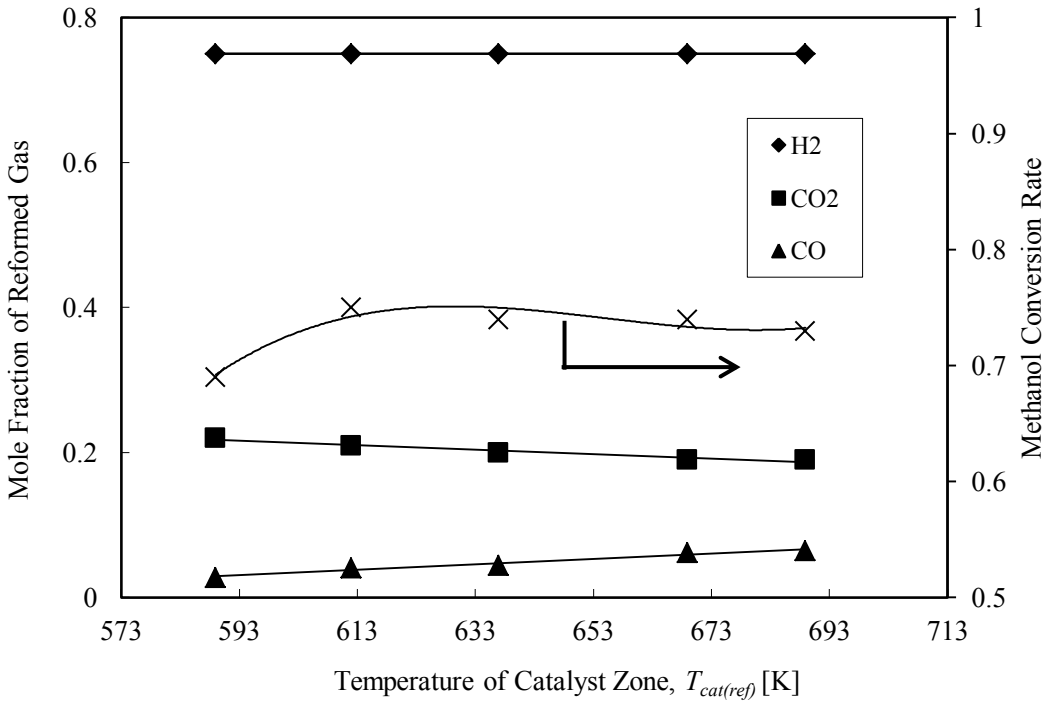

Fig. 2.5 Effect of reference catalyst zone temperature on mole fraction of reformed gas and methanol conversion rate (P_0: 0.4MPa, α: 1, F_{reac}: 2.8×10^{-4} mol/s)

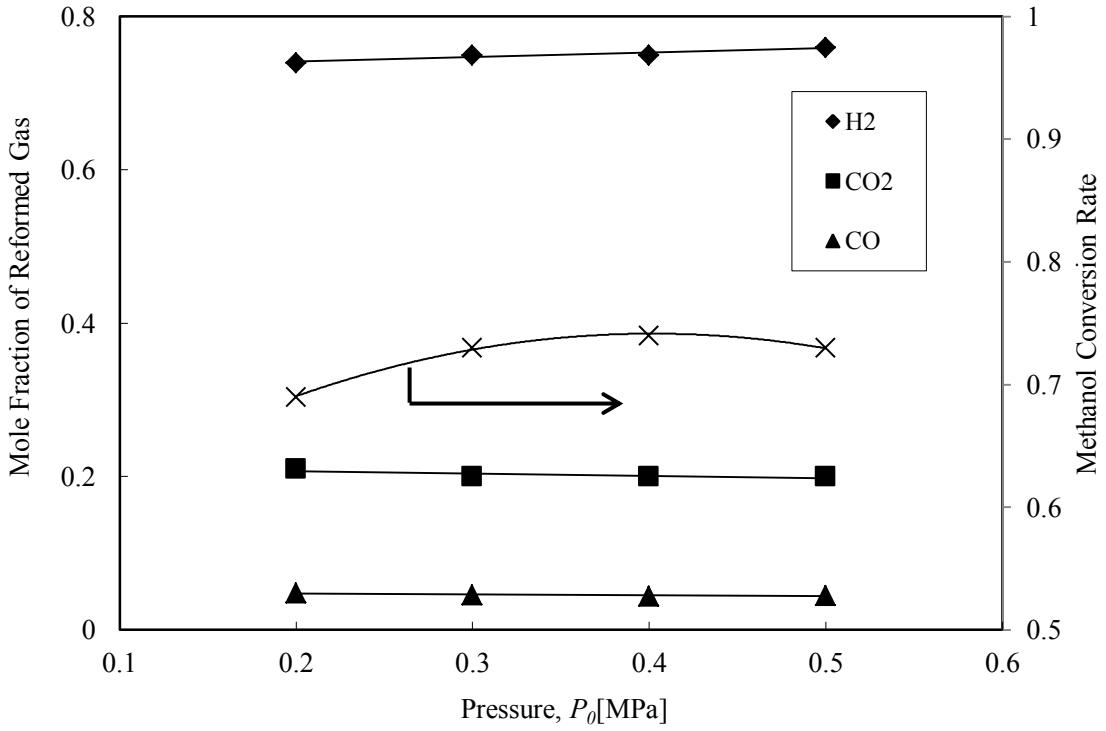

Fig. 2.6 Effect of pressure at upstream side on mole fraction of reformed gas and methanol conversion rate ($T_{cat(ref)}$: 637K, α: 1, F_{reac}: 2.8×10^{-4} mol/s)

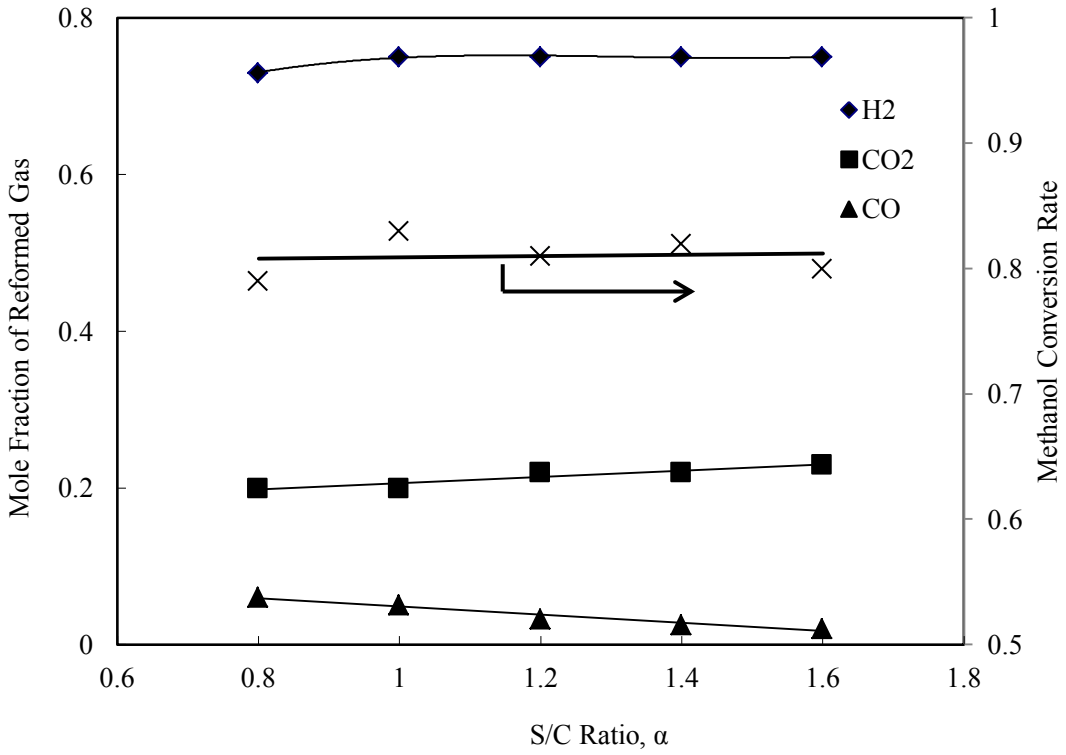

Fig. 2.7 Effect of S/C ratio on mole fraction of reformed gas and methanol conversion rate ($T_{cat(ref)}$: 637K, P_0: 0.40MPa)

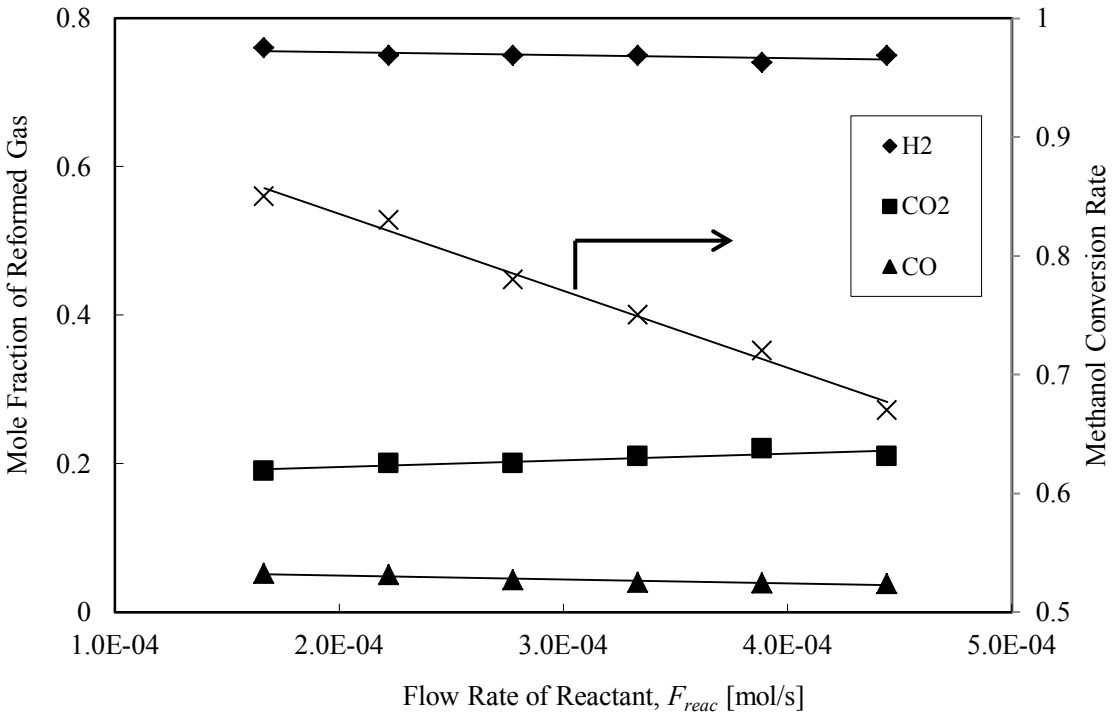

Fig. 2.8 Effect of reactant flow rate on mole fraction of reformed gas and methanol conversion rate ($T_{cat(ref)}$: 637K, P_0: 0.40MPa, α: 1)

2.3.2 Hydrogen Purification

In this section, the results of the hydrogen permeation rate under various operating parameters including the reference membrane temperature, pressure at the upstream side, S/C ratio and reactant flow rate are described.

2.3.2.1 Dependence on Temperature

Figure 2.9 shows the hydrogen permeation rate under various reference membrane temperatures. The figure shows that initially, the hydrogen permeation rate increases significantly with an increase in the reference membrane temperature. This is caused by the increase in the hydrogen permeance coefficient and significant increase in methanol conversion rate shown in Fig. 2.5, when the reference temperature is increased. Figure 2.9 shows that the increase rate of the permeation rate gradually decreases when the reference temperature becomes higher than 580K, which is caused by the almost constant and slight decrease in the methanol conversion rate at this temperature range.

The CO concentration contained in the permeated gas under various operating reference membrane temperatures is mentioned. This indicates that high purity hydrogen with a very low CO concentration can be obtained for all temperature ranges, which is able to be used for PEFC application (< 10 ppm) (Katsuki 2005).

2.3.2.2 Dependence on Pressure

Figure 2.10 shows the effect of upstream side pressure on the hydrogen permeation rate. The hydrogen permeation rate increases with an increase in the pressure, which is caused by the larger difference between hydrogen partial pressure at the upstream side and the permeated side. The figure shows that the increase rate of the hydrogen permeation rate gradually decreases. Details of this trend are discussed in Section 2.3.4.

Table 2.3 shows the high purity hydrogen with low CO concentration, which is less than 0.3 ppm, is obtained under various pressures.

2.3.2.3 Dependence on Steam/Methanol (S/C) Ratio

Figure 2.11 shows the effect of the S/C ratio on the hydrogen permeation rate. The figure

shows that the hydrogen permeation rate reaches maximum at the S/C ratio around unity and decreases on both sides. When the S/C ratio is decreased from 1 to 0.8, the hydrogen permeation rate decreases. This is mainly due to the decrease in the hydrogen mole fraction in the reformed gas when the S/C ratio is decreased. The decrease in the hydrogen mole fraction decreases the permeation rate because the hydrogen partial pressure decreases. On the other hand, when the S/C ratio becomes higher than 1, the permeation rate tends to decrease gradually. When the S/C ratio is increased from unity, more excessive steam at the upstream side exists, which causes the decrease in the hydrogen mole fraction. As a result, the permeation rate decreases with an increase in the S/C ratio because the hydrogen partial pressure at the upstream side decreases. As shown in Table 2.4, all values of CO concentration are very small and fulfil the PEFC requirement (<10ppm) (Katsuki 2005).

2.3.2.4 Dependence on Reactant Flow Rate

Figure 2.12 shows the effect of the reactant flow rate on the hydrogen permeation rate. The permeation rate initially increases with an increase in the reactant flow rate, and reaches a maximum when the reactant flow rate is around 2.8×10^{-4} mol/s. When the reactant flow rate is increased from 1.7 to 2.8×10^{-4} mol/s, the flow velocity towards the membrane surface increases. The higher flow velocity produces a higher hydrogen concentration at the membrane surface, which causes an increase in the hydrogen permeation rate. However, once the reactant flow rate exceeds 2.8×10^{-4} mol/s, the effect of the decrease in the methanol conversion rate mentioned in Section 2.3.1.4 on the decrease in H_2 partial pressure is considered to overcome the effect of the increase in the flow velocity towards the membrane. Consequently, less hydrogen is permeated due to the decrease in hydrogen partial pressure at the upstream side.

Table 2.5 shows that CO concentration in the permeated gas is very small, and thus is suitable for the PEFC application.

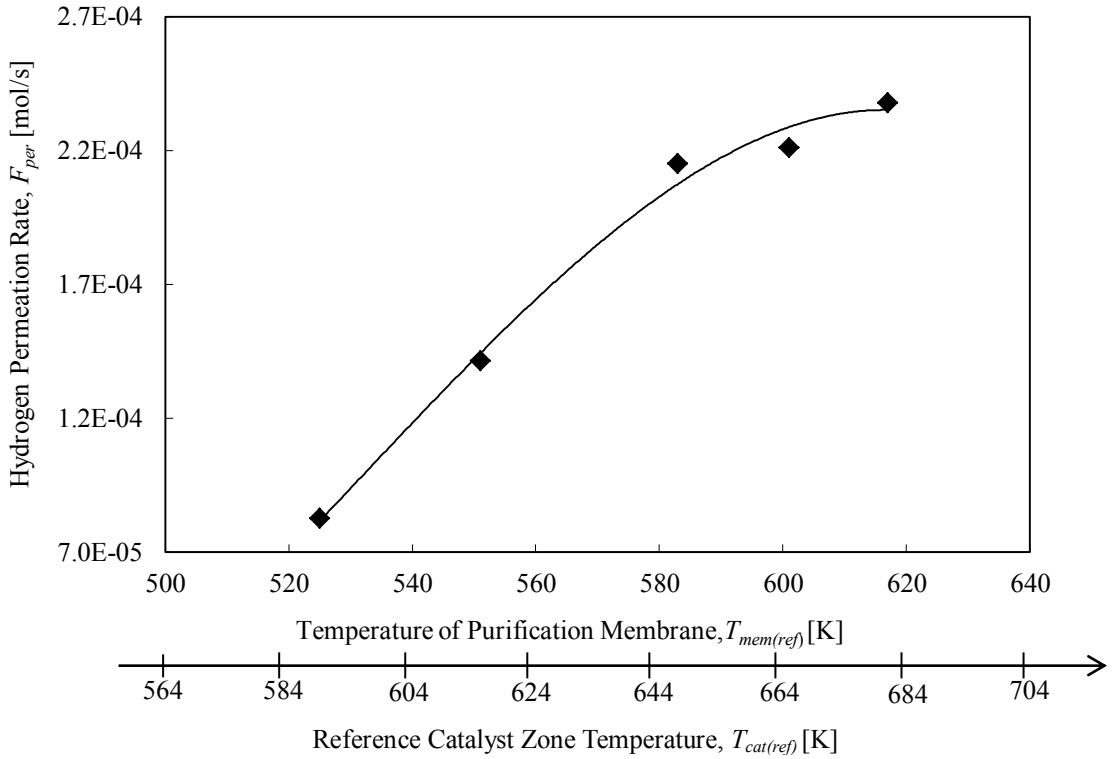

Fig.2.9 Effect of reference membrane temperature on hydrogen permeation rate (P_1: 0.4 MPa, α: 1, F_{reac}: 2.8×10^{-4} mol/s)

Table 2.2 CO concentration at different reference membrane temperatures

Reference Membrane Temperature, $T_{mem(ref)}$ [K]	525	551	583	601	617
CO concentration [ppm]	0.01	0.00	0.15	0.15	0.26

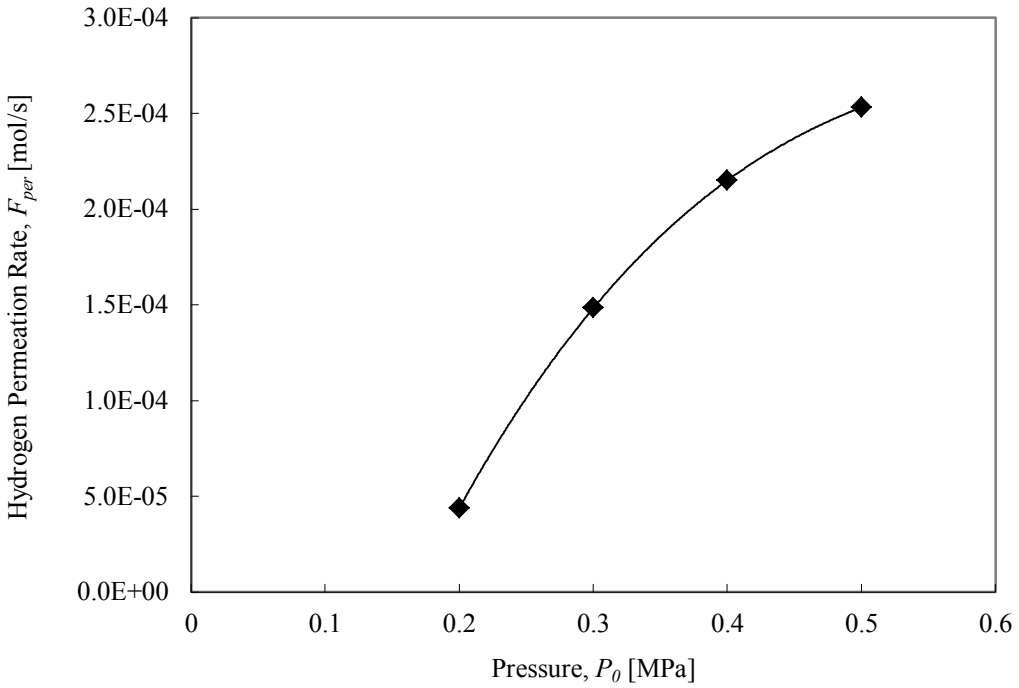

Fig. 2.10 Effect of upstream side pressure on hydrogen permeation rate ($T_{mem(ref)}$: 583K, α: 1, F_{reac}: 2.8×10^{-4} mol/s)

Table 2.3 CO concentration at different pressures

Pressure, P_0 [MPa]	0.20	0.30	0.40	0.50
CO concentration [ppm]	0.09	0.16	0.15	0.22

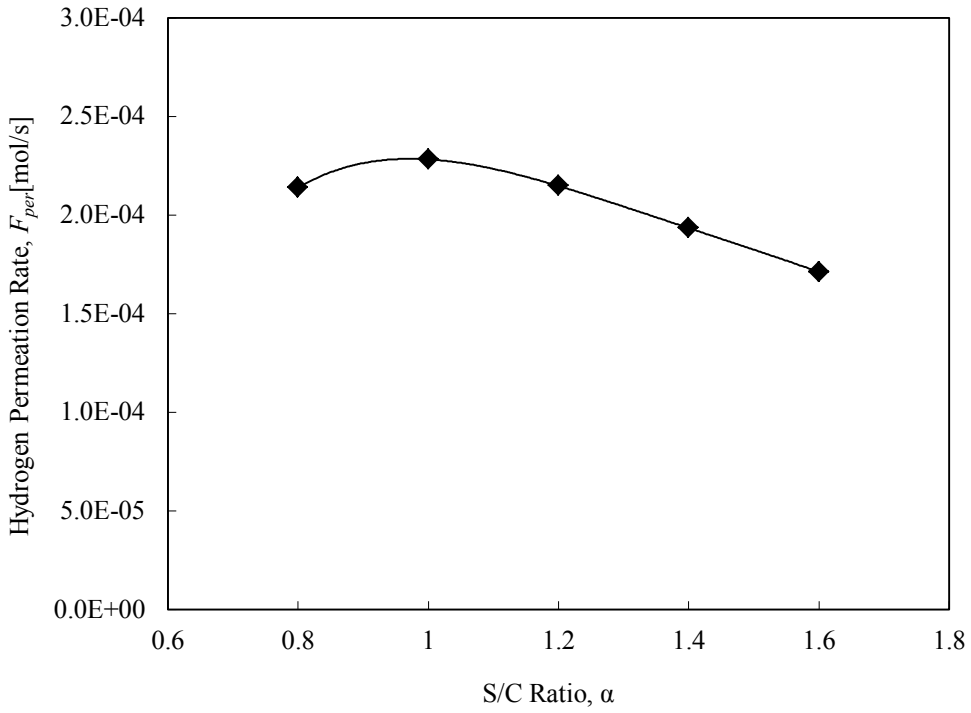

Fig. 2.11 Effect of S/C ratio on hydrogen permeation rate ($T_{mem(ref)}$: 583K, P_0: 0.40 MPa, F_{reac}: 2.8×10^{-4} mol/s)

Table 2.4 CO concentration at different S/C ratios

S/C ratio, α	0.8	1	1.2	1.4	1.6
CO concentration [ppm]	0.15	0.18	0.33	0.14	0.20

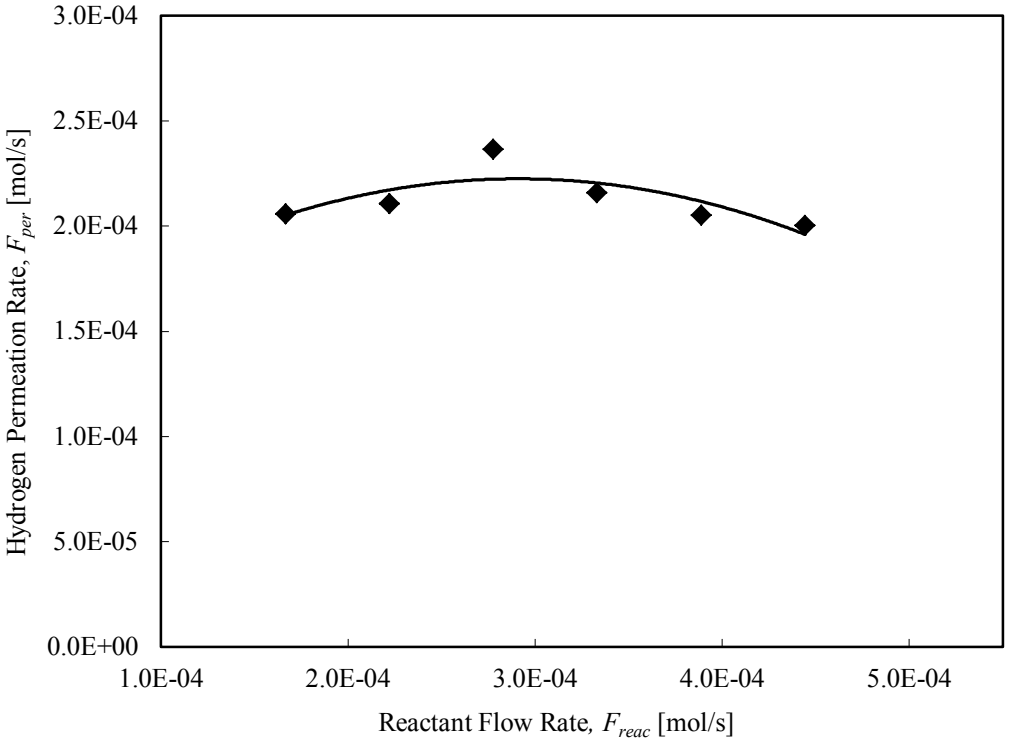

Fig. 2.12 Effect of reactant flow rate on hydrogen permeation rate ($T_{mem(ref)}$: 583K, P_0: 0.40 MPa, α: 1)

Table 2.5 CO concentration at different reactant flow rates

Reactant Flow Rate, F_{reac} [$\times 10^{-4}$ mol/s]	1.7	2.2	2.8	3.3	3.9	4.4
CO concentration [ppm]	0.00	0.08	0.05	0.08	0.06	0.05

2.3.3 Example of System of Compact Methanol Steam Reformer with PEFC

In our research, the compact reformer that we proposed is for small electrical device application, with the power output of around 35W. In this case, when 50% efficiency is assumed for a fuel cell (Su, 2009), the required hydrogen production rate for the power output of 35W is calculated to be around 0.90 mol/h (2.5×10^{-4}mol/s). Here, 0.90 mol/h (2.5×10^{-4}mol/s) is the maximum hydrogen permeation rate which is obtained when the compact reformer operates under reference membrane temperature ($T_{mem(ref)}$) of 583K, upstream pressure (P_0) of 0.50MPa, steam to methanol ratio (α) of 1 and methanol flow rate(F_{reac}) of 1mol/h.

Let say we have a system of a compact reformer in connection with Polymer Electrolyte Fuel Cell (PEFC) with the efficiency of 50% (Su, 2009) as shown below.

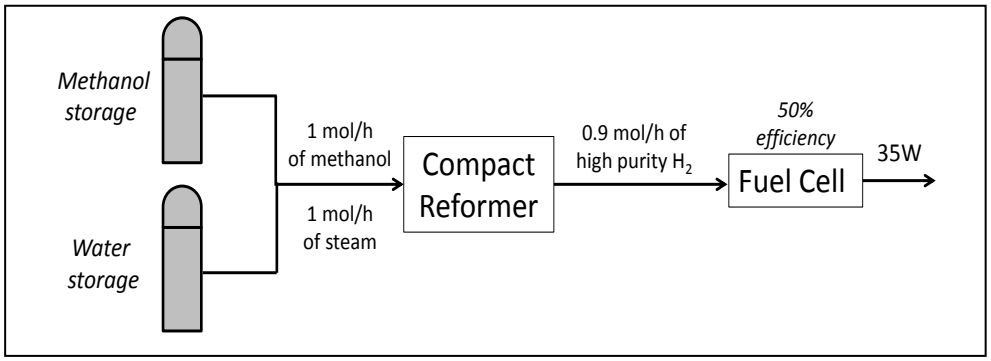

Fig. 2.13 Compact reformer in connection with PEFC

The size of the system depends on the purpose. Based on Fig. 2.13, it can be said that the size of methanol and water storage plays an important role to ensure the portability of the system. In this case, the size of storage is supposed to be as small as possible. Table 2.6 shows the various sizes of storage and the respective time available to use the system, based on the condition as shown in Fig. 2.13. Here, the properties of methanol and water that are used for the calculations are shown in Table 2.7.

Table 2.6 Size of storage and time available to use the system

	Storage Size [ml]	Mass Content [kg]	Time Available [hr] -limited by methanol storage
Methanol	**250**	0.20	~6
Water		0.25	
Methanol	**500**	0.40	~12
Water		0.50	
Methanol	**1000**	0.79	~24
Water		1.00	

Table 2.7 Properties of methanol and water

	Molar mass [g/mol]	Density [kg/m^3]
Methanol (CH_3OH)	32	791.8
Water (H_2O)	18	1000

Based on Table 2.6, when a bigger storage is used in the system, the time available to use the system becomes longer. It can be said that even the storage with the smallest size of 250ml is used, the available time to use the system is still reasonable (~6 hours). However, as mentioned previously, the size of the storage strongly depends on the purpose. For instance, if the user wants to use the system to run a laptop computer continuously for more than 1 day, then the storage of methanol should be bigger than 1000ml. But, it is important to note that it is desirable the storage with smaller size is used in the system, because the portability of the system is more possible. In this case, the fuel top-up is more preferable than to increase the size of fuel storage.

2.3.4 Estimation of Hydrogen Permeation Rate

The hydrogen permeation rate under various pressures at the upstream side is estimated by Eq. (2.9). The estimated values are compared with experimental data.

2.3.4.1 Dependence on Pressure

Figure 2.14 shows the results of estimation for the hydrogen permeation rate under various (a) pressures at the upstream side and (b) differences in square root of the hydrogen partial pressures, along with the experimental data. Here, $P_{H_2,1(ref)}$ is the reference partial pressure of hydrogen at the upstream side, which is equal to $P_{H_2,in}$. The values for hydrogen permeance coefficient (q) are estimated from Fig. 2.3, as 2.0×10^{-8}

mol.m^{-1}.s^{-1}.Pa$^{-0.5}$ and 1.4×10^{-8} mol.m^{-1}.s^{-1}.Pa$^{-0.5}$.

The figure shows that when the total pressure at the upstream side (P_1) is increased, the corresponding difference in square root of hydrogen partial pressures ($\sqrt{P_{H_2,1(ref)}} - \sqrt{P_{H_2,2}}$) also increases due to the almost constant inlet hydrogen concentration and the constant atmospheric pressure of $P_{H_2,2}$. As a result, the estimated hydrogen permeation rate increases, as well as experimental result. Figure 2.14(b) shows that the permeation rate estimated by the Eq.(2.9) increases linearly with an increase in difference of the square root of hydrogen partial pressures, whereas the experimental result shows that the increase rate of the permeation rate gradually decreases. In this case, a more fundamental study is necessary to make clear the reason why such significant difference between the prediction by Sieverts' equation and experimental result occurs. This fundamental study is further discussed in Chapter 3.

2.3.5 Membrane Surface Variation During Permeation

For further discussion, we observed the surface topography of the purification membrane by a Scanning Electron Microscope (SEM). Figure 2.15 shows SEM images of an unused membrane and a used membrane. Figure 2.15(a) shows that the unused membrane has a smooth surface while Fig. 2.15(b) shows that the used membrane has a rough surface and uneven distribution of the black and white area, which probably causes a non-uniform permeation to occur at the surface.

The changes in the physical characteristics of the membrane surface after the permeation as shown by the figure are supposed to be due to the blockage or adsorption of non-H_2 species on the surface, which decreases the hydrogen permeation.

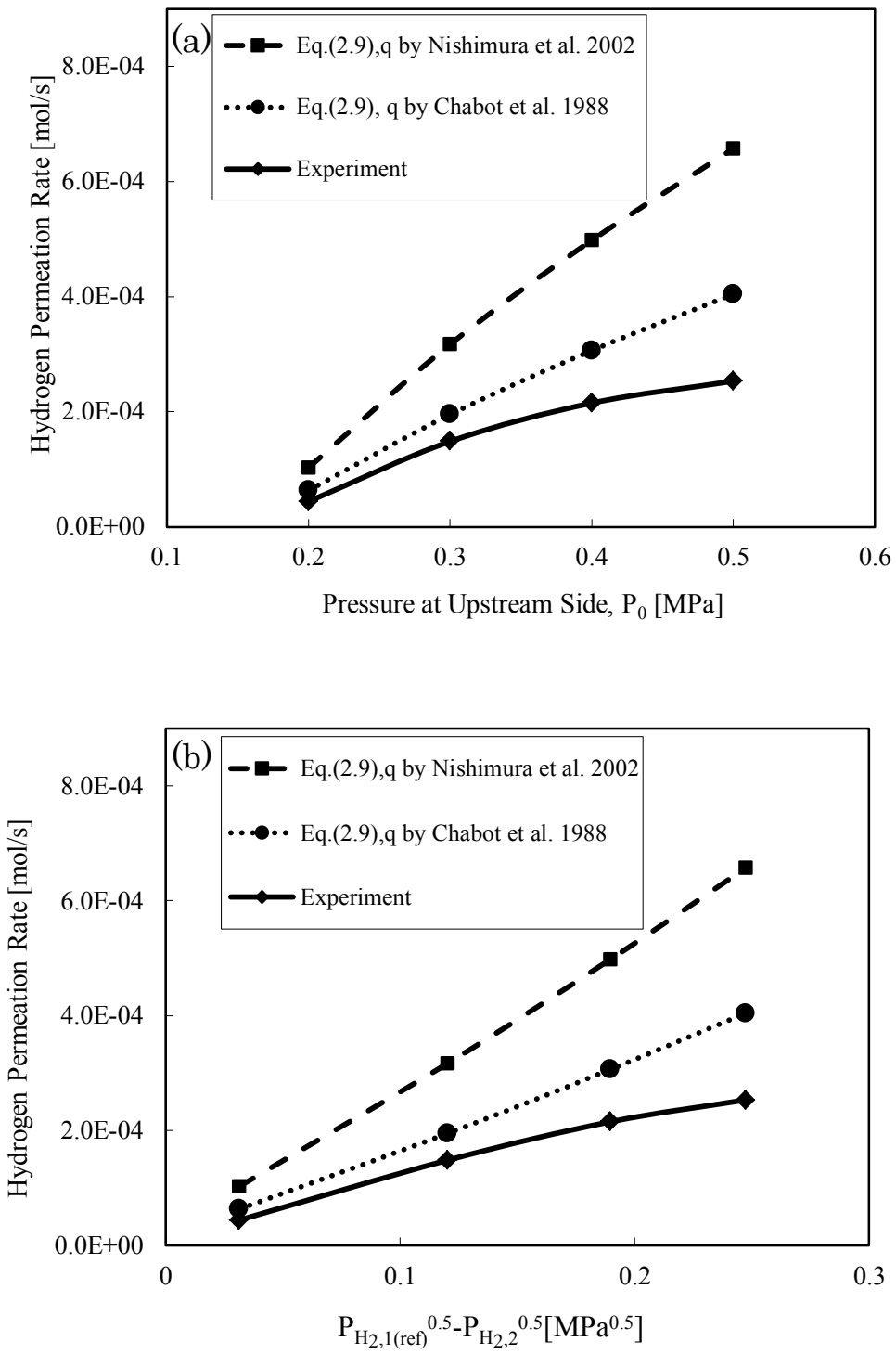

Fig. 2.14 Effect of (a) pressure at upstream side and (b) difference in square root of hydrogen partial pressures on hydrogen permeation rate, based on experiment and estimation ($T_{mem(ref)}$: 583K, α: 1, F_{reac}: 2.8×10^{-4} mol/s)

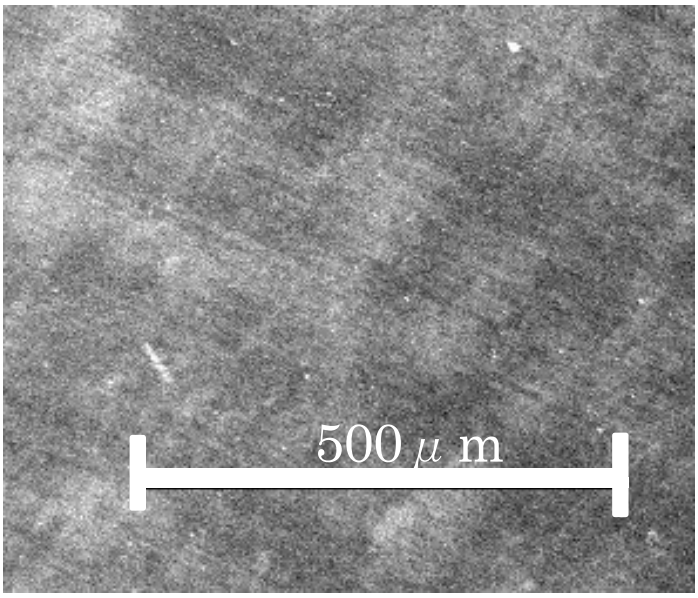

(a) unused membrane

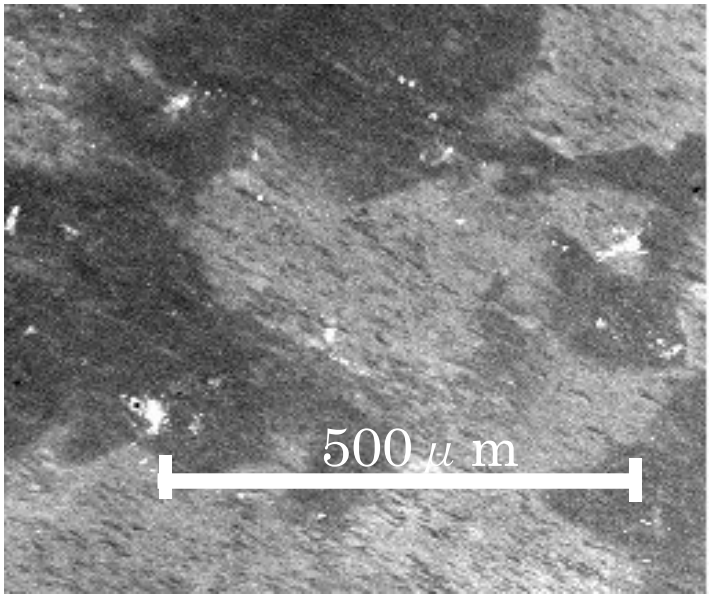

(b) used membrane

Fig. 2.15 The SEM images of (a) unused membrane and (b) used membrane

2.4 Conclusions

The performance of a compact methanol steam reformer using catalyst $CuO/ZnO/Al_2O_3$ for methanol steam reforming reaction and a Pd/Ag membrane for hydrogen purification was studied experimentally. The mole fraction of reformed hydrogen under various reference catalyst zone temperatures, pressures at the upstream side, S/C ratios and reactant flow rates is almost constant at 0.75, which corresponds to the mole fraction of H_2 estimated by the overall steam reforming reaction formula.

The higher hydrogen permeation rate is attained when we use the higher reference membrane temperature and higher pressure. For the S/C ratio, we obtain the maximum permeation rate when the ratio is around 1 because the hydrogen partial pressure at the upstream side becomes highest when no excessive reactant at the upstream side exists. For the reactant flow rate, the permeation rate is maximum at a certain value where the hydrogen concentration at the membrane surface becomes highest due to the maximum effect of high flow velocity towards the membrane. The significant difference between the prediction by Sieverts' equation and experimental H_2 permeation rate demonstrates that the prediction method is not going well in this case. Therefore, a more fundamental study is necessary to make clear the reason why such significant difference occurs.

Chapter 3

Experimental Investigation on the Hydrogen Permeation with Flat Sheet Pd/Ag Membrane

3.1 Introduction

Recent studies have revealed that for the case of hydrogen mixture with high fraction of H_2 feed rate that permeates membrane (high H_2 permeation ratio), the well-known Sieverts' equation alone still could not estimate the hydrogen permeation flux accurately even though only non-inhibiting gases were used in the hydrogen mixture. Several researchers (Caravella *et al.* 2009, Catalano *et al.* 2009, Chen *et al.* 2011, Chen *et al.* 2012) have revealed that not only feed concentration of mixture, but feed flow rate also becomes an important parameter in such condition which could affect the permeation characteristics for tubular type membrane.

Based on previous studies, the permeation characteristics for flat sheet Pd/Ag membrane was less explored, unlike that for the long tubular type membrane (Zhang *et al.* 2006, Caravella *et al.* 2009, Catalano *et al.* 2009, Chen *et al.* 2011, Chen *et al.* 2012). As mentioned in Chapter 2, the H_2 permeation rate for compact methanol steam reformer is much lower than the prediction by Sieverts' equation. Then, in this chapter, a more fundamental study on H_2 permeation for flat sheet Pd/Ag membrane was performed experimentally. Differ from the experimental study in Chapter 2, the study in this chapter used the unsupported membrane with stagnating flow at the upstream side of the membrane surface, to study the effect of feed flow rate without considering any possible influence from metal support. In addition, the non-inhibiting N_2 was used in binary hydrogen mixture to neglect any adsorption effect of non-H_2 species. The experimental results were then compared with prediction by the Sieverts' equation.

3.2 Experimental Methods and Procedures

An experimental setup for the hydrogen permeation test is shown in Fig. 3.1. Hydrogen/Nitrogen mixture was used because nitrogen is a non-inhibiting inert gas (Barbieri *et al.* 2008). For the purification process, a flat sheet, dense 77wt.% Pd/23wt.% Ag membrane with a thickness of 25μm, diameter of 0.02m and effective surface area of 3.14×10^{-4} m^2 was set inside the test module. Meanwhile, the position of K-type thermocouple (sheath diameter 1.6mm) for measurement of the reference membrane temperature ($T_{mem(ref)}$) was set at 10mm above the membrane at downstream side along centerline. The heating was performed by a ribbon heater, which covers the entire body of the module. Then, the whole covered module body was insulated to prevent heat loss. The leakage check was conducted by Swagelok liquid leak detector before and after the experiment for safety and to confirm no leakage occurs. In addition, we confirmed that no permeation of nitrogen occurs through the membrane.

Initially, the experimental module was purged by nitrogen and then, the module was heated by the ribbon heater. Once the reference temperature reached the desired temperature, the mixture of hydrogen and nitrogen was supplied to the module through the inlet which was set at 3.2mm atop the membrane surface at the upstream side. The flow rate of each gas was controlled by mass flow controllers (Horiba STEC, model: SEC-E40 MK3 300sccm for H_2, and 100 sccm for N_2). The total pressure of the gas mixture at the upstream side was controlled by a needle valve when hydrogen started to permeate the membrane. In this case, the permeated (downstream) pressure was atmospheric pressure. The flow rate of purified gas was measured by a soap-film flow meter (GL Sciences 50ml) once the reading of the flow rate became stable.

In this study, the effect of the feed flow rate of H_2/N_2 mixture on the hydrogen permeation rate was investigated experimentally as a function of reference membrane temperatures ($T_{mem(ref)}$), total pressures at the upstream side (P_0) and inlet H_2 mole fractions ($X_{H2,in}$). Meanwhile, the results of the experiments with pure hydrogen were used to obtain the value of the hydrogen permeance coefficient.

3.2.1 Experimental Conditions for Pure Hydrogen

The hydrogen permeation rate was measured as a function of the feed flow rate for the case of pure hydrogen to determine the hydrogen permeance coefficient of the purification membrane. The experimental conditions are presented in Tables 3.1 and 3.2.

Table 3.1 Dependence of permeation on hydrogen feed flow rate

No. of series	**1**
Reference membrane temperature, $T_{mem(ref)}$ [K]	523
Total pressure, P_0 [MPa]	0.20
Inlet hydrogen flow rate, F_{in,H_2} [mol/s]	$6.69\text{x}10^{-5}$~$2.23\text{x}10^{-4}$

Table 3.2 Permeation test

No. of Series	**1**	**2**	**3**
Reference membrane temperature, $T_{mem(ref)}$ [K]	523	623	723
Total pressure, P_0 [MPa]	0.20-0.30		
Inlet hydrogen flow rate, F_{in,H_2} [mol/s]	$2.23\text{x}10^{-4}$		

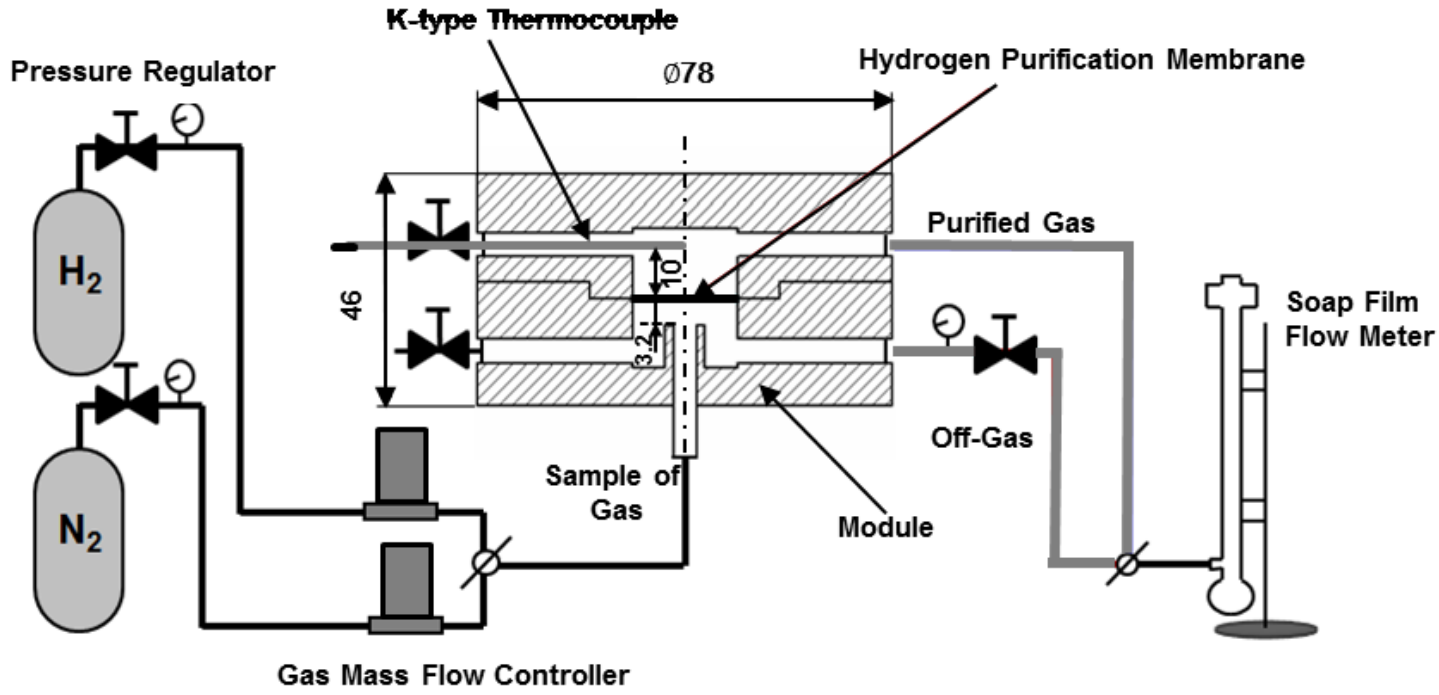

Fig. 3.1 Experimental Setup

3.2.2 Experimental Conditions for Hydrogen Mixture

3.2.2.1 Reference Condition (Effect of Feed Flow Rate)

The experiments were conducted under various conditions, as shown in Tables 3.3 and 3.4. For the cases with various pressures and temperatures, the inlet hydrogen mole fraction was set to 0.75 ($X_{H_2,in} : X_{N_2,in}$=0.75:0.25). This mole fraction was selected based on the overall methanol steam reforming reaction model, as demonstrated in Chapter 2.

Meanwhile, for the cases with various inlet H_2 mole fractions, the pressure and temperature were set constant at 0.25MPa and 623K, respectively. For all cases, the downstream side was at atmospheric pressure.

Table 3.3 Experimental conditions for various pressures and temperatures

No. of Series	1	2	3
Upstream pressure, P_0 [MPa]	0.20	0.25	0.30
Reference membrane temperature, $T_{mem(ref)}$ [K]	623	523-723	623
Feed flow rate, F_{in} [mol/s]	$1.5\text{x}10^{-5}$~$2.98\text{x}10^{-4}$		

Table 3.4 Experimental conditions for various inlet H_2 mole fractions

(P_0 :0.25MPa, $T_{mem(ref)}$:623K)

No. of Series	1	2	3
Inlet H_2 mole fraction, $X_{H2,in}$	0.70	0.75	0.80
Feed flow rate, F_{in} [mol/s]	$2.78\text{x}10^{-5}$~$1.94\text{x}10^{-4}$	$2.78\text{x}10^{-5}$~$2.50\text{x}10^{-4}$	

3.3 Theoretical Background

In this section, the Sieverts' equation is reconsidered to estimate H_2 permeation mole flux.

The hydrogen permeation mole flux through a dense Pd-based membrane can be estimated by Sieverts' law, which is quantified with Fick's First law as shown in Eq. (3.1)(Uemiya *et al.* 1991):

$$f = \frac{q}{d}\left(\sqrt{P_{H_2,1}} - \sqrt{P_{H_2,2}}\right) \tag{3.1}$$

where f is the hydrogen permeation mole flux, q is the hydrogen permeance coefficient, d is the membrane thickness, $P_{H_2,1}$ is the hydrogen partial pressure at the membrane surface of upstream side and $P_{H_2,2}$ is the hydrogen partial pressure at the membrane surface of downstream side.

Figure 3.2 shows the hydrogen partial pressure profile near the membrane surface of the upstream side. Here, P_{in} is total pressure at the inlet, P_0 is total pressure at the upstream side, P_1 is total pressure at the membrane surface of upstream side, $P_{H_2,in}$ is the hydrogen partial pressure at the inlet, f_{mean} is the mean mole flux (feed flow rate per effective membrane surface area) and f_{mean,H_2} is the mean hydrogen mole flux. As shown in Fig. 3.2, Line 1 represents the hydrogen partial pressure profile when the decrease in the H_2 concentration toward the membrane is not taken into account. In this case, the H_2 partial pressure at the membrane surface as represented by Point A is assumed to be the same as that far from the membrane surface. Therefore, $P_{H_2,1}$ can be estimated by Eq. (3.2) as follows,

$$P_{H_2,1} = P_{H_2,in} = \frac{f_{mean,H_2}}{f_{mean}} P_{in} \tag{3.2}$$

where $f_{mean,H_2} = X_{H_2,in} \times f_{mean}$. By substituting $P_{H_2,1}$ in Eq. (3.1) with Eq. (3.2), the following Eqs. (3.3) is obtained. .

$$f = \frac{q}{d}\left(\sqrt{\frac{f_{mean,H_2}}{f_{mean}} P_{in}} - \sqrt{P_{H_2,2}}\right) \tag{3.3}$$

Equation (3.3) then is used to estimate H_2 permeation mole flux for the reference conditions.

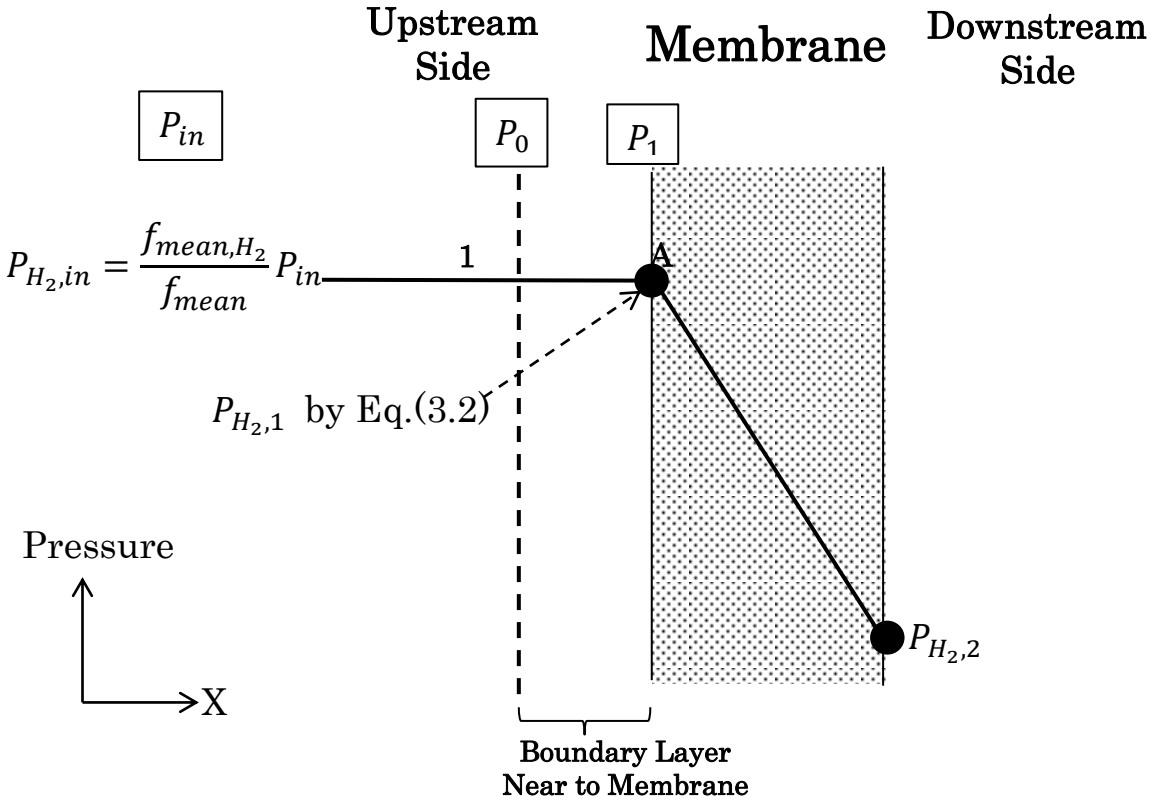

Fig. 3.2 Pressure profile of the permeation system

3.4 Results and Discussion

3.4.1 Pure Hydrogen Case

3.4.1.1 Permeation Characteristics for Pure Hydrogen

Figure 3.3 shows the permeation characteristics of a Pd/Ag membrane used in this study when the upstream side of the membrane was pressurized with pure hydrogen. These experiments were carried out at 523K, 623K and 723K. The figure shows that the H_2 flux was linear with respect to the difference in square root of hydrogen partial pressures between the upstream side and downstream side. This demonstrates that the purification membrane follows the Sieverts' law, which means that the H_2 flux was controlled by diffusion of H atom across the membrane.

Figure 3.4 shows the effect of the feed flow rate on the H_2 permeation rate through a Pd/Ag membrane for the case of pure H_2. The figure shows that the permeation rate does not depend on the feed flow rate, and thus demonstrates that the hydrogen permeance coefficient is not affected by the feed flow rate. The minimum inlet H_2 flow rate that was set for the experiment was about 6.694×10^{-5} mol/s (~0.241 mol/h) to ensure the pressure at the upstream side could be sustained. In Fig. 3.4, the dotted line shows the condition of H_2 permeation rate is equal to the inlet H_2 flow rate. Thus, the area where F_{in,H_2} is equal or lower than that of the dotted line cannot be realized.

3.4.1.2 Permeance Coefficient

Figure 3.5 shows the hydrogen permeance coefficient for Pd based membranes as a function of a reciprocal temperatures. It was found that the permeance coefficient for the membrane of the present study was relatively higher in comparison to that for other membranes. However, similar trend was obtained with other membranes, in that the coefficient of the membranes increases with an increase in temperature and gradually becomes flat with further increase in temperature.

The values of the hydrogen permeance coefficient (q) used for the estimation for case of H_2 mixture with various inlet H_2 partial pressures are presented in Table 3.5. In addition, the values used for the estimation for case of H_2 mixture with various inlet H_2 mole

fractions are presented in Table 3.6. For the latter case, other piece of flat sheet Pd/Ag membrane with the same thickness was used, in which it has been confirmed to follow Sieverts' Law.

All the values of the coefficient were determined by substituting Eq.(3.1) with the experimental data in the present study.

Table 3.5 Values of hydrogen permeance coefficient for the case of H_2 mixture with various inlet H_2 partial pressures

Total Pressure, P_0 [MPa]	Reference Membrane Temperature, $T_{mem(ref)}$ [K]	Hydrogen Permeance Coefficient, q [molm^{-1}s^{-1}Pa$^{-1/2}$]
0.20	623	3.9x10^{-8}
0.25	523	2.8x10^{-8}
	623	3.8x10^{-8}
	723	4.0x10^{-8}
0.30	623	3.6x10^{-8}

Table 3.6 Values of hydrogen permeance coefficient for the case of H_2 mixture with various inlet H_2 mole fractions

Inlet H_2 mole fraction, $X_{H_2,in}$	Hydrogen Permeance Coefficient, q [molm^{-1}s^{-1}Pa$^{-1/2}$]
0.70	4.0x10^{-8}
0.75	4.3x10^{-8}
0.80	4.3x10^{-8}

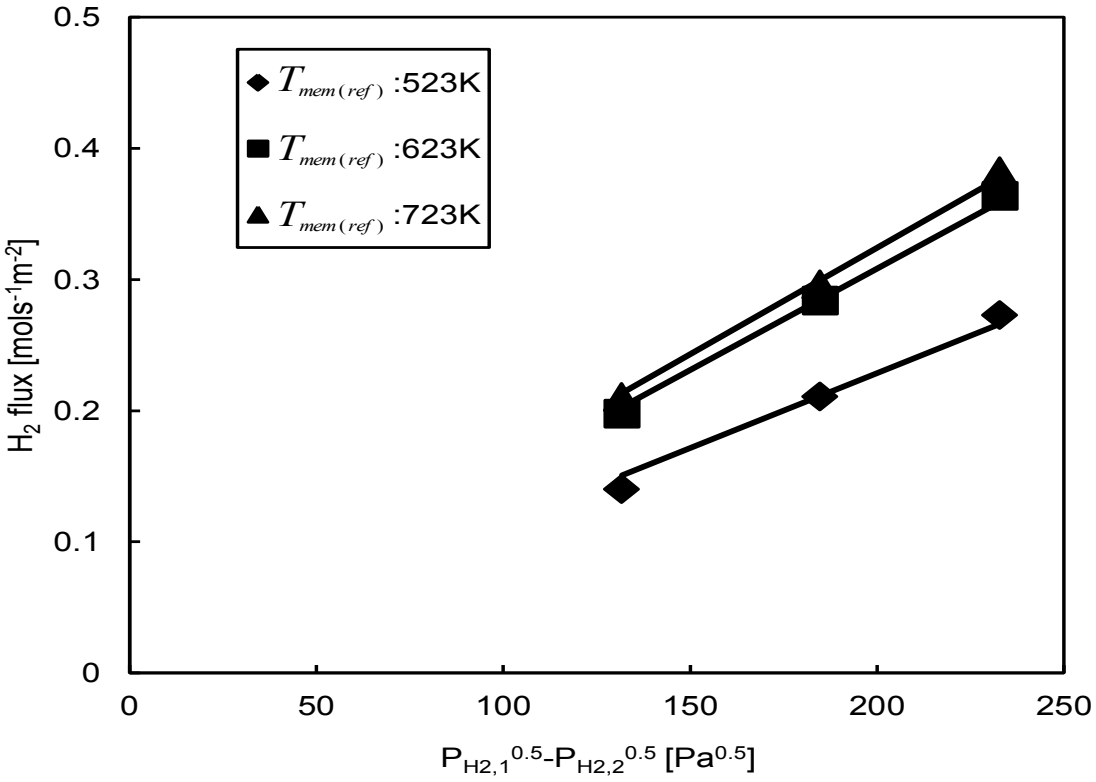

Fig. 3.3 Pure H_2 permeation characteristics of Pd/Ag membrane

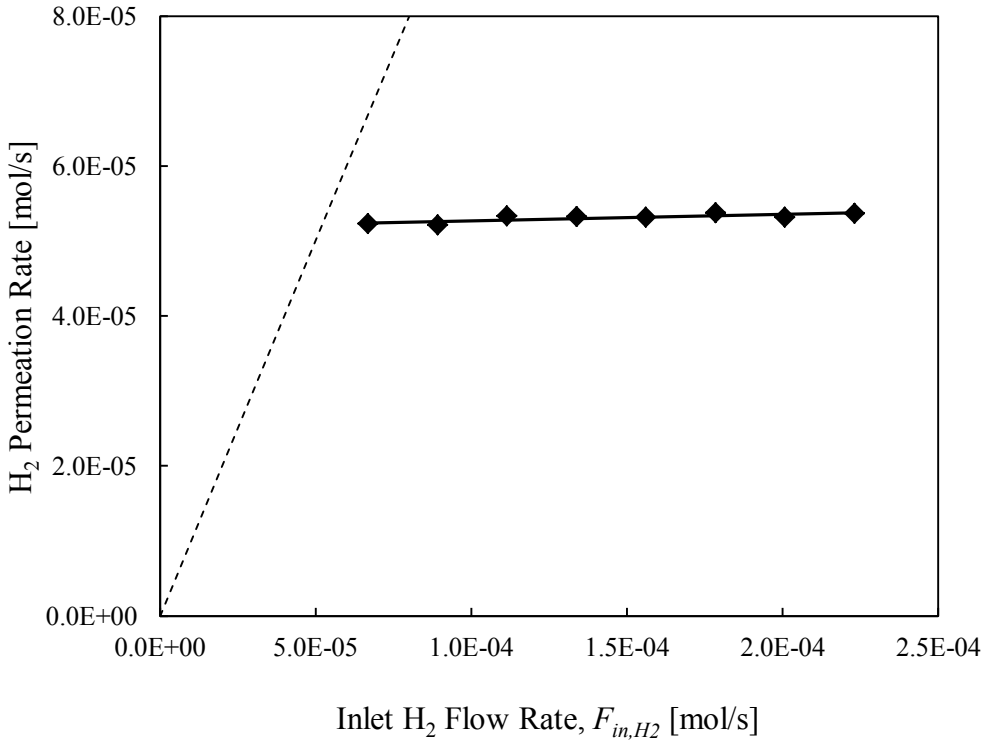

Fig. 3.4 Effect of inlet H_2 flow rate on H_2 permeation rate for pure H_2 ($T_{mem(ref)}$:523K, P_0:0.20MPa)

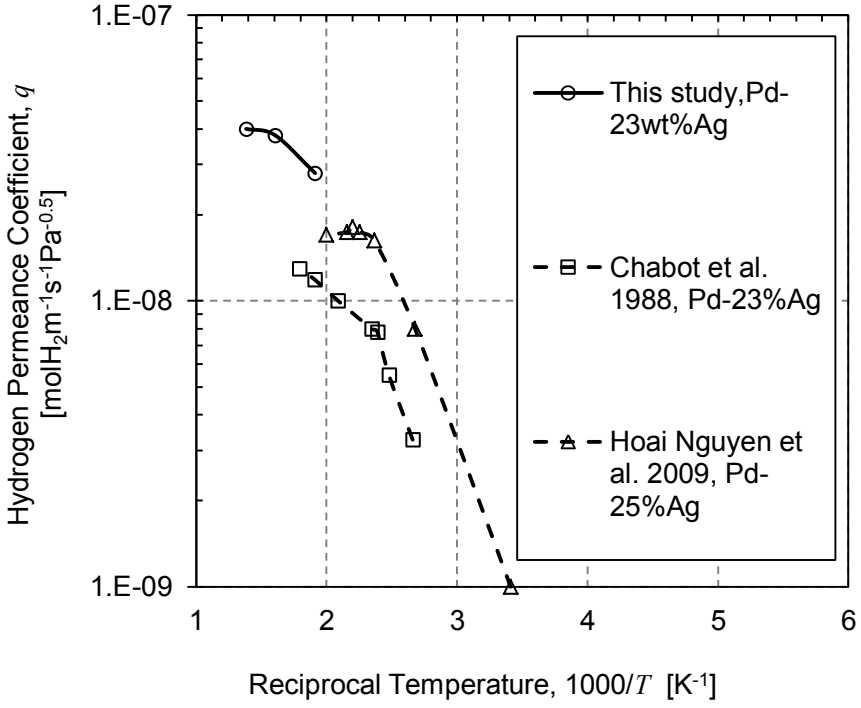

Fig. 3.5 Hydrogen permeance coefficient(q) for Pd based membranes

3.4.2 Hydrogen Mixture Case

3.4.2.1 Dependence on Feed Flow Rate

Figure 3.6 shows the effect of the feed flow rate on the H_2 permeation rate, for different reference membrane temperatures. The figure shows that the H_2 permeation rate increases with an increase in the feed flow rate. This is supposed due to the increase in flow velocity towards the membrane surface of the upstream side, which causes the increase in hydrogen concentration at the membrane surface of upstream side. Due to the increase in hydrogen concentration, the hydrogen partial pressure at the membrane surface also increases when the feed flow rate is increased. In addition, it was a reasonable result that the H_2 permeation rate increases with an increase in reference membrane temperature, which corresponds to the increase in the hydrogen permeance coefficient, as shown in Fig. 3.5. Figure 3.6 shows that for most of the feed flow rates, the difference in the permeation rate between the case of $T_{mem(ref)}$ =523K and $T_{mem(ref)}$=623K is much larger than the difference between the case of $T_{mem(ref)}$= 623K and $T_{mem(ref)}$ =723K. These significant differences correspond to the trend of changes in the hydrogen permeance coefficient when the reference temperature was increased, as shown in Fig. 3.5.

Figure 3.7 shows the effect of the feed flow rate on the H_2 permeation rate, for different inlet hydrogen partial pressures at the upstream side. Similar to the observation by previous researchers for the case of tubular type membrane (Catalano *et al.* 2009), the permeation rate is higher for a higher feed flow rate. This is supposed to be due to the increase in the hydrogen partial pressure at the membrane surface of the upstream side when the feed flow rate is increased, as already mentioned above.

Figure 3.8 shows the effect of the feed flow rate on the H_2 permeation rate, for different inlet hydrogen mole fractions. The figure demonstrates that the permeation rate is higher for a higher feed flow rate, in which the reason has already been mentioned in the previous paragraph. The figure also shows that when the inlet H_2 mole fraction is increased, the H_2 permeation rate increases. This is supposed due to the increase in H_2 concentration at the membrane surface, that is H_2 partial pressure at the membrane surface when the inlet H_2 mole fraction is increased.

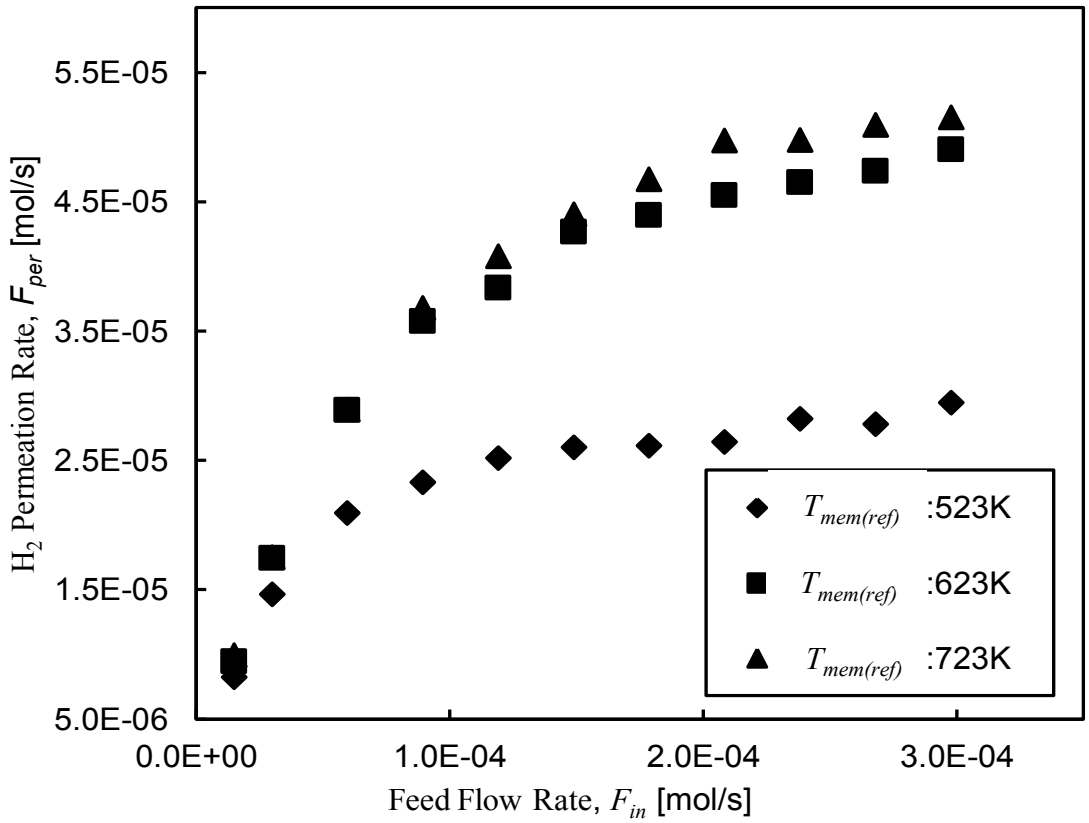

Fig. 3.6 Effect of feed flow rate on H_2 permeation rate, for different reference membrane temperatures ($P_{H_2,in}$: 0.19MPa, $P_{H_2,2}$: 0.10MPa)

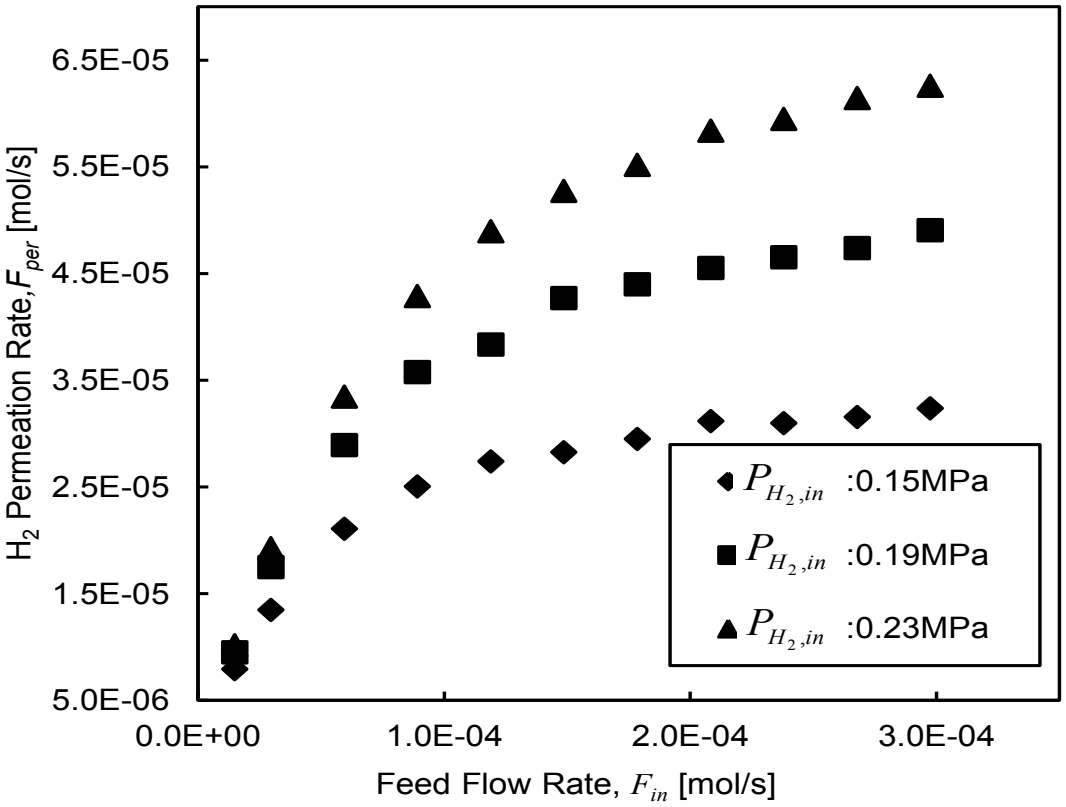

Fig. 3.7 Effect of feed flow rate on H_2 permeation rate, for different inlet hydrogen partial pressures ($T_{mem(ref)}$: 623K, $P_{H_2,2}$: 0.10MPa)

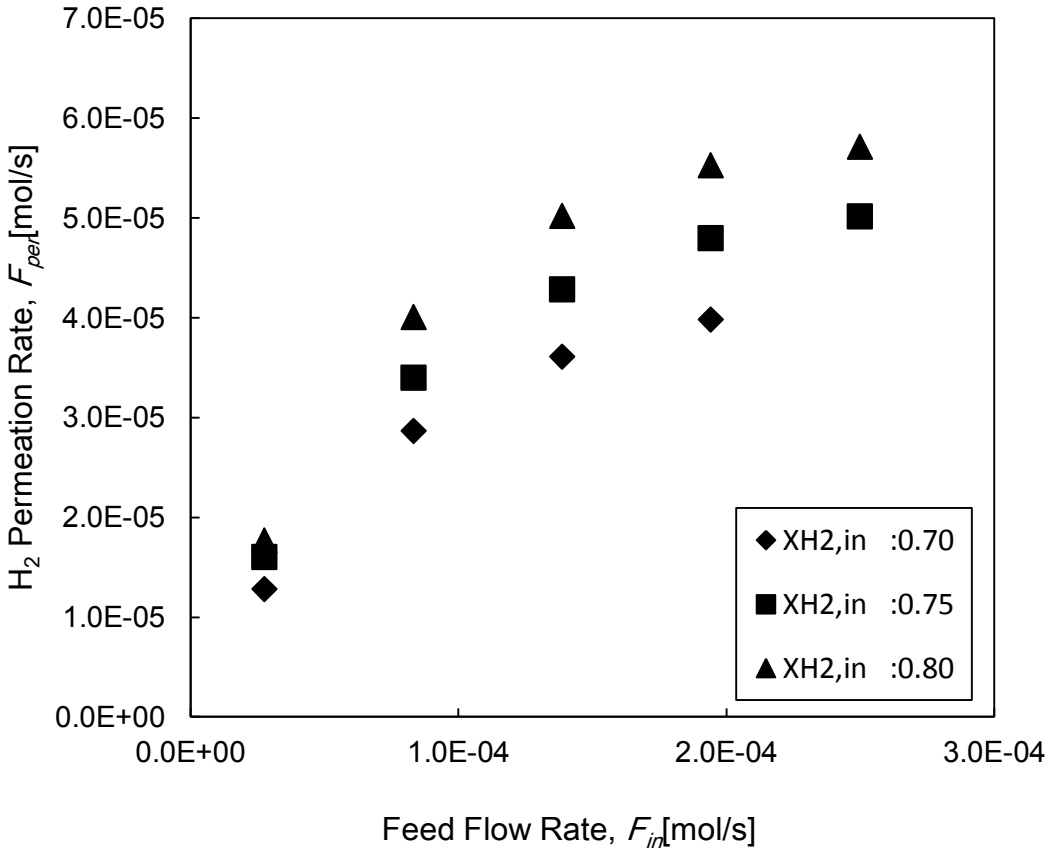

Fig. 3.8 Effect of feed flow rate on H_2 permeation rate, for different inlet hydrogen mole fractions ($T_{mem(ref)}$: 623K, $P_{H_2,in}$: 0.19MPa, $P_{H_2,2}$: 0.10MPa)

3.4.2.2 Comparison Between Estimation by Sieverts' Equation and Experimental Results

Figures 3.9(a)-(c) and 3.10(a)-(c) show the H_2 permeation mole flux as a function of mean mole flux. Here, the feed flow rate in the experiment was converted to mean mole flux, which represents the feed flow rate divided by the effective membrane surface area. In Figs. 3.9(a)-(c) and 3.10(a)-(c), the experimental result, estimation by Eq.(3.3) along with the limitation line of which H_2 permeation mole flux is equal to the mean H_2 mole flux, are presented.

Experimental results show that the H_2 permeation mole flux generally decreases with a decrease in the mean mole flux, and becomes very close to the limitation when the mean mole flux is very low. This trend cannot be estimated by Eq.(3.3) because Eq.(3.3) demonstrates constant H_2 permeation mole flux, independence from the mean mole flux by definition. Furthermore, the prediction by Sieverts' equation also gives the unrealistic results, once the estimated H_2 permeation mole flux exceeds the limitation line, which means the permeation mole flux becomes higher than the mean mole flux. Even when the inlet hydrogen partial pressure or inlet hydrogen mole fraction is changed, the same trend is obtained.

As shown by Figs 3.9(a)-(c) and 3.10(a)-(c), the experimental results are much lower than the estimation by the Sieverts' equation, that is Eq.(3.3). This elucidates that when $P_{H_2,in}$ is used in the Eq.(3.3), the $P_{H_2,1}$ is overestimated, thus the estimation gives much higher permeation mole flux in comparison to the permeation flux obtained from the experiment. On the other hand, when the mean mole flux is increased, the H_2 permeation mole flux becomes closer to the estimation by Eq.(3.3), thus demonstrates that $P_{H_2,1}$ approaching to $P_{H_2,in}$.

Thus, it is suggested that a new prediction method based on Sieverts' equation which considers the decrease in hydrogen concentration at the membrane surface, is necessary to estimate H_2 permeation rate for H_2 mixture. Corresponding to previous study (Catalano *et al.* 2009) for tubular type membrane, H_2 permeation flux itself is supposed to become an important parameter in this case. This will further discussed in Chapter 4.

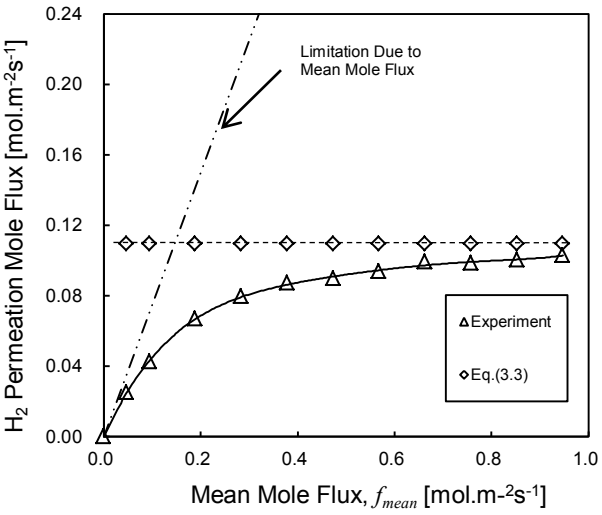

(a) $P_{H_2,in}$: 0.15MPa, $P_{H_2,2}$: 0.10MPa

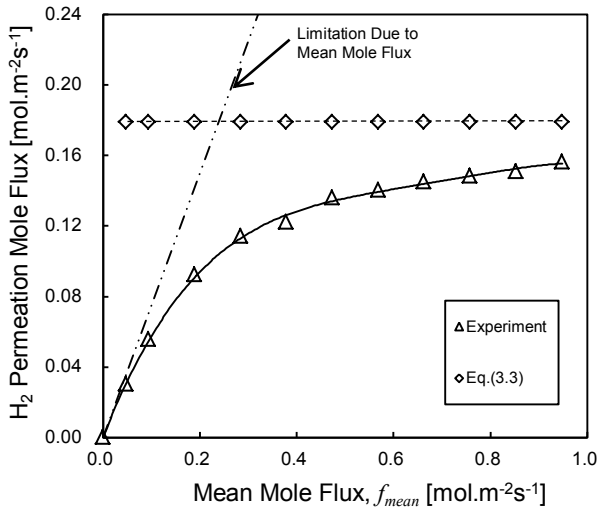

(b) $P_{H_2,in}$: 0.19MPa, $P_{H_2,2}$: 0.10MPa

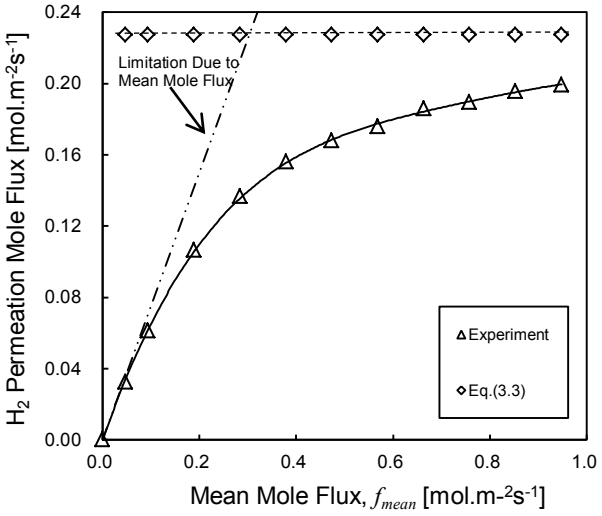

(c) $P_{H_2,in}$: 0.23MPa, $P_{H_2,2}$: 0.10MPa

Fig. 3.9 Effect of mean mole flux on H_2 permeation mole flux ($T_{mem(ref)}$: 623K)

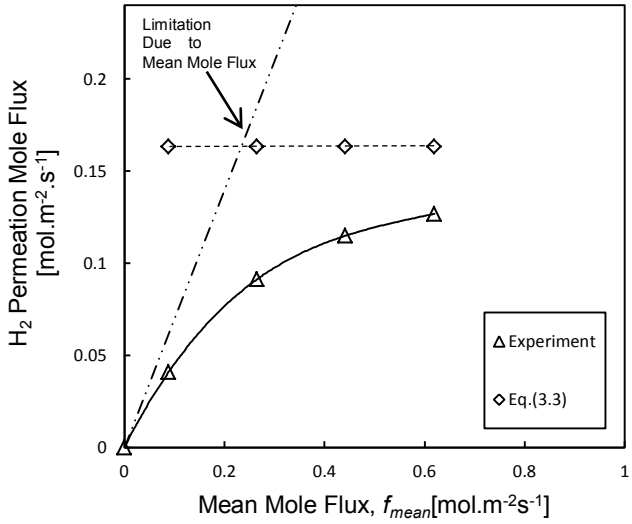

(a) $X_{H_2,in}$:0.70, $P_{H_2,in}$: 0.19MPa, $P_{H_2,2}$: 0.10MPa

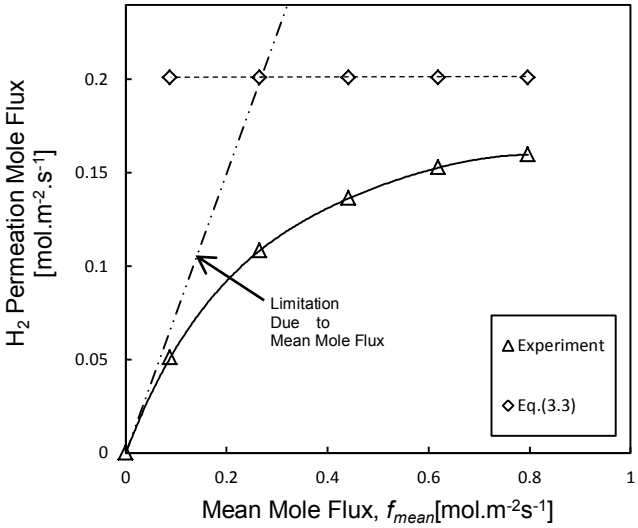

(b) $X_{H_2,in}$:0.75, $P_{H_2,in}$: 0.19MPa, $P_{H_2,2}$: 0.10MPa

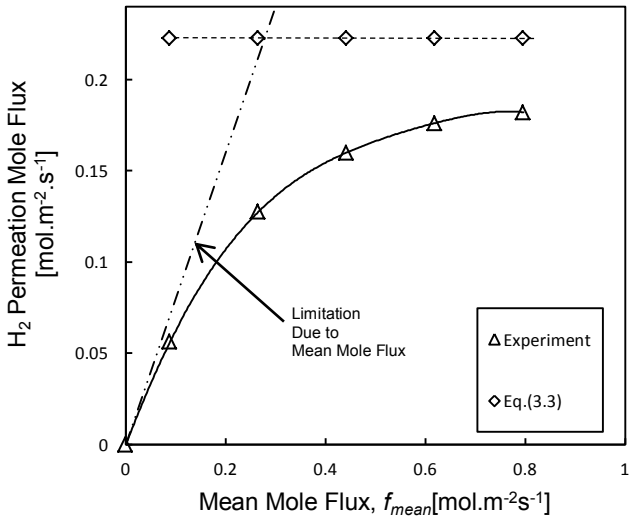

(c) $X_{H_2,in}$:0.80, $P_{H_2,in}$: 0.19MPa, $P_{H_2,2}$: 0.10MPa

Fig. 3.10 Effect of mean mole flux on H_2 permeation mole flux ($T_{mem(ref)}$: 623K)

3.5 Conclusion

In the present study, the effect of feed flow rate of hydrogen mixture on the hydrogen permeation for flat sheet Pd/Ag membrane was investigated experimentally.

The test for pure hydrogen demonstrates that the Pd/Ag membranes used in the present study follows the Sieverts' Law. In addition, it was found that the hydrogen permeance coefficient of the Pd/Ag membranes in this study is relatively higher in comparison to that in the other studies, but the trend of changes in the permeance coefficient with temperature is similar.

For the hydrogen mixture, the experimental results showed that the H_2 permeation rate decreases when the feed flow rate is decreased, regardless of temperatures, inlet H_2 partial pressures and inlet H_2 mole fractions. This trend cannot be estimated by the Sieverts' equation, thus elucidates that the hydrogen partial pressure at membrane surface is overestimated when the inlet hydrogen partial pressure is used in the equation. Then, the phenomenon of hydrogen concentration decrease at membrane surface is confirmed, which is supposed due to the effect of H_2 permeation itself.

Chapter 4

Theoretical Analysis on Hydrogen Permeation with Flat Sheet Pd/Ag Membrane for Hydrogen Mixture

4.1 Introduction

Recent studies have revealed that for the case of hydrogen mixture with high fraction of H_2 feed rate that permeates membrane (high H_2 permeation ratio), the well-known Sieverts' equation alone still could not estimate the hydrogen permeation flux accurately even though only non-inhibiting gases were used in the hydrogen mixture (Chen *et al.* 2008, Catalano *et al.* 2009, Chen *et al.* 2011). Catalano *et al.* (2009) reported that during this condition, H_2 permeation flux is one of the important factors that could affect the flow properties near the membrane surface of the upstream side. This reveals that the use of feed flow rate in the Sieverts' equation without considering the effect of H_2 flux could cause deviation from the actual H_2 permeation flux. Several researchers have studied the effect of feed flow rate on permeation characteristics in such condition for tubular type membrane, experimentally (Catalano *et al.* 2009, Zhang *et al.* 2006) and numerically (Zhang *et al.* 2006, Caravella *et al.* 2009, Chen *et al.* 2011, Chen *et al.* 2012). They have demonstrated the phenomena of concentration polarization, which could be clearly observed when a long tubular membrane was used.

To describe the permeation characteristics in such condition, Gaohong *et al.*(1999) asserted that a better correlation to describe the gas separation needs to be investigated, which can explain the effect of permeation itself clearly, while Mourgues and Sanchez (2005) concluded that the general relation for multiple parameters such as permeate flux, operating pressure and feed velocity is difficult to obtain because these parameters depend on each other. Several studies (Caravella *et al.* 2009, Catalano *et al.* 2009, Caravella *et al.* 2010) have been conducted to introduce new methods for estimating hydrogen permeation flux for the case of high H_2 permeation ratio. Catalano *et al.* (2009) used a mass transport coefficient to consider the major contribution of diffusion due to permeation. Semi-empirical equations were proposed to estimate the hydrogen permeation rate, in which some experimental data is necessary in order to use the equations. A polarization map has also been created by Caravella *et al.* (2009) as a useful tool to evaluate the concentration polarization manually once the inlet and outlet conditions are specified. In

another study (Caravella *et al.* 2010), a novel permeation reduction coefficient was introduced to consider the inhibition by CO and concentration polarization simultaneously. Even though many researchers (Gaohong *et al.* 1999, Mourgues and Sanchez 2005, Catalano *et al.* 2009, Chen *et al.* 2011) pointed out that the permeation flux (or permeation rate) plays a significant role in such condition in addition to the other parameters, it seems that the relation for multiple parameters including H_2 permeation flux has not been proposed yet.

As mentioned in Chapter 3, the actual H_2 permeation mole flux for H_2 mixture decreases with a decrease in mean mole flux, and this could not be predicted by Sieverts' equation. Then, in this chapter, such trend is discussed by using a proposed theoretical equation that takes into account the effect of H_2 permeation itself. The estimation of H_2 permeation mole flux by Sieverts' equation is quantitatively reconsidered by taking into account the hydrogen concentration decrease at the membrane surface of the upstream side due to permeation. The proposed analytical method is supposed to be practically useful for the permeation system with similar geometry, in which the similar geometry has been implemented for many applications (Arstad *et al.* 2006, Unemoto *et al.* 2007, S. Damle 2009).

4.2 Theoretical Background

In this section, the Sieverts' equation is reconsidered quantitatively to take into account the decrease in hydrogen concentration at the membrane surface due to permeation.

As mentioned in Chapter 3, the hydrogen permeation mole flux through a dense Pd-based membrane can be estimated by Sieverts' law, which is quantified with Fick's First law as shown in Eq. (4.1)(Uemiya *et al.* 1991):

$$f = \frac{q}{d}\left(\sqrt{P_{H_2,1}} - \sqrt{P_{H_2,2}}\right) \tag{4.1}$$

Figure 4.1 shows the hydrogen partial pressure profile near the membrane surface of the upstream side. Here, P_{in} is total pressure at the inlet, P_0 is total pressure at the upstream side, P_1 is total pressure at the membrane surface of upstream side, $P_{H_2,in}$ is the

hydrogen partial pressure at the inlet, f_{mean} is the mean mole flux (feed flow rate per effective membrane surface area) and f_{mean,H_2} is the mean hydrogen mole flux. As described in Chapter 3, Line 1 in Fig. 4.1 represents the hydrogen partial pressure profile when the decrease in the H_2 concentration toward the membrane is not taken into account. In this case, $P_{H_2,1}$ can be estimated by Eq. (4.2) as follows,

$$P_{H_2,1} = P_{H_2,in} = \frac{f_{mean,H_2}}{f_{mean}} P_{in} \tag{4.2}$$

which is same with Eq.(3.2) in Chapter 3. In this case, $f_{mean,H_2} = X_{H_2,in} \times f_{mean}$. In the case of pure hydrogen, no hydrogen concentration decrease occurs and Eq. (4.2) can be used to estimate the hydrogen permeation mole flux accurately.

However, for the case of hydrogen mixture, the hydrogen partial pressure varies as represented by Line 2 schematically and the hydrogen permeation mole flux is overestimated when Eq. (4.2) is used. In our study, Eq. (4.2) is extended to take into account the decrease in hydrogen concentration at the membrane surface due to permeation, as represented by Point B. In this case, $P_{H_2,1}$ can be estimated by Eq. (4.3) as follows,

$$P_{H_2,1} = \frac{f_{mean,H_2} - f}{f_{mean} - f} P_{in} \tag{4.3}$$

where $P_{in} = P_0 = P_1$. By substituting $P_{H_2,1}$ in Eq. (4.1) with Eqs. (4.2) and (4.3), the following Eqs. (4.4) and (4.5) are obtained. .

$$f = \frac{q}{d}\left(\sqrt{\frac{f_{mean,H_2}}{f_{mean}} P_{in}} - \sqrt{P_{H_2,2}}\right) \tag{4.4}$$

which is same with Eq.(3.3) in Chapter 3, and

$$f = \frac{q}{d}\left(\sqrt{\frac{f_{mean,H_2} - f}{f_{mean} - f} P_{in}} - \sqrt{P_{H_2,2}}\right) \tag{4.5}$$

In this case, $\frac{f_{mean,H_2} - f}{f_{mean} - f}$ in Eq. (4.5) represents H_2 mole fraction at the membrane surface of the upstream side with consideration of the decrease in hydrogen concentration due to permeation.

Equation (4.5) is then rewritten as follows,

$$0 = f^3 + f^2\left(2\frac{q}{d}\sqrt{P_{H_2,2}} - f_{mean}\right) + f\left(\frac{q^2}{d^2}P_{H_2,2} - \frac{q^2}{d^2}P_{in} - 2\frac{q}{d}f_{mean}\sqrt{P_{H_2,2}}\right) + \left(-\frac{q^2}{d^2}f_{mean}P_{H_2,2} + \frac{q^2}{d^2}f_{mean,H_2}P_{in}\right) \quad (4.6)$$

Equation (4.6) is solved using Newton-Raphson method (S. Rao 2002). As shown in Eq. (4.6), f can be obtained when the boundary conditions are determined.

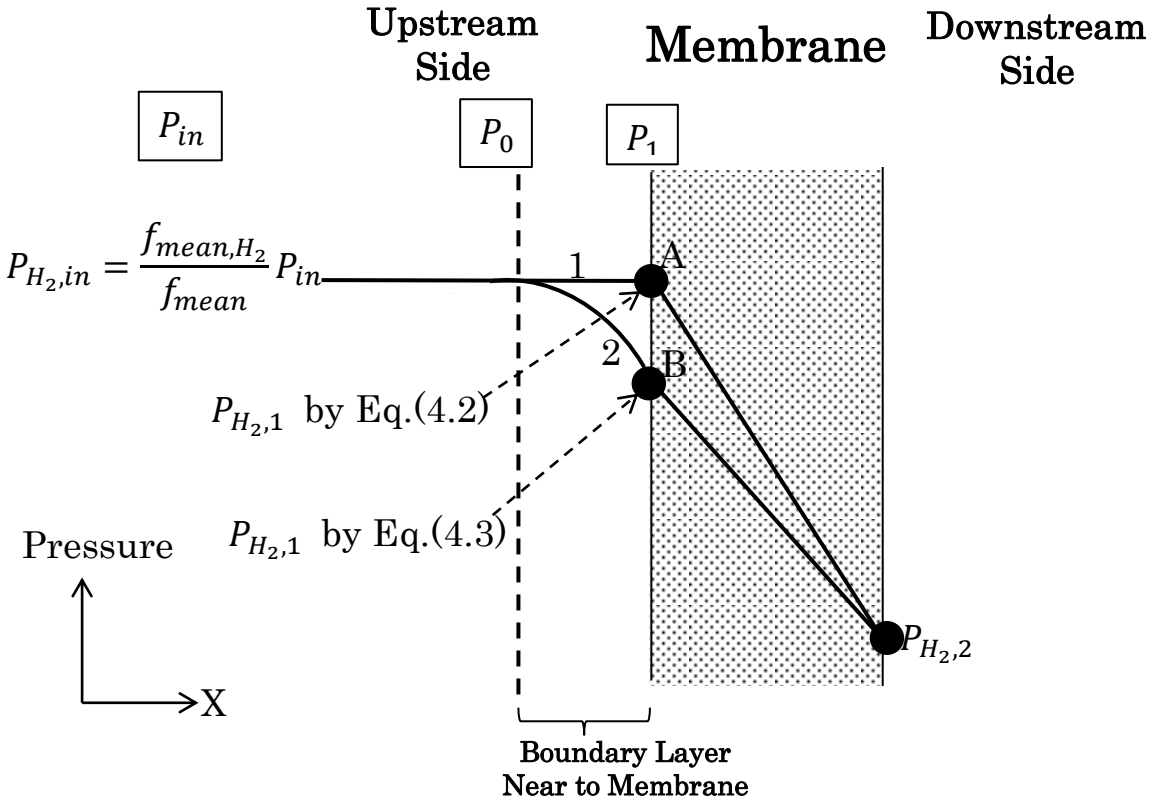

Fig. 4.1 Pressure profile of the permeation system

4.3 Results and Discussion

4.3.1 Comparison Between Estimation by Theoretical Equation and Experimental Results

In this section, the experimental result for the case of H_2 mixture with various inlet H_2 partial pressures and various inlet H_2 mole fractions in Chapter 3 is used for comparison with H_2 permeation mole flux estimated by the proposed theoretical equation.

Figures 4.2(a)-(c) and 4.3(a)-(c) show the H_2 permeation mole flux as a function of mean mole flux for H_2 mixture with various inlet H_2 partial pressures and various inlet H_2 mole fractions, respectively. Here, the feed flow rate in the experiment was converted to mean mole flux, which represents the feed flow rate divided by the effective membrane surface area. In Figs. 4.2(a)-(c) and 4.3(a)-(c), the experimental result, estimation by Eq.(4.4), estimation by Eq.(4.5) along with the limitation line of which H_2 permeation mole flux is equal to the mean H_2 mole flux, are presented.

Experimental results show that the H_2 permeation mole flux generally decreases with a decrease in the mean mole flux, and becomes very close to the limitation when the mean mole flux is very low. This trend can be estimated quantitatively by Eq.(4.5), but not by Eq.(4.4). In this case, Eq.(4.4) demonstrates constant H_2 permeation mole flux, independence from the mean mole flux by definition. Even when the inlet hydrogen partial pressure or inlet hydrogen mole fraction is changed, the same trend is obtained.

Figures 4.2(a)-(c) and 4.3(a)-(c) also demonstrate that the H_2 permeation mole flux gradually reaches to estimation by Eq.(4.4) when the mean mole flux is increased. This trend is supposed to be similar to the mechanism of first order lag function. Therefore, a straight line with gradient of the curved line of Eq.(4.5) at (0,0) is created as shown by Figs. 4.2(a)-(c) and 4.3(a)-(c) to estimate the value of mean mole flux for normalization ($f_{mean,o}$) which corresponds to "time constant" in the first order lag function. Then, the intersection between this line and the line of estimation by Eq.(4.4) gives the value of $f_{mean,o}$. In this case, the value estimated by Eq.(4.4) in Figs. 4.2(a)-(c) and 4.3(a)-(c) corresponds to "gain" in the first order lag function. Then, the result for each case is normalized to describe similarity of the mechanism of H_2 permeation according to the first

order lag function, for the cases with different inlet H_2 partial pressure and different inlet H_2 mole fraction. This is further discussed in Section 4.3.3.

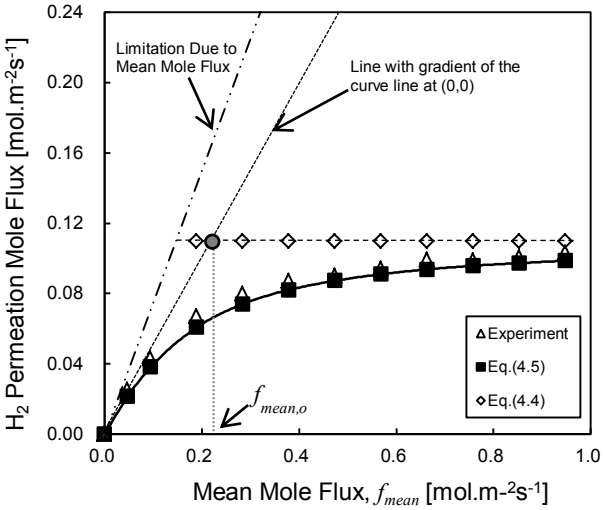

(a) $P_{H_2,in}$: 0.15MPa, $P_{H_2,2}$: 0.10MPa

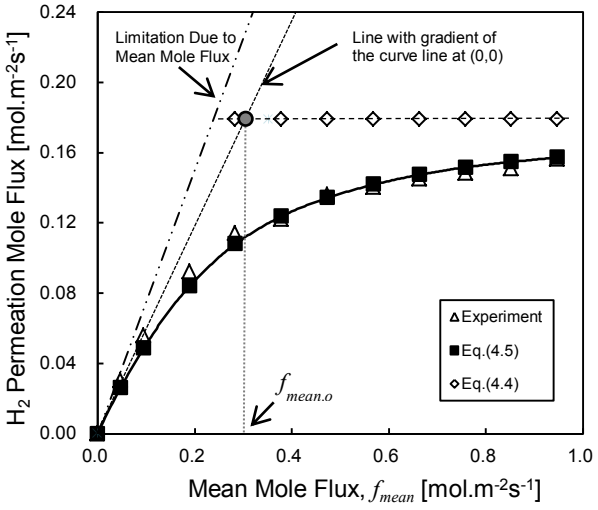

(b) $P_{H_2,in}$: 0.19MPa, $P_{H_2,2}$: 0.10MPa

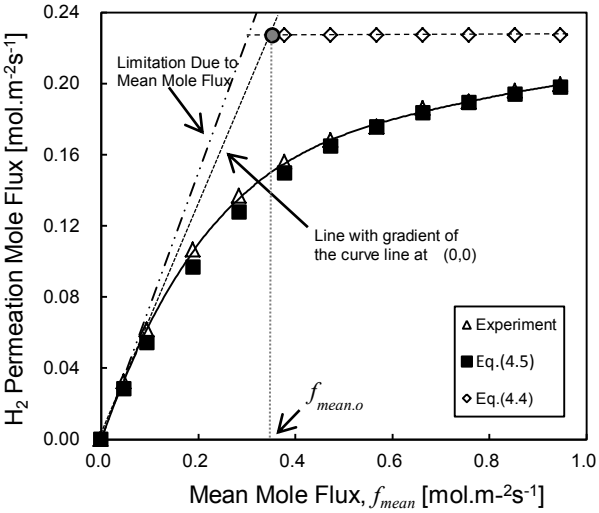

(c) $P_{H_2,in}$: 0.23MPa, $P_{H_2,2}$: 0.10MPa

Fig. 4.2 Effect of mean mole flux on H_2 permeation mole flux ($X_{H_2,in}$:0.75, $T_{mem(ref)}$: 623K)

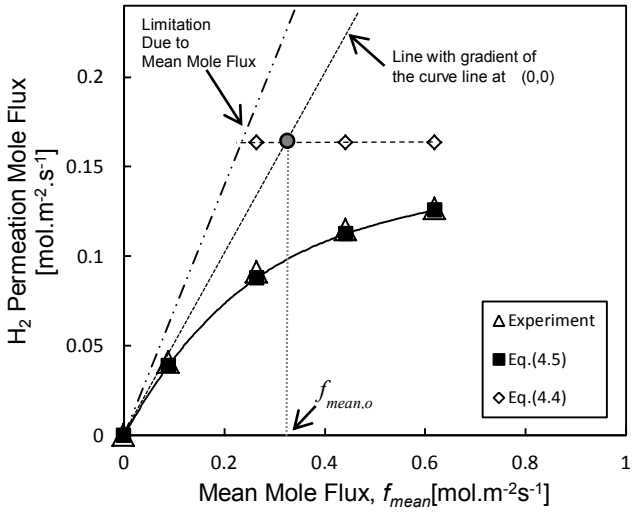

(a) $X_{H_2,in}$:0.70, $P_{H_2,in}$: 0.19MPa, $P_{H_2,2}$: 0.10MPa

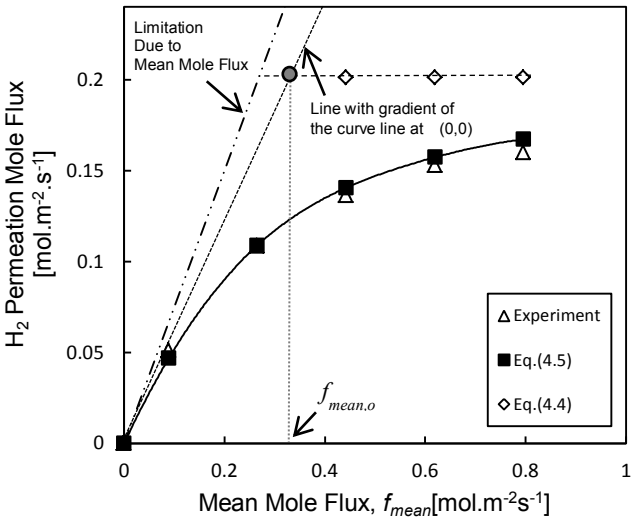

(b) $X_{H_2,in}$:0.75, $P_{H_2,in}$: 0.19MPa, $P_{H_2,2}$: 0.10MPa

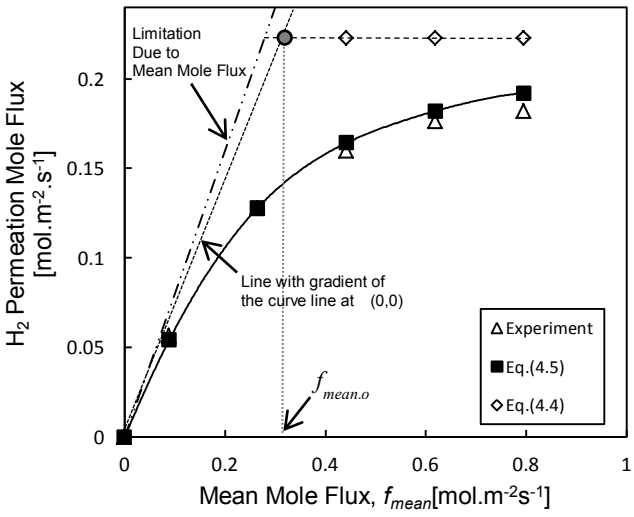

(c) $X_{H_2,in}$:0.80, $P_{H_2,in}$: 0.19MPa, $P_{H_2,2}$: 0.10MPa

Fig. 4.3 Effect of mean mole flux on H_2 permeation mole flux ($T_{mem(ref)}$: 623K)

4.3.2 Mechanism of Proposed Theoretical Equation

In this section, the theoretical result for the case of H_2 mixture with various inlet H_2 partial pressures is used to describe the mechanism of the proposed theoretical equation.

Figure 4.4 shows H_2 partial pressure at the membrane surface of the upstream side estimated by Eq. (4.5), as a function of mean mole flux. Meanwhile, Fig. 4.5 shows the H_2 mole fraction at the membrane surface of the upstream side estimated by $\frac{f_{mean,H_2} - f}{f_{mean} - f}$, as a function of mean mole flux.

Figure 4.4 shows that for any inlet hydrogen partial pressure, the H_2 partial pressure at the membrane surface decreases with a decrease in the mean mole flux. In addition, the figure shows that the H_2 partial pressure at the membrane surface is always lower than the inlet value ($P_{H_2,in}$), which is represented by straight dotted lines. It is interesting to note that the H_2 partial pressure goes to 0.10MPa when the mean mole flux is approaching to 0 mol/(m^2s), which is the same as H_2 partial pressure at the membrane surface of downstream side ($P_{H_2,2}$).

Meanwhile, Fig. 4.5 demonstrates that the H_2 mole fraction at the membrane surface decreases with a decrease in the mean mole flux, and is always smaller than the inlet mole fraction ($X_{H_2,in}$). This is caused by the diffusion effect due to hydrogen concentration decrease at the membrane surface. It is interesting to note that the H_2 mole fractions for 0.15MPa, 0.19MPa and 0.23MPa go to different values with a decrease in mean mole flux as shown in Fig. 4.5, which are 0.50,0.40 and 0.33, respectively. These values represent the minimum mole fraction, when the hydrogen partial pressure at the membrane surface of the upstream side becomes equal to that of the downstream side ($P_{H_2,2}$=0.10MPa), as shown in Fig. 4.4. In addition, the H_2 mole fraction at the membrane surface is always lower for higher inlet hydrogen partial pressure, which is supposed due to the stronger effect of diffusion when the inlet hydrogen partial pressure is increased.

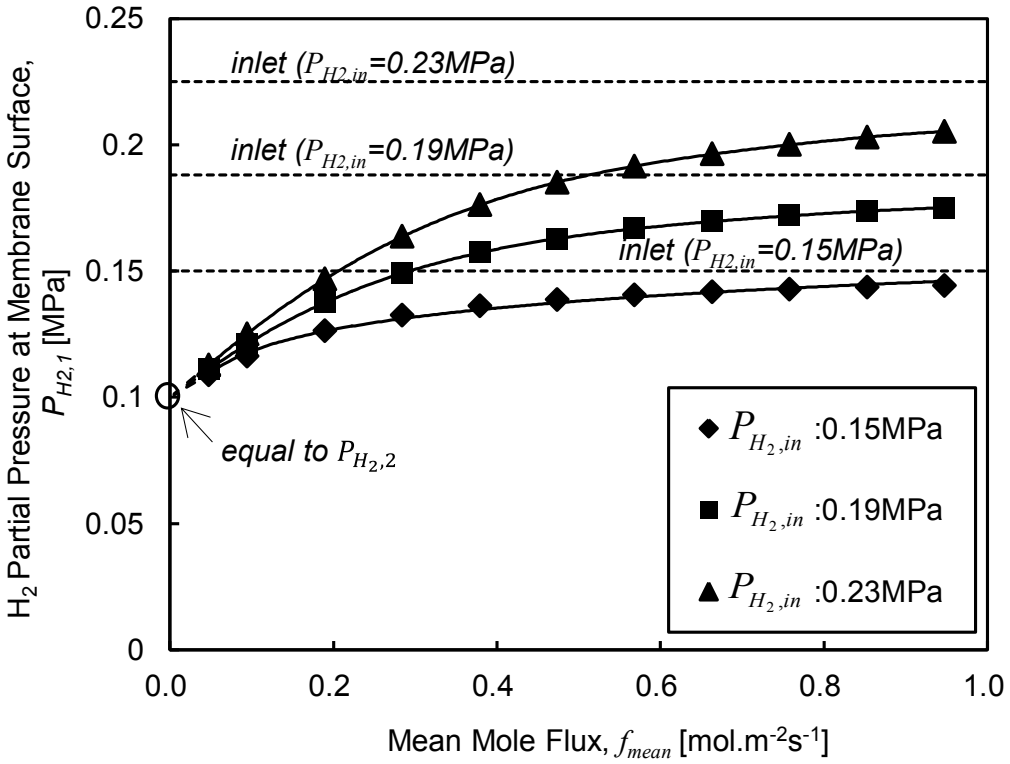

Fig. 4.4 H_2 partial pressure at the membrane surface of the upstream side with consideration of decrease in hydrogen concentration, under various mean mole fluxes ($T_{mem(ref)}$: 623K, $P_{H_2,2}$: 0.10MPa)

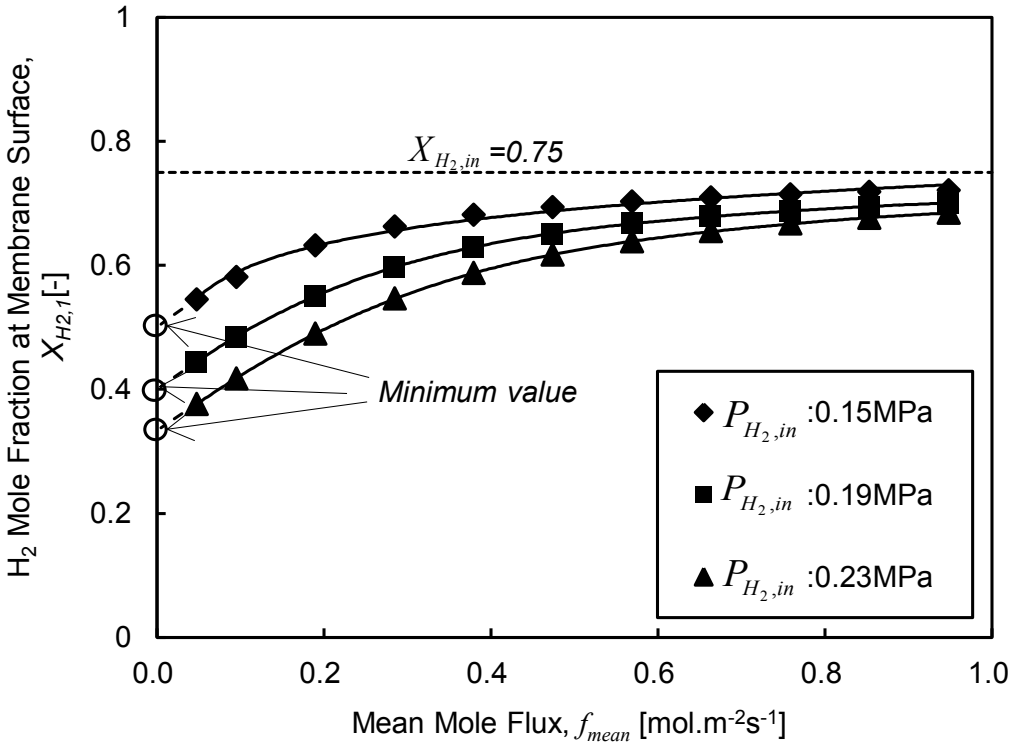

Fig. 4.5 H_2 mole fraction at the membrane surface of the upstream side with consideration of decrease in hydrogen concentration, under various mean mole fluxes ($T_{mem(ref)}$: 623K, $P_{H_2,2}$: 0.10MPa)

4.3.3 Normalization of Theoretical Results

Figures 4.6 and 4.7 show the normalized permeation mole flux (δ) as a function of the normalized mean mole flux (ε) for the H_2 mixture with various inlet H_2 partial pressures and inlet H_2 mole fractions, respectively. In both cases, the reference membrane temperature ($T_{mem(ref)}$) is 623K. Here, ε and δ are given as follows:

$$\varepsilon = \frac{f_{mean}}{f_{mean,o}} \tag{4.7}$$

$$\delta = \frac{Permeation\ Mole\ Flux\ Estimated\ by\ Eq.(4.5)}{Permeation\ Mole\ Flux\ Estimated\ by\ Eq.(4.4)} \tag{4.8}$$

A dashed curved line which represents the first order lag function is also created in Figs. 4.6 and 4.7. In the present study, the "gain" in the first order lag function is renamed as "normalized flux estimated by Eq.(4.4)" while the "time constant" is renamed as "normalized mean mole flux constant" to fit with the phenomena. Similar to the method to estimate $f_{mean,o}$, the normalized mean mole flux constant is obtained from the intersection between the line of normalized flux estimated by Eq.(4.4) and the line with gradient of the dashed curved line at (0,0) as shown in Figs. 4.6 and 4.7. In this case, the value of normalized flux estimated by Eq.(4.4) is 1 and the value of normalized mean mole flux constant is also 1.

Figures 4.6 and 4.7 show that the changes in δ with respect to ε can be expressed by a single curved line without regard to the inlet H_2 partial pressures and inlet H_2 mole fractions, respectively. Initially, this trend is found to follow the mechanism of first order lag function, with the equation as follows:

$$\delta = 1 - \exp(-\varepsilon) \tag{4.9}$$

When ε is 1, that is ε is that of the normalized mean mole flux constant, the

normalized permeation mole flux(δ) is 63% of the normalized flux estimated by Eq.(4.4), which means the first order lag function. When ε is further increased, the δ approaches 1. The value of δ, however deviates from the curve of the first order lag function. This indicates that the effect of diffusion does not disappear so quickly with an increase in the mean mole flux.

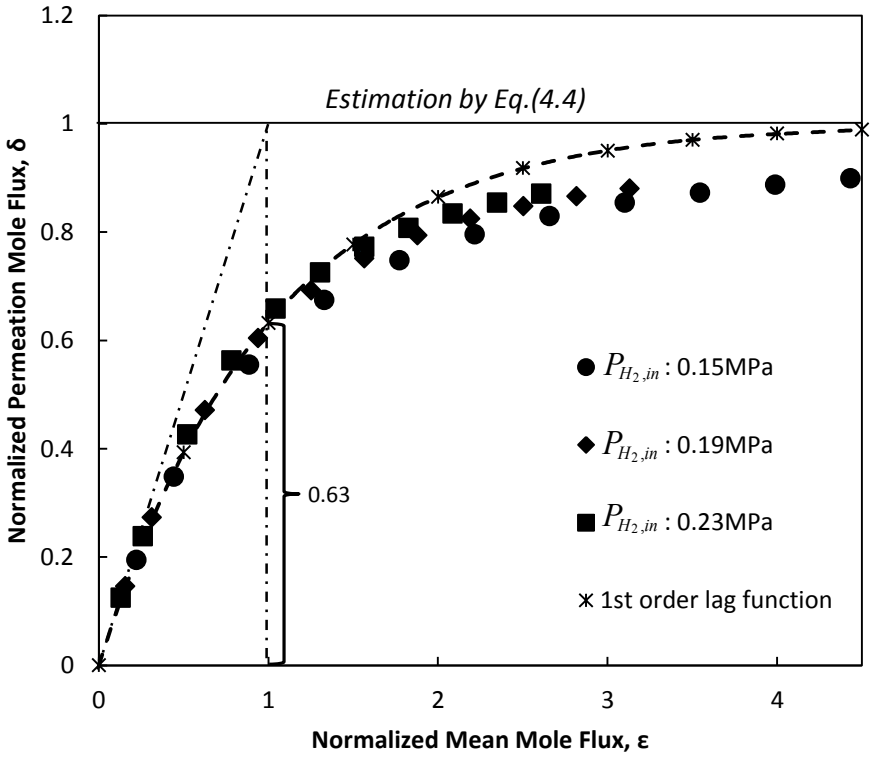

Fig. 4.6 Normalization of theoretical results for various pressures ($T_{mem(ref)}$:623K, $P_{H_2,2}$: 0.10MPa)

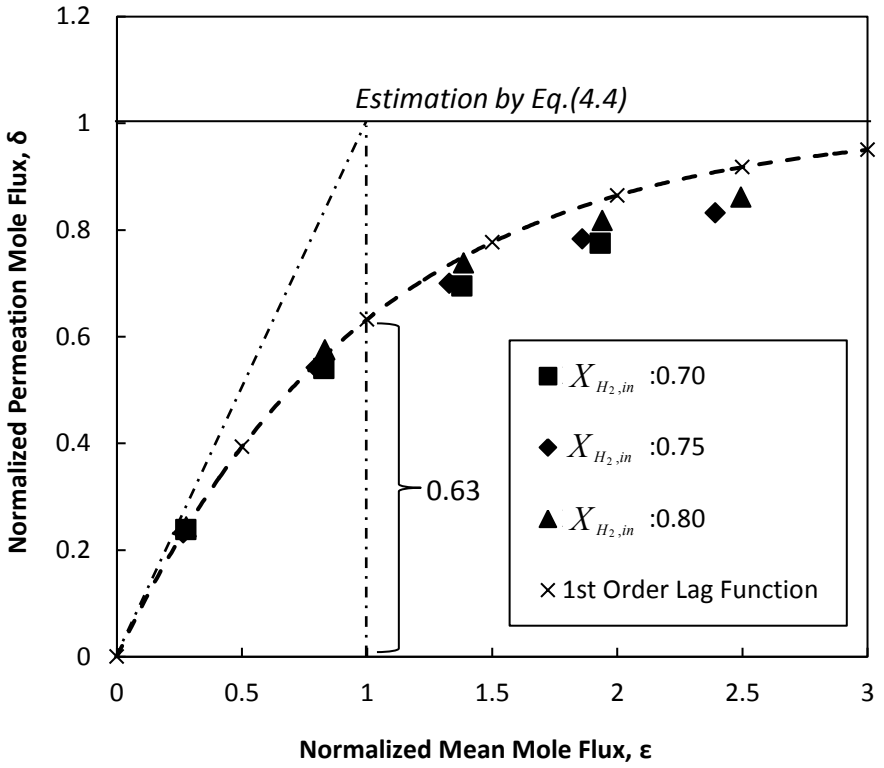

Fig. 4.7 Normalization of theoretical results for various inlet H_2 mole fractions ($T_{mem(ref)}$:623K, $P_{H_2,in}$: 0.19MPa, $P_{H_2,2}$: 0.10MPa)

4.4 Conclusion

In the present study, a theoretical equation to estimate hydrogen permeation mole flux was proposed, by taking into account the decrease in hydrogen concentration at the membrane surface of the upstream side due to permeation.

As described in Chapter 3, for the hydrogen mixture, the experimental results showed that the H_2 permeation rate decreases when the feed flow rate is decreased. This trend of the H_2 permeation mole flux can be analytically estimated when the effect of the permeation flux of H_2 itself is taken into account in the Sieverts' equation. As a result, the H_2 permeation mole flux can be predicted by using concentration of H_2 of the feed mixture. This demonstrates that the diffusive transport effect around the membrane plays an important role as well as the convective transport effect in determining the H_2 mole fraction at the membrane surface. On the other hand, when the mean mole flux is sufficiently high, the role of diffusion transport becomes negligibly small compared to the convection transport, thus the permeation mole flux can be well estimated by the original Sieverts' equation without taking into account the effect of permeation flux of H_2 itself.

For sufficiently low mean mole flux, the dependence of H_2 permeation mole flux on the mean mole flux follows the first order lag function without regard to the inlet H_2 partial pressures and inlet H_2 mole fractions. When the mean mole flux is further increased, the normalized permeation mole flux starts to deviate from the function. It means that the diffusion transport effect does not disappear so quickly with an increase in the mean mole flux.

Chapter 5

Numerical Analysis on Hydrogen Permeation with Flat Sheet Pd/Ag Membrane for Hydrogen Mixture

5.1 Introduction

Number of studies asserted that the permeation flux itself is one of the important factors which could affect the flow properties near the membrane surface for the case of H_2 mixture with high H_2 permeation ratio (Ludtke *et al.* 1998, Gaohong *et al.* 1999, Mourgues and Sanchez 2005, Pizzi *et al.* 2008, Catalano *et al.* 2009, Chen *et al.* 2013). They have demonstrated the phenomena of concentration polarization along the horizontal direction of tubular type membrane, which becomes more pronounced when longer membrane is used. Numerical investigation by Chen *et al.* (2011) for tubular type membrane with H_2 mixture cross flow elucidates that the concentration polarization becomes stronger when the pressure difference or membrane permeance is increased. Then, further investigation on the phenomena of concentration polarization for the same type of membrane was performed to consider the effect of sweep gas which was supplied at the permeated side (Chen *et al.* 2012). They found that the better performance of hydrogen separation could be obtained when counter-current mode was applied, in which the flowing direction of sweep gas is opposite with that of feed gas.

For the case of high H_2 permeation ratio, Catalano *et al.* (2009) have introduced the mass transport coefficient to consider the effect of H_2 permeation flux. They have proposed the semi-empirical equation to predict the H_2 permeation flux in such situation, in which some experimental data are necessary in order to use the equation. Meanwhile, a polarization map has been introduced by Caravella *et al.* (2009) to evaluate the strength of concentration polarization when the inlet and outlet condition are specified. For permeation system with sweep gas supplied at the permeated side, concentration polarization index has

been created by Chen *et al.* (2012) in order to evaluate the behavior of H_2 permeation. To consider the effect of polarization and inhibition by CO simultaneously, the novel permeation reduction coefficient was introduced by Caravella *et al.*(2010). Nagy *et al.*(2013) introduced a model which can be used to know the best operating condition to obtain high separation efficiency for a dense polymer membrane. They have concluded that the convective velocity of the feed gas mixture causes the curvature effect on the concentration distribution in boundary layer near the membrane (Nagy 2010, Nagy 2012).

Based on previous studies, in the case of high H_2 permeation ratio, it is suggested that the fundamental study on characteristics of H_2 permeation for a flat sheet Pd/Ag membrane was less explored, unlike for tubular type membrane (Catalano *et al.* 2009, Chen *et al.* 2011, Chen *et al.* 2012, Caravella *et al.* 2009). Even though the analytical method of H_2 permeation mole flux has been introduced in previous chapters, a numerical analysis to clearly describe the H_2 concentration distribution for such geometry and condition, has not been performed yet. Therefore, in this study, the numerical investigation was performed to understand the H_2 concentration distribution in such case fundamentally without considering the effect of membrane support (Liang and Hughes 2005). The geometry used in the present investigation was similar with the membrane module used in the experiment to imitate the real hydrogen purification process.

5.2 Numerical Simulation

5.2.1 Computational Domain

The numerical simulation was performed in two-dimensional axi-symmetric

configuration using Fluent 13.1(ANSYS) software to discuss the hydrogen permeation mechanism for mixture from the viewpoint of transport phenomena. The centerline of the module for the permeation test corresponds to the axis of symmetry. The geometry is determined following the experimental apparatus in Chapter 3.

The flow condition is assumed to be a steady and laminar, incompressible flow of binary hydrogen mixture. Ideal gas assumption is applied and the mixture is treated as isothermal. Fick's Law was used for molecular diffusion, which indicates the mass flux of molecular diffusion is proportional to the gradient of mass fraction. In addition, the gravitational effect was negligible in this analysis. Species conservation condition was applied at the inlet to allow the inlet diffusion.

The computational domain along with the boundary conditions and coordinate system for the case of binary H_2:N_2 mixture are shown in Fig. 5.1. The binary hydrogen mixture was issued from the inlet. The gases that do not permeate the membrane flow out from the outlet. The wall was set as an impermeable wall and no slip boundary condition was assumed for velocity. The boundary conditions for the membrane is described in detail in Section 5.2.3.

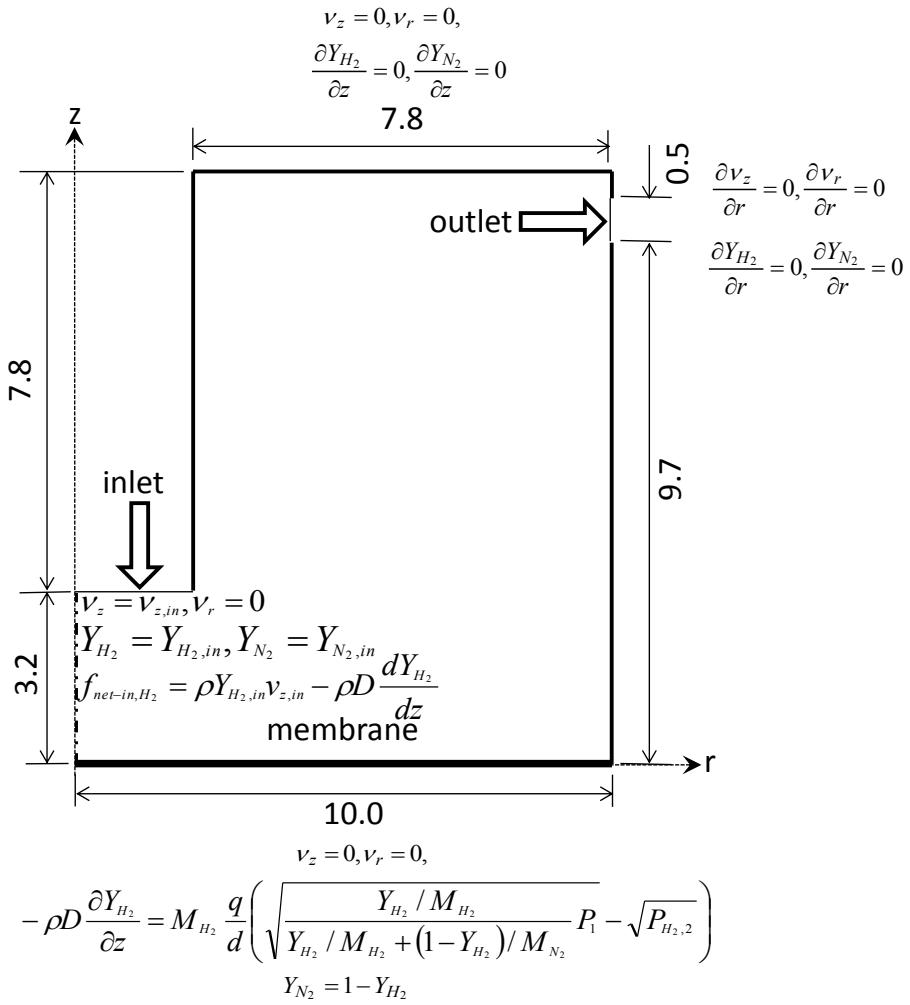

Fig. 5.1 Computational domain with boundary conditions

5.2.2 Governing Equations

The equations of continuity, momentum conservation and species conservation used are as follows:

Continuity equation:

$$\frac{\partial \rho}{\partial t}+\frac{\partial(\rho v_z)}{\partial z}+\frac{\partial(\rho v_r)}{\partial r}+\frac{\rho v_r}{r}=0 \tag{5.1}$$

Momentum conservation equation in z-direction:

$$\frac{\partial \rho v_z}{\partial t}+\frac{1}{r}\frac{\partial(\rho r v_z v_z)}{\partial z}+\frac{1}{r}\frac{\partial(\rho r v_r v_z)}{\partial r}$$

$$=-\frac{\partial p}{\partial z}+\frac{1}{r}\frac{\partial}{\partial z}\left(r\mu\left(2\frac{\partial v_z}{\partial z}-\frac{2}{3}\nabla\cdot\vec{v}\right)\right)+\frac{1}{r}\frac{\partial}{\partial r}\left(r\mu\left(\frac{\partial v_z}{\partial r}+\frac{\partial v_r}{\partial z}\right)\right)+F_z \tag{5.2}$$

Momentum conservation equation in r-direction:

$$\frac{\partial \rho v_r}{\partial t}+\frac{1}{r}\frac{\partial(\rho r v_z v_r)}{\partial z}+\frac{1}{r}\frac{\partial(\rho r v_r v_r)}{\partial r}$$

$$=-\frac{\partial p}{\partial r}+\frac{1}{r}\frac{\partial}{\partial r}\left(r\mu\left(2\frac{\partial v_r}{\partial r}-\frac{2}{3}\nabla\cdot\vec{v}\right)\right)+\frac{1}{r}\frac{\partial}{\partial z}\left(r\mu\left(\frac{\partial v_z}{\partial r}+\frac{\partial v_r}{\partial z}\right)\right)-2\mu\frac{v_r}{r^2}+\frac{2}{3}\frac{\mu}{r}(\nabla\cdot\vec{v})+F_r \tag{5.3}$$

Species conservation equation:

$$\frac{\partial(\rho Y_i)}{\partial t}+\frac{1}{r}\frac{\partial(\rho v_r Y_i)}{\partial r}+\frac{\partial(\rho v_z Y_i)}{\partial z}=\frac{1}{r}\frac{\partial}{\partial r}\left(D_i\frac{\partial Y_i}{\partial r}\right)+\frac{\partial}{\partial z}\left(D_i\frac{\partial Y_i}{\partial z}\right) \tag{5.4}$$

where z is the axial coordinate, r is the radial coordinate, v_z and v_r are the axial and radial velocities, p is the static pressure, F_z and F_r are the external forces and μ is

the viscosity. In addition, Y_i is the mass fraction of species i and D_i is the mass diffusivity for species i in the gas mixture.

5.2.3 Boundary Conditions for Membrane

Based on the surface conservation condition (Williams 1985, Ueda and Mizumoto 1989), the transportation of species at the penetrating surface is shown by Eq.(5.5) as follows:

$$\rho Y_{H_2} v_b - \rho D \frac{\partial Y_{H_2}}{\partial z} = f_{mass,d} \tag{5.5}$$

where ρ is mixture density, Y_{H_2} is mass fraction of hydrogen, v_b is the flow velocity towards membrane surface at very close to membrane, D is the diffusion coefficient and $f_{mass,d}$ is the mass flux of hydrogen which comes out from the membrane at downstream side. In this case, $\rho Y_{H_2} v_b$ is the mass flux by convection and $-\rho D \frac{\partial Y_{H_2}}{\partial z}$ is the mass flux by diffusion.

The value of v_b can be estimated as follows:

$$v_b = \frac{f_{mass,u}}{\rho} \tag{5.6}$$

where $f_{mass,u}$ is the mass flux of hydrogen towards the membrane surface at the upstream side.

By inserting Eq.(5.6) into Eq.(5.5), the following Eq.(5.7) is obtained. Then, the permeation model based on Eq.(5.7) is shown by Fig. 5.2 below.

$$Y_{H_2} f_{mass,u} - \rho D \frac{\partial Y_{H_2}}{\partial z} = f_{mass,d} \tag{5.7}$$

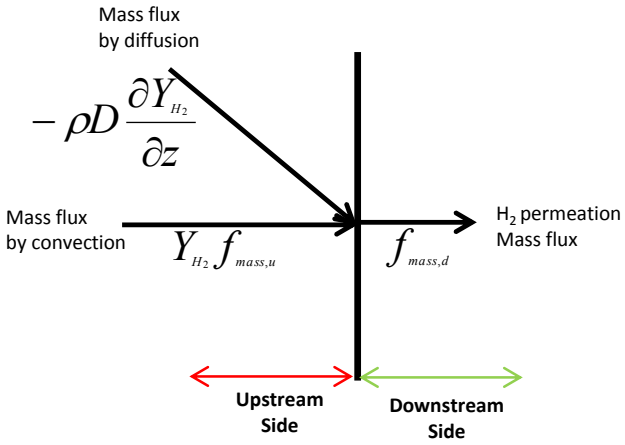

Fig. 5.2 Permeation model

As mentioned in Chapter 1.1.2, in the view point of separation mechanism, inorganic membrane can be divided into porous and nonporous(dense) membrane (Adhikari and Fernando, 2006). For porous membrane, the penetration of H_2 occurs through the membrane, thus

$$f_{mass,u} = f_{mass,d} \tag{5.8}$$

which shows the importance of convective transport at very close to the porous membrane.

However, in the present study, a nonporous(dense) Pd/Ag membrane was used for hydrogen purification. In this case, no penetration occurs through the membrane and hydrogen gas is dissociated into ion at the membrane surface prior to permeating through the membrane (Adhikari and Fernando 2006, Phair and Donelson 2006, Chen *et al.* 2011, Chen *et al.* 2012). Therefore, the flow velocity at the membrane surface of upstream side

can be expressed as $v_b = 0$(Chen *et al.* 2011, Chen *et al.* 2012). As a result, $f_{mass,u}$ becomes zero and then, $Y_{H_2} f_{mass,u} = 0$ is assumed. Due to this assumption, based on Eq.(5.7), the transportation of species at the membrane surface of Pd/Ag membrane is given as follows:

$$-\rho D \frac{\partial Y_{H_2}}{\partial z} = f_{mass,d} \tag{5.9}$$

At the membrane surface, the driving force for hydrogen permeation is the difference in hydrogen partial pressure between the upstream and downstream side. Hydrogen permeates the membrane based on Sieverts' equation as follows (Uemiya *et al.* 1991[(ii)]):

$$F = \frac{qA}{d}\left(\sqrt{P_{H_2,1}} - \sqrt{P_{H_2,2}}\right) \tag{5.10}$$

where F is hydrogen permeation rate, q is hydrogen permeance coefficient, A is effective membrane surface area, d is membrane thickness, $P_{H_2,1}$ is hydrogen partial pressure at membrane surface of upstream side and $P_{H_2,2}$ is hydrogen partial pressure at membrane surface of downstream side.

In the present numerical simulation, $P_{H_2,1}$ could not be obtained directly . Therefore, Eq.(5.10) is modified to Eq.(5.15) as the following steps.

Initially, when Eq.(5.10) is divided by A and multiplied by the molecular weight of hydrogen(M_{H_2}), the following equation is obtained.

$$f_{mass,d} = M_{H_2} \frac{q}{d}\left(\sqrt{X_{H_2} P_1} - \sqrt{P_{H_2,2}}\right) \tag{5.11}$$

where X_{H_2} is the mole fraction of hydrogen and P_1 is the total pressure at the membrane surface of upstream side. From this point, further explanation on the derivation of membrane boundary condition is made based on binary H_2:N_2 mixture. Then, the X_{H_2}, mass fraction (Y_{H_2}) and mass concentration (ρ_{H_2}) for hydrogen were obtained using Eqs.(5.12) –(5.14).

$$X_{H_2} = \frac{C_{H_2}}{C_{H_2} + C_{N_2}} \tag{5.12}$$

$$Y_{H_2} = \frac{\rho_{H_2}}{\rho_{H_2} + \rho_{N_2}} = \frac{\rho_{H_2}}{\rho} \tag{5.13}$$

$$\rho_{H_2} = C_{H_2} M_{H_2} \tag{5.14}$$

where C_{H_2} and C_{N_2} are the mole concentrations for hydrogen and nitrogen, respectively. Meanwhile, ρ_{N_2} is the mass concentration for nitrogen. Then, by substituting Eqs. (5.12)-(5.14) into Eq.(5.11), the following equation was obtained.

$$f_{mass,d} = M_{H_2} \frac{q}{d}\left(\sqrt{\frac{Y_{H_2} / M_{H_2}}{Y_{H_2} / M_{H_2} + (1 - Y_{H_2}) / M_{N_2}}} P_1 - \sqrt{P_{H_2,2}} \right) \tag{5.15}$$

Finally, by inserting Eq.(5.15) into Eq.(5.9), the boundary condition for the membrane is obtained as follows;

$$-\rho D\frac{\partial Y_{H_2}}{\partial z}=M_{H_2}\frac{q}{d}\left(\sqrt{\frac{Y_{H_2}/M_{H2}}{Y_{H_2}/M_{H_2}+\left(1-Y_{H_2}\right)/M_{N_2}}P_1}-\sqrt{P_{H_2,2}}\right) \tag{5.16}$$

in which Eq.(5.9) is rewritten as follows,

$$-\rho D\frac{\partial Y_{H_2}}{\partial z}=f_{mass,d} \tag{5.9}$$

Based on Eq.(5.9) and (5.16), it can be said that the mass diffusion at the membrane surface is determined by the mass flux of hydrogen which comes out from the membrane at downstream side, that is hydrogen permeation mass flux.

For calculation of diffusion coefficient (D), Chapman-Enskog formula (Bird *et al.* 1960, Caravella *et al.* 2008) as shown by Eq. (5.17) was used.

$$D_{ij}=0.00186\left[T^3\left(1/M_i+1/M_j\right)\right]^{0.5}\frac{1}{P\sigma^2{}_{ij}\Omega_{ij}} \tag{5.17}$$

where D_{ij} represents diffusion coefficient for binary mixture of species i and species j. T is absolute temperature, M is the molecular weight, P is the absolute pressure, σ is collision diameter and Ω is the collision integral.

5.2.4 Calculation Conditions

The H_2 concentration distribution was investigated numerically for various feed flow rates, total pressures, inlet H_2 mole fractions and species in binary H_2 mixtures. For various feed flow rates, the calculation condition for numerical simulation is similar to the

experimental conditions as mentioned in Chapter 3.

5.2.4.1 For various total pressures

The binary H_2:N_2 mixture was considered in this part. The inlet H_2 mole fraction ($X_{H_2,in}$) and total downstream pressure ($P_{H_2,2}$) were set as 0.75 and 0.10MPa, respectively. The calculation condition is shown in Table 5.1.

Table 5.1 Calculation condition for various total pressures

No. of Series	1	2	3
Upstream Pressure, P_0 [MPa]	0.20	0.25	0.30
Membrane Temperature, $T[K]$	623	623	623
Feed Flow Rate, F_{in} [mol/s]	$1.5\text{x}10^{-5}$ - $2.98\text{x}10^{-4}$	$1.5\text{x}10^{-5}$ - $2.98\text{x}10^{-4}$	$1.5\text{x}10^{-5}$ - $2.98\text{x}10^{-4}$

5.2.4.2 For various inlet H_2 mole fractions

In this part, H_2:N_2 mixture was considered. For all fractions, the value of hydrogen permeance coefficient(q) is taken as $3.86\text{x}10^{-8}$ mol.m^{-1}.s^{-1}.Pa$^{-0.5}$.The downstream pressure at the membrane surface ($P_{H_2,2}$) was set constant at 0.10MPa. The calculation condition is shown in Table 5.2.

Table 5.2 Calculation condition for various inlet H_2 mole fractions

No. of Series	1	2	3
Inlet mole fraction of H_2, $X_{H_2,in}$	0.70	0.75	0.80
Total pressure, P_0 [MPa]	0.25	0.25	0.25
Membrane temperature, T [K]	623	623	623
Feed Flow Rate, F_{in} [mol/s]	$2.98\text{x}10^{-5}$~ $2.98\text{x}10^{-4}$	$2.98\text{x}10^{-5}$~ $2.98\text{x}10^{-4}$	$2.98\text{x}10^{-5}$~ $2.98\text{x}10^{-4}$

5.2.4.3 For various H_2 mixtures with different species

The permeation characteristic for various H_2 mixtures with different species was investigated. For all cases, the value of hydrogen permeance coefficient(q) is taken as $3.86\text{x}10^{-8}$ $\text{mol.m}^{-1}\text{.s}^{-1}\text{.Pa}^{-0.5}$. The diffusivity for each binary H_2 mixture is calculated by Chapman-Enskog formula as shown by Eq. (5.17), and the calculated values are shown in Table 5.4. In this part, the downstream pressure at the membrane surface ($P_{H_2,2}$) was set constant at 0.10MPa. The calculation condition is shown in Table 5.3.

Table 5.3 Calculation condition for H_2 mixtures with different species

No. of Series	1	2	3	4
H_2 mixture	H_2:N_2	H_2:Ar	H_2:He	H_2:CO_2
Total pressure, P_0 [MPa]	0.25	0.25	0.25	0.25
Membrane temperature, T [K]	623	623	623	623
Feed Flow Rate, F_{in} [mol/s]	$2.98\text{x}10^{-5}$~ $2.98\text{x}10^{-4}$	$2.98\text{x}10^{-5}$~ $2.98\text{x}10^{-4}$	$2.98\text{x}10^{-5}$~ $2.98\text{x}10^{-4}$	$2.98\text{x}10^{-5}$~ $2.98\text{x}10^{-4}$

Table 5.4 Binary Mixture Diffusivity at T : 623K and P_0 :0.25MPa

Gas mixture	H_2:N_2	H_2:Ar	H_2:He	H_2: CO_2
Diffusivity [x10^{-4} m^2/s]	1.07	1.10	2.17	0.903

5.3 Results and Discussion

5.3.1 Comparison with Experimental and Analytical Results

Figure 5.3 shows the comparison between simulation, experimental and analytical results for various total upstream pressures. In this case, the analytical results are obtained by Eq. (4.5) in Chapter 4.

Based on Fig. 5.3, it can be said that the numerical result is quantitatively fit with experimental and analytical result, which indicates that the numerical result is reliable to describe the H_2 concentration distribution during H_2 permeation. Figure 5.3 demonstrates that the H_2 permeation mole flux increases with an increase in the mean mole flux (feed flow rate/effective membrane surface area). When the mean mole flux is increased, H_2 partial pressure at the membrane surface also increases which is further described in Section 5.3.2.

Figures 5.4 and 5.5 show the comparison between simulation and analytical results for the case of various inlet H_2 mole fractions and binary H_2 mixtures, respectively. Figure 5.4 demonstrates that the simulation result is quantitatively fits with the analytical result regardless of inlet H_2 mole fraction. For various binary H_2 mixtures except H_2:He mixture, the simulation result shows very good agreement with analytical result both qualitatively and quantitatively. The deviation of H_2:He mixture from the analytical result is supposed due to the significant difference in binary diffusivity. This is further described in Section

5.3.5.

5.3.2 H_2 concentration profile for various feed flow rates

Radial profile of H_2 concentration on the membrane surface and profile of H_2 along the central axis of the membrane were plotted and discussed for various feed flow rates. In addition, the velocity profile along the central axis of the membrane for each feed flow rate was also presented. As mentioned previously, the feed flow rate was converted to mean mole flux, which represents the feed flow rate per effective membrane surface area. In this study, the net transport of species at the inlet consists of both convection and diffusion components. In this simulation, the $X_{H_2,in}$ is considered as a reference value, which is the H_2 mole fraction that specifies the convection component at the inlet. Then, for each mean mole flux, the H_2 mole fraction is normalized by dividing it to the reference inlet H_2 mole fraction ($X_{H_2,in}$), that is 0.75. The dashed line of normalized H_2 mole fraction is equal to 1, that is when the H_2 mole fraction is equal to reference inlet H_2 mole fraction, is also presented.

Figure 5.6 shows the radial profile of H_2 concentration on the membrane surface as a function of mean mole flux. The figure shows that for all mean mole fluxes, the normalized H_2 mole fraction at the membrane surface gradually decreases with an increase in normalized radial distance of membrane, and is always lower than the maximum normalized value of 1. Here, the average H_2 permeation mole flux is calculated from this H_2 concentration distribution. Figure 5.6 demonstrates that when the mean mole flux is increased, the H_2 mole fraction at the membrane surface increases due to the effect of the increase in flow velocity towards the membrane surface. Thus, H_2 permeation mole flux

increases due to the increase in H_2 partial pressure at the membrane surface, following Sieverts' Law. It is interesting to note that the H_2 permeation mole flux obtained from the simulation could be well estimated by the proposed analytical method. When the mean mole flux is increased, the normalized concentration along the radial distance approaches to the maximum normalized value of 1, that is when radial H_2 mole fraction along the membrane surface becomes 0.75.

Figure 5.7 shows the H_2 concentration profile along the central axis of the membrane as a function of mean mole flux. The figure shows that for all mean mole fluxes, the normalized mole fraction of H_2 decreases towards the membrane surface, which is caused by the effect of H_2 permeation. Thus, it confirms that concentration polarization happens in the permeation system. When the mean mole flux is decreased, the deviation of normalized H_2 mole fraction at the membrane surface from the maximum normalized value of 1 becomes larger, which means the molecular diffusion due to the effect of H_2 permeation becomes stronger. Even though the H_2 permeation mole flux decreases when the mean mole flux is decreased, the effect of the H_2 permeation mole flux which causes the decrease in H_2 concentration at the membrane surface becomes stronger, thus the concentration polarization is more clearly formed.

When the mean mole flux is increased, the normalized H_2 mole fraction at the membrane surface approaches to the maximum normalized value of 1. This is caused by the shorter residence time when the mean mole flux is increased, thus relatively smaller fraction of feed hydrogen permeates the membrane. In this case, the effect of convective transport starts to play an important role in the region at around the membrane, thus the concentration polarization is weakened. When the mean mole flux is sufficiently high, the effect of decrease in H_2 mole fraction at the membrane surface can be negligible, thus the

H_2 mole fraction is supposed to be almost same with the reference inlet H_2 mole fraction. In addition, it is interesting to note that when the mean mole flux is sufficiently low, the net inlet H_2 mole fraction ($X_{H_2,net-in}$) becomes lower than the reference inlet H_2 mole fraction of 0.75, which is mainly due to the very low inlet velocity and strong effect of molecular diffusion.

Figure 5.8 shows the velocity profile along the central axis of the membrane as a function of mean mole flux. Figure 5.8 demonstrates that for all mean mole fluxes, the velocity decreases towards the membrane surface, and finally becomes zero when reaching membrane surface. As mentioned previously, we used a dense(nonporous) Pd/Ag membrane for hydrogen purification.. Thus, the velocity at the membrane surface can be assumed as zero.

5.3.3 H_2 concentration profile for various pressures

Figure 5.9 shows the H_2 concentration profile along the central axis of the membrane as a function of total upstream pressure. The figure shows that for all pressures, the normalized H_2 mole fraction decreases towards the membrane surface due to the effect of H_2 permeation, which means concentration polarization happens. When the pressure difference (or upstream pressure) is increased, higher H_2 permeation flux is obtained, but at the same time the effect of the H_2 permeation flux on the H_2 concentration decrease at the membrane surface becomes stronger, thus the deviation of normalized H_2 mole fraction from the maximum normalized value of 1 becomes larger. In this case, diffusive effect becomes stronger for higher pressure, thus concentration polarization becomes more pronounced.

5.3.4 H_2 concentration profile for various inlet H_2 mole fractions

Figure 5.10 shows the H_2 concentration profile along the central axis of the membrane as a function of inlet H_2 mole fraction. For each case, the local H_2 mole fraction is normalized to respective reference inlet H_2 mole fraction, to investigate the behavior of concentration polarization for various inlet H_2 mole fractions. The figure shows that for all cases, the normalized H_2 mole fraction decreases towards the membrane surface due to the effect of H_2 permeation. The figure also demonstrates the redundancy of normalized H_2 mole fraction for different inlet H_2 mole fraction, thus elucidates that the strength of concentration polarization effect is almost same regardless of the reference inlet H_2 mole fraction.

Figure 5.11 shows the radial profile of H_2 concentration on the membrane surface as a function of inlet H_2 mole fraction. For all inlet H_2 mole fractions, the normalized H_2 mole fraction at the membrane surface decreases with an increase in normalized radial distance, in which the average H_2 permeation mole flux calculated from this H_2 concentration distribution can be quantitatively estimated by the proposed analytical method as shown by Fig. 5.4. Based on Fig. 5.11, it can be said the radial profile for all cases are almost same, and the significant difference was not observed in our fraction range.

5.3.5 H_2 concentration profile for various binary H_2 mixtures

Figure 5.12 shows the radial profile of H_2 concentration on the membrane surface for various binary H_2 mixtures. The figure demonstrates that the normalized H_2 mole fraction at the membrane surface for H_2:CO_2 is highest while for H_2:He is lowest. Meanwhile, the

radial profiles of H_2 concentration for H_2:N_2 and H_2:Ar have almost same trend, both qualitatively and quantitatively. The various trends of the profile are supposed due to the difference in diffusivity of binary gas mixture, as shown by Table 5.4. It is interesting to note that the H_2 permeation mole flux calculated from these various H_2 concentration distributions except for the case of H_2:He can be estimated quantitatively by the proposed analytical method.

Figure 5.13 demonstrates the H_2 concentration along the central axis of the membrane as a function of species in binary H_2 mixture. When sufficiently low feed flow rate is used for H_2 mixture with higher diffusivity, H_2 permeation mole flux becomes less due to the stronger effect of concentration polarization. In this case, the effect of the H_2 permeation mole flux on decrease in H_2 concentration at membrane surface becomes stronger, thus the H_2 mole fraction at membrane surface becomes lower. Due to the larger deviation of the normalized H_2 mole fraction at membrane surface from the maximum normalized value of 1, the concentration polarization effect becomes stronger when the H_2 mixture with higher diffusivity is used. Therefore, the sequence of strength of concentration polarization effect can be shown as H_2:He> H_2:Ar> H_2:N_2> H_2:CO_2.

The numerical results for various H_2 mixtures elucidate that when the permeation system is switched from low to high H_2 permeation ratio, the diffusivity of the gas mixture starts to play an important role which can significantly affects the H_2 permeation flux through the membrane. The different behavior of H_2 permeation could be clearly observed among the mixtures with inert gas (N_2,Ar and He) when the permeation system undergoes the condition of high H_2 permeation ratio, even though the similarity of these mixtures is well known for the case of low H_2 permeation ratio.

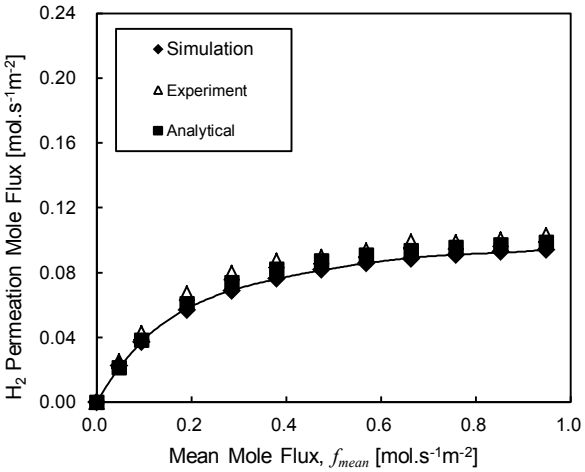

(a) P_0 : 0.20 MPa

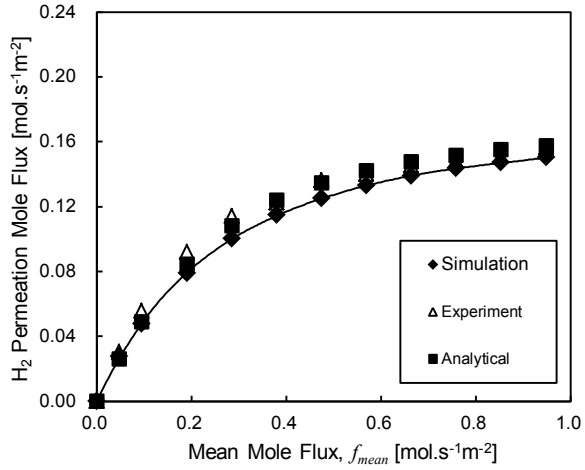

(b) P_0 : 0.25 MPa

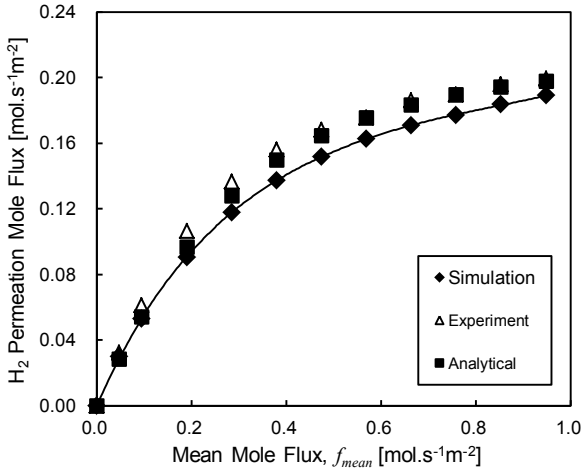

(c) P_0 : 0.30 MPa

Fig. 5.3 Comparison between simulation, experimental and analytical results for various total upstream pressures ($X_{H_2,in}$: 0.75, $T_{mem(ref)}$: 623 K, $P_{H_2,2}$: 0.10 MPa)

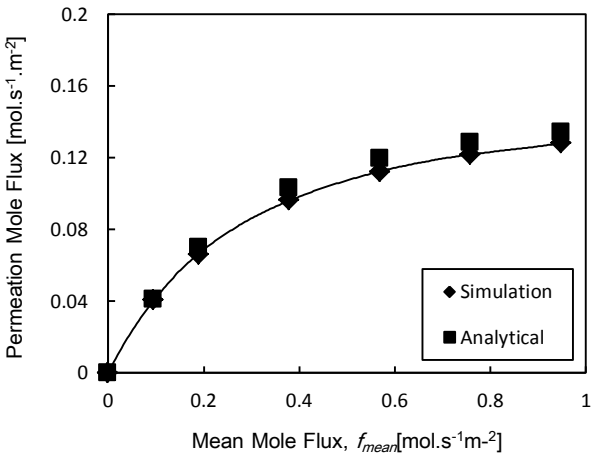

(a) $X_{H_2,in}$: 0.70

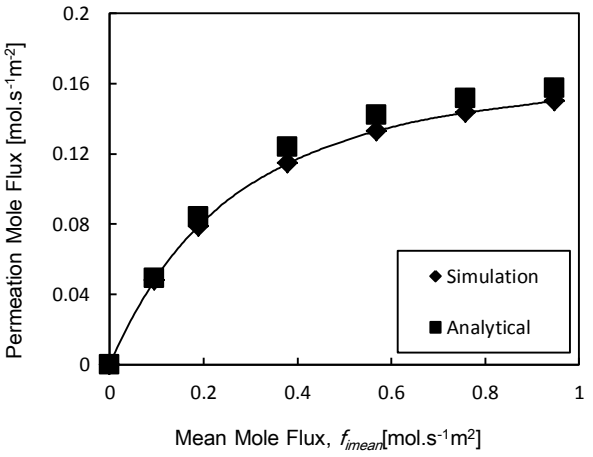

(b) $X_{H_2,in}$: 0.75

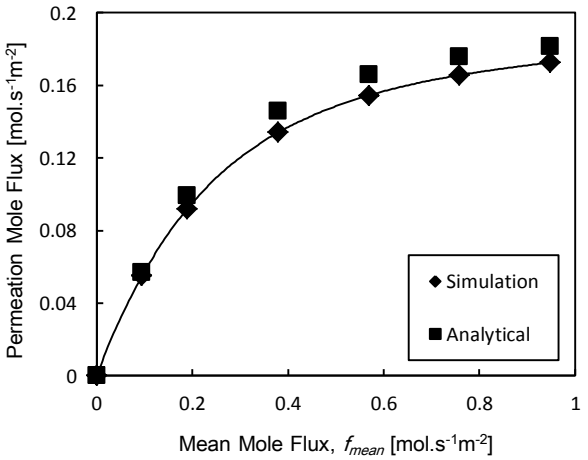

(c) $X_{H_2,in}$: 0.80

Fig. 5.4 Comparison between simulation and analytical results for various inlet H_2 mole fractions (T_{mem} : 623K, P_0 :0.25MPa, $P_{H_2,2}$: 0.10 MPa)

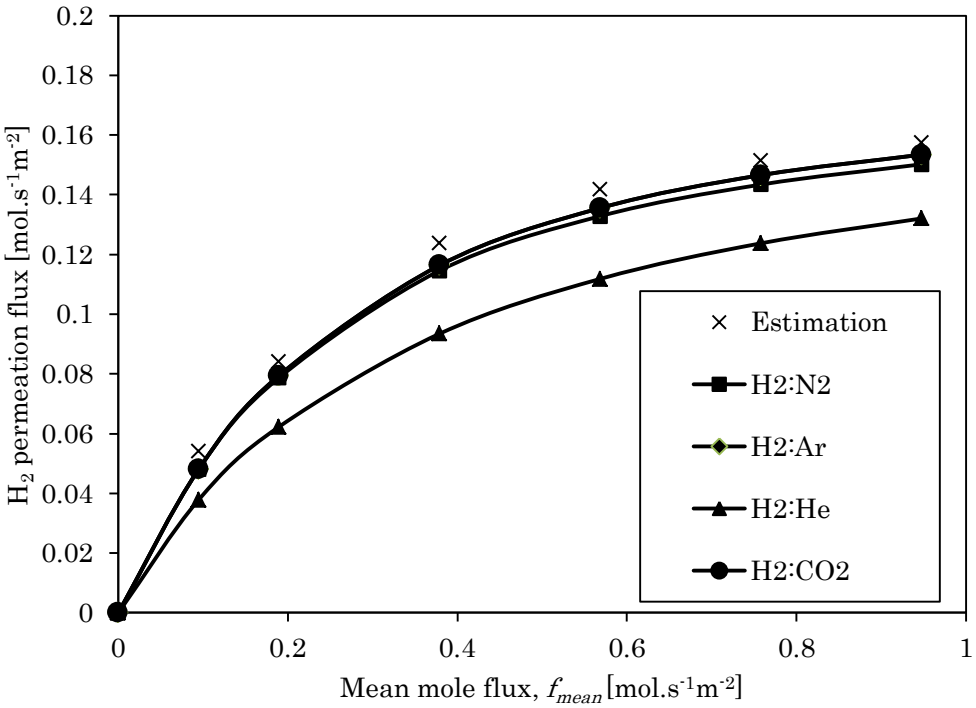

Fig. 5.5 Comparison between simulation and analytical results for various binary H_2 mixtures ($X_{H_2,in}$: 0.75, T_{mem}: 623K, P_0:0.25MPa, $P_{H_2,2}$: 0.10 MPa)

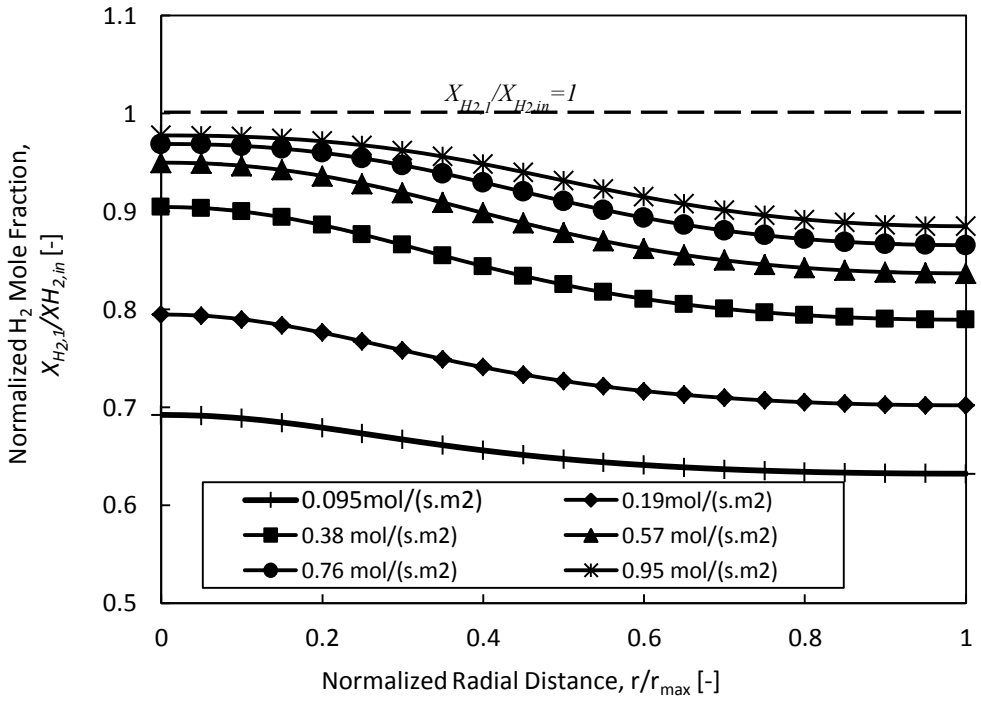

Fig. 5.6 Radial profile of H_2 concentration on the membrane surface as a function of mean mole flux ($X_{H_2,in}$: 0.75, T_{mem}: 623K, P_0 :0.25MPa , $P_{H_2,2}$: 0.10 MPa)

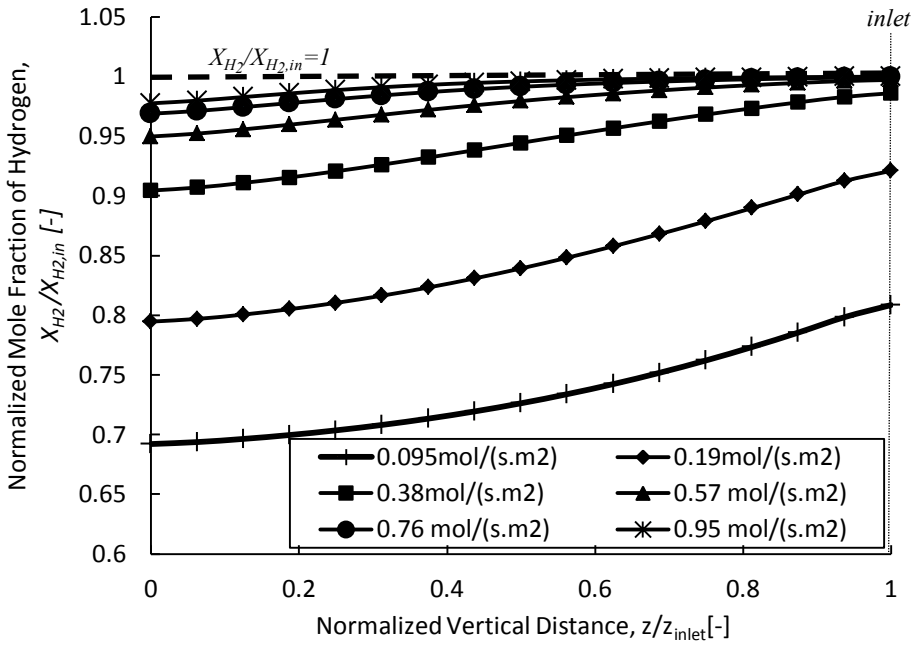

Fig. 5.7 H_2 concentration profile along the central axis of the membrane as a function of mean mole flux ($X_{H_2,in}$: 0.75, T_{mem}: 623K, P_0:0.25MPa , $P_{H_2,2}$: 0.10 MPa)

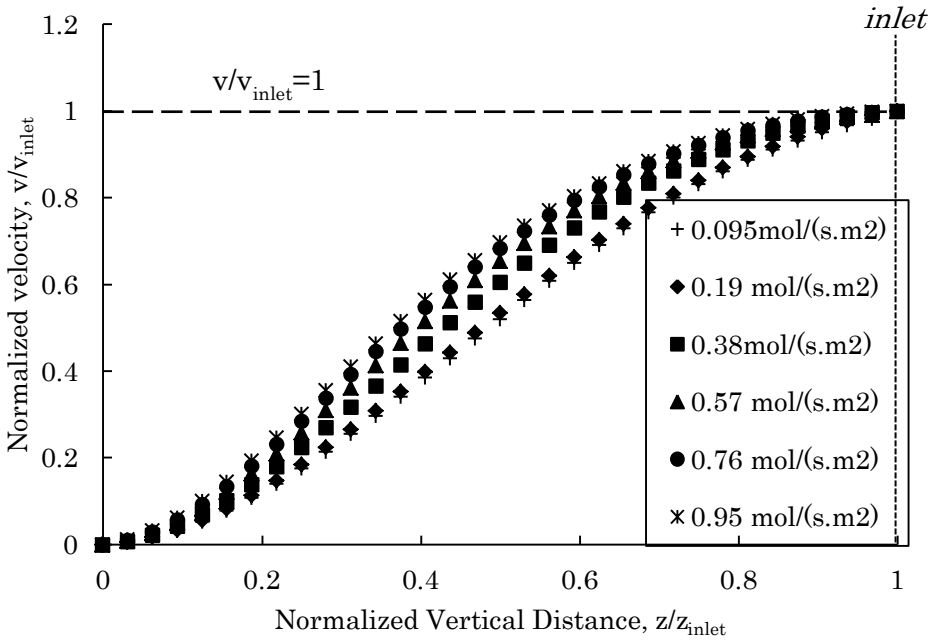

Fig. 5.8 Velocity profile along the central axis of the membrane as a function of mean mole flux ($X_{H_2,in}$: 0.75, T_{mem}: 623K, P_0:0.25MPa , $P_{H_2,2}$: 0.10 MPa)

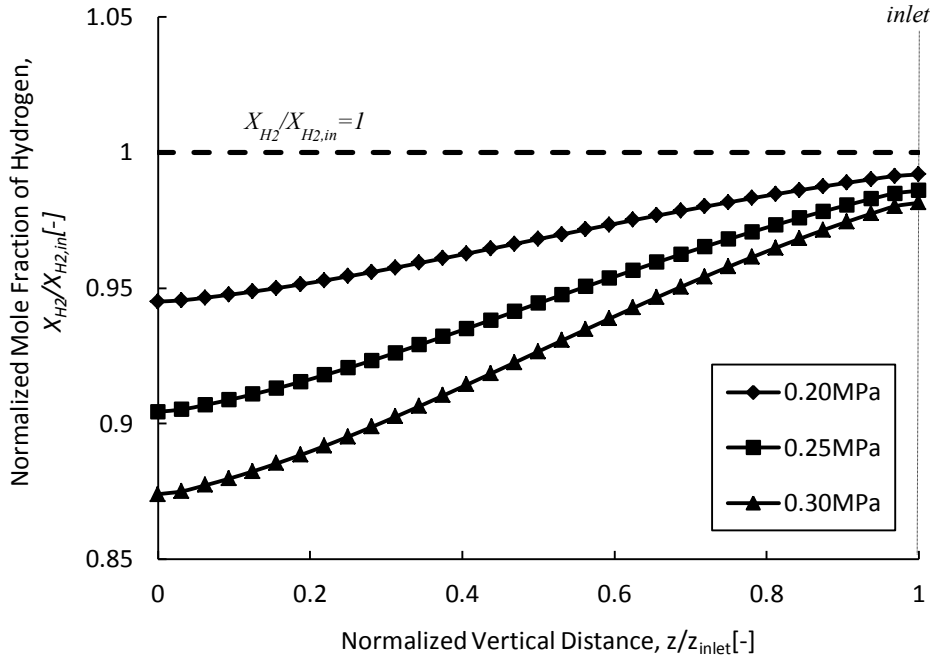

Fig. 5.9 H_2 concentration profile along the central axis of the membrane as a function of total upstream pressure ($X_{H_2,in}$: 0.75, T_{mem}: 623K, $P_{H_2,2}$: 0.10 MPa, f_{mean}: 0.38 mol.s^{-1}m^{-2})

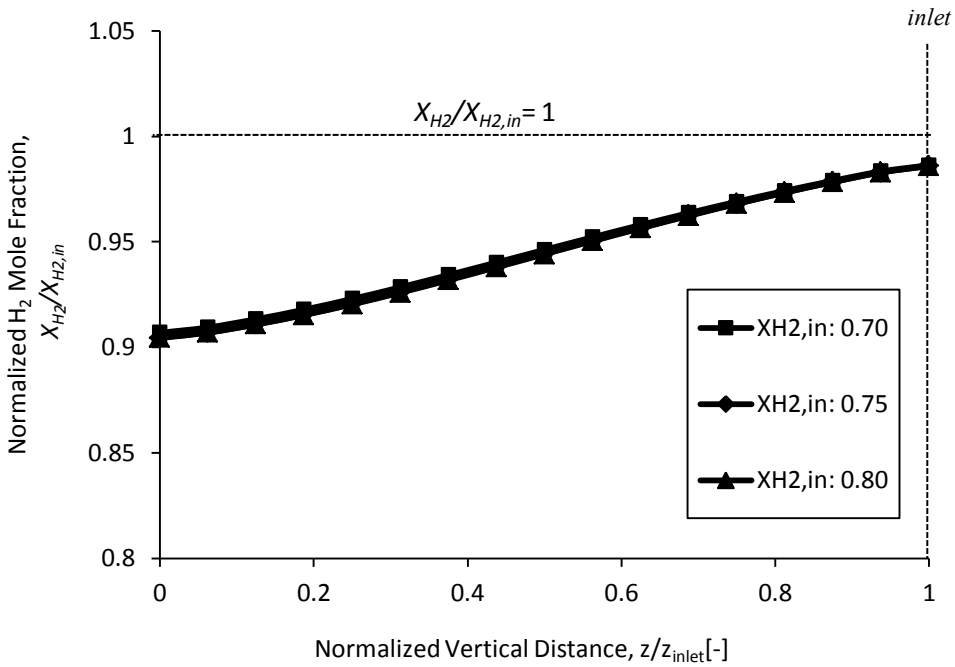

Fig. 5.10 H_2 concentration profile along the central axis of the membrane as a function of inlet H_2 mole fractions (T_{mem}: 623K, P_0:0.25MPa, $P_{H_2,2}$: 0.10 MPa, f_{mean}: 0.38 mol.s^{-1}m^{-2})

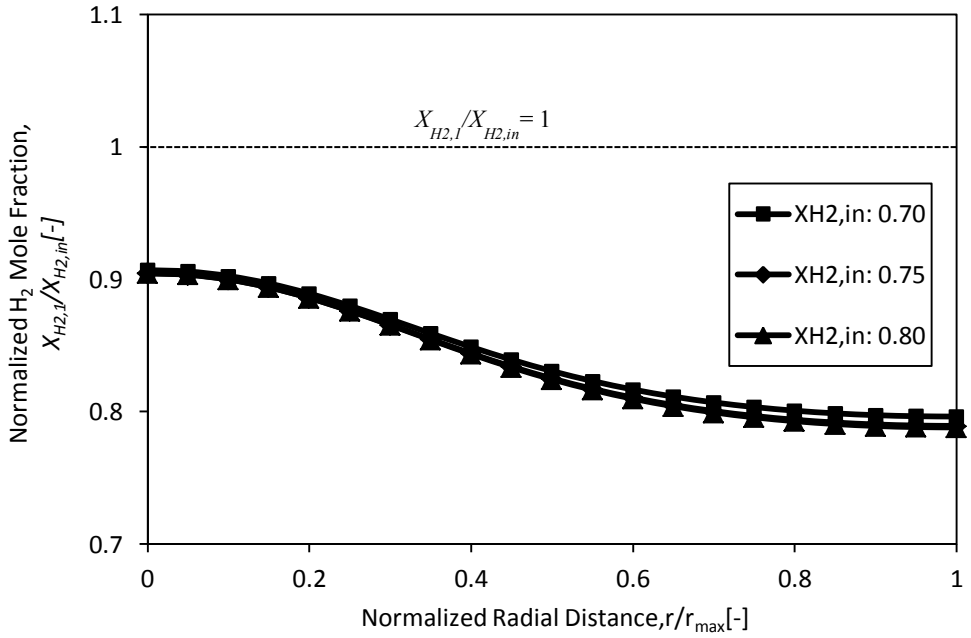

Fig. 5.11 Radial profile of H_2 on the membrane surface as a function of inlet H_2 mole fractions (T_{mem} : 623K, P_0 :0.25MPa, $P_{H_2,2}$: 0.10 MPa, f_{mean} : 0.38 mol.$s^{-1}m^{-2}$)

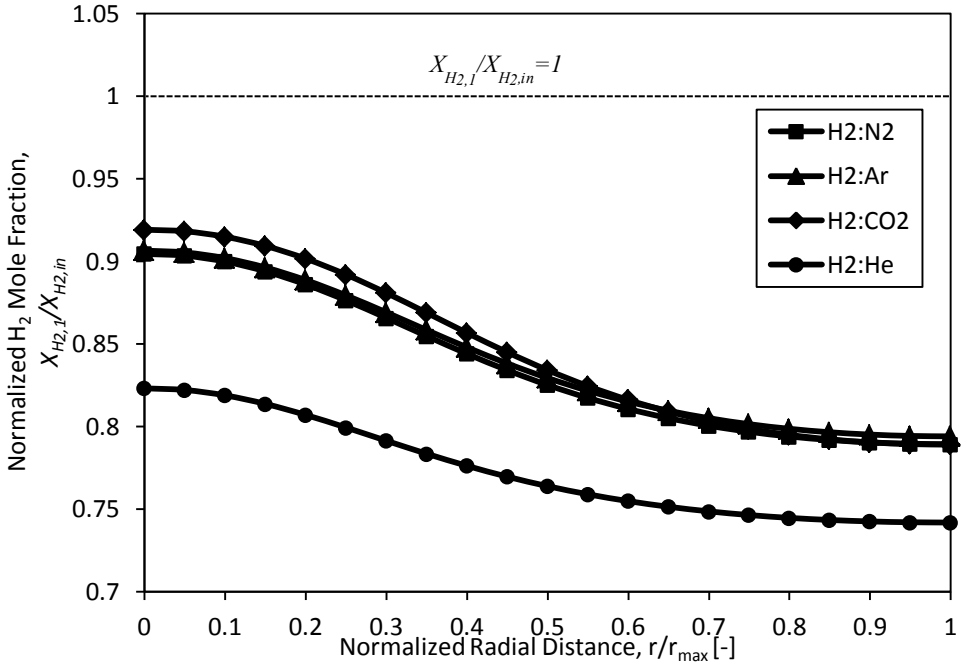

Fig. 5.12 Radial profile of H_2 concentration on the membrane surface as a function of species in H_2 mixture ($X_{H_2,in}$: 0.75, T_{mem}: 623K, P_0 :0.25MPa, $P_{H_2,2}$: 0.10 MPa, f_{mean}: 0.38 mol.s^{-1}m^{-2})

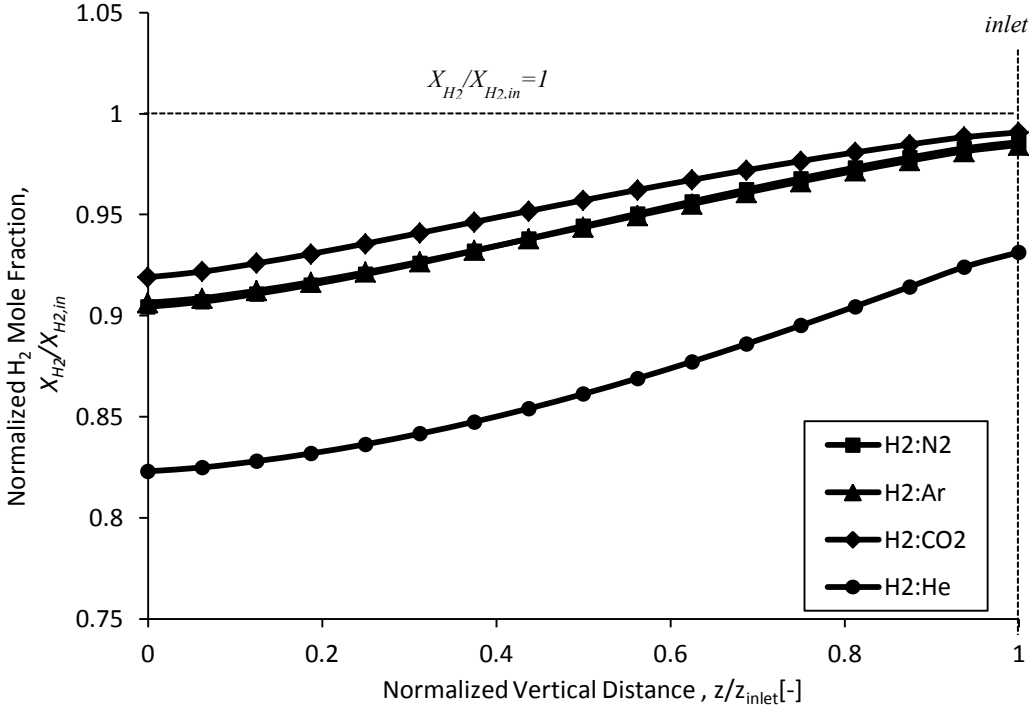

Fig. 5.13 H_2 concentration profile along the central axis of the membrane as a function of species in H_2 mixture ($X_{H_2,in}$: 0.75, T_{mem}: 623K, P_0 :0.25MPa, $P_{H_2,2}$: 0.10 MPa, f_{mean}: 0.38 mol.s^{-1}m^{-2})

5.4 Conclusions

The H_2 permeation through a flat sheet Pd/Ag membrane for H_2 mixture was investigated numerically. In the present investigation, the mean mole flux is varied for each total upstream pressure, inlet H_2 mole fraction and binary H_2 mixture.

The numerical result for the case of H_2:N_2 mixture ($X_{H_2,in}$=0.75) has been validated experimentally, and is found quantitatively fit with analytical result based on the Sieverts' equation. For the cases with different inlet H_2 mole fraction and species in binary H_2 mixture, the numerical results show very good agreement with the analytical results except for the case of H_2:He mixture.

The numerical results show a decrease in H_2 mole fraction towards the membrane surface, which makes clear the concentration polarization near the membrane surface. Furthermore, the H_2 mole fraction at the membrane surface approaches to the reference inlet H_2 mole fraction when the mean mole flux is increased, which means the strength of molecular diffusion becomes less for larger mean mole flux and then, the concentration polarization is weakened. When the mean mole flux is decreased or the total upstream pressure is increased, the effect of molecular diffusion on the flow near the membrane becomes stronger, thus concentration polarization could be clearly formed. The numerical result for various inlet H_2 mole fractions demonstrate the redundancy of normalized H_2 mole fraction profile, thus the difference in strength of concentration polarization effect was not observed in the present investigation. The numerical results also demonstrate that the role of mixture diffusivity becomes important when the permeation system is switched from low to high H_2 permeation ratio, in which concentration polarization could be clearly observed in such situation. The concentration polarization effect becomes more important when the H_2 mixture with higher binary diffusivity is used.

Overall, it can be said that the molecular diffusion, that is concentration polarization plays a significant role for H_2 permeation with flat sheet Pd/Ag membrane.

Chapter 6

Summary and Concluding Remarks

6. Summary and Concluding Remarks

The performance of a compact methanol steam reformer with flat sheet Pd/Ag membrane for hydrogen purification was studied experimentally. The mole fraction of reformed hydrogen under various reference catalyst zone temperatures, upstream side pressures, S/C ratios and reactant flow rates is almost constant at 0.75, which corresponds to the mole fraction of H_2 estimated by the overall methanol steam reforming reaction formula.

The higher hydrogen permeation rate is attained when we use the higher reference membrane temperature and higher pressure. For the S/C ratio, we obtain the maximum permeation rate when the ratio is around 1 because the hydrogen partial pressure at the upstream side becomes highest when no excessive reactant at the upstream side exists. For the reactant flow rate, the permeation rate is maximum at a certain value where the hydrogen concentration at the membrane surface becomes highest due to the maximum effect of high flow velocity towards the membrane. Experimentally obtained H_2 permeation rate is much lower than the prediction by Sieverts' equation, which indicates that the Sieverts' equation is not going well in this case. In addition, the compact reformer with a purification membrane produces hydrogen with a very low CO concentration, less than 10ppm which is suitable for the PEFC application.

To make clear the significant difference between the experimental H_2 permeation rate and the prediction by Sieverts' equation, hydrogen permeation for flat sheet Pd/Ag membrane was investigated experimentally by using H_2:N_2 mixture to neglect any adsorption effect of non-H_2 species. For the hydrogen mixture, the experimental results

showed that the H_2 permeation rate decreases when the feed flow rate is decreased while it is constant for pure hydrogen. This trend of the H_2 permeation mole flux can be analytically estimated when the effect of the permeation flux of H_2 itself is taken into account in the Sieverts' equation. As a result, the H_2 permeation mole flux can be predicted by using H_2 concentration of the feed mixture. On the other hand, when the mean mole flux is increased, the permeation mole flux can be well estimated by the Sieverts' equation without taking into account the effect of permeation flux of H_2 itself.

For sufficiently low mean mole flux, the dependence of H_2 permeation mole flux on the mean mole flux follows the first order lag function without regard to the inlet H_2 partial pressures and inlet H_2 mole fractions. However, when the mean mole flux is further increased, the normalized permeation mole flux starts to deviate from the function. It means that the diffusive transport effect does not disappear so quickly with an increase in the mean mole flux.

The numerical investigation on H_2 permeation with flat sheet Pd/Ag membrane for H_2 mixture was performed to describe clearly the H_2 concentration distribution during permeation. In the present investigation, the mean mole flux is varied for each total upstream pressure, inlet H_2 mole fraction and binary H_2 mixture. The numerical result for the case of H_2:N_2 mixture has been validated experimentally, and is found quantitatively fit with analytical result based on the Sieverts' equation. For the cases with different inlet H_2 mole fraction and species in H_2 mixture, the numerical results show very good agreement with the analytical results except for the case of H_2:He mixture. The numerical results show a decrease in H_2 mole fraction toward the membrane surface for various conditions, which makes clear the concentration polarization near the membrane surface. Furthermore, the H_2 concentration gradient decreases and H_2 mole fraction at the membrane surface

approaches to the maximum inlet H_2 mole fraction when the mean mole flux is increased, which means the role of molecular diffusion becomes less important for larger mean mole flux and then, the concentration polarization is weakened. When the mean mole flux is decreased or the total upstream pressure is increased, the effect of molecular diffusion becomes more important, thus concentration polarization could be clearly formed. Therefore, it is elucidated that the diffusive effect plays an important role as well as convective effect in determining H_2 mole fraction at membrane surface. The numerical result for various inlet H_2 mole fractions demonstrate the redundancy of H_2 mole fraction profile, thus the difference in strength of concentration polarization effect was not observed in the present investigation. The numerical results demonstrate that the role of mixture diffusivity becomes important during the permeation, in which concentration polarization could be clearly observed. The concentration polarization effect becomes stronger when the H_2 mixture with higher binary diffusivity is used. Overall, it can be said that the molecular diffusion, that is concentration polarization plays a significant role for permeation with flat sheet Pd/Ag membrane when H_2 mixture is used.

References

Adhikari, S. and Fernando, S., Reviews-Hydrogen Membrane Separation Techniques, *Ind. Eng. Chem. Res.*, Vol. 45(2006), pp. 875-881.

Agrell, J., Birgersson, H. and Boutonnet, M., Steam Reforming of Methanol over a $Cu/ZnO/Al_2O_3$ Catalyst: A Kinetic Analysis and Strategies for Suppression of CO Formation, *Journal of Power Sources*, Vol. 106(2002), pp. 249-257.

Amandusson. H., Ekedahl, L.-G., and Dannetun, H., The effect of CO and O_2 on hydrogen permeation through a palladium membrane. *Appl. Surf. Sci.*, Vol. 153(2000), pp.259-267.

Amano, M., Nishimura, C., and Komaki, M., Effects of high concentration CO and CO_2 on hydrogen permeation through the palladium membrane, *Mater. Trans. JIM* 31(1990), pp. 404.

Antoniazzi, A.B., Haasz, A.A., Stangeby, P.C., The effect of adsorbed carbon and sulphur on hydrogen permeation through palladium, *J. Nucl. Mater.*, Vol. (162-164) (1989), pp. 1065.

Arstad, B., Venvik, H., Klette, H., Walmsley, J.C., Tucho, W.M., Holmestad, R., Holmen, A. and Bredesen, R., Studies of self-supported 1.6 μm Pd/23 wt.% Ag Membranes during and after Hydrogen Production in a Catalytic Membrane Reactor, *Catalysis Today*, Vol.118 (2006), pp. 63-72.

Baker, R. W., Membrane Technology and Applications (3rd Edition), A John Wiley & Sons, Ltd. Publication; 2012.

Barbieri, G., Scura, F., Lentini, F., De Luca, G. and Drioli, E., A novel model equation for the permeation of hydrogen in mixture with carbon monoxide through Pd-Ag membranes, *Separation and Purification Technology*, Vol.61(2008), pp. 217-224.

Basile, A., Iulianelli, A., Longo, T., Liguori, S., De Falco, M., Membrane Reactors for Hydrogen Production Processes, Springer-Verlag, London Limited: 2011.

Basile, A., Tereschenko, G.F., Orekhova, N.V., Ermilova, M.M., Gallucci, F. and Iulianelli, A., An Experimental Investigation on Methanol Steam Reforming with Oxygen Addition in a Flat Pd-Ag Membrane Reactor, *International Journal of Hydrogen Energy* ,Vol.31 (2006), pp. 1615-1622.

Bird, R.B., Stewart, W.E. and Lightfoot, E.N., Transport Phenomena, Wiley, New York, 1960.

Caravella A, Barbieri G, Drioli E., Modelling and simulation of hydrogen permeation through supported Pd-alloy membranes with a multicomponent approach, *Chemical Engineering Science*, Vol.63 (2008), pp. 2149-2160.

Caravella, A., Barbieri, G. and Drioli, E., Concentration polarization analysis in self-supported Pd-based membranes, *Separation and Purification Technology*, Vol. 66(2009), pp. 613-624.

Caravella, A., Scura, F., Barbieri, G. and Drioli, E., Inhibition by CO and Polarization in Pd-Based Membranes: A Novel Permeation Reduction Coefficient, *The Journal of Physical Chemistry B*, Vol. 114 (2010), pp. 12264-12276.

Catalano, J., Giacinti Baschetti, M., and C. Sarti, G., Influence of the gas phase resistance on hydrogen flux through thin palladium-silver membranes, *Journal of Membrane Science*, Vol.339(2009), pp. 57-67.

Catalano, J., Baschetti, M. G. and C. Sarti, G., Hydrogen permeation in palladium-based membranes in the presence of carbon monoxide, *Journal of Membrane Science*, Vol. 362 (2010), pp. 221-233.

Chabot, J., Lemonte, J., Grumet, C. and Sannier, J., Fuel Clean-up System: Poisoning of Palladium-silver Membranes by Gaseous Impurities, *Fusion Tech.*, Vol. 14(1988), pp. 614-618.

Chein, R-.Y., Chen, Y.-C., Lin, Y.-S. and Chung, J.N., Hydrogen production using integrated methanol-steam reforming reactor with various reformer designs for PEM fuel cells, *International Journal of Energy Research*, Vol. 36 (2012), pp. 466-476.

Chen, S.C., Caryat, Hung, C.Y., Tu, G.C. and Rei, M.H., Perturbed Hydrogen Permeation of a Hydrogen Mixture-New Phenomena in Hydrogen Permeation by Pd Membrane, *International Journal of Hydrogen Energy*,Vol. 33(2008),pp. 1880-1889.

Chen,W.-H., Syu, W.-Z. and Hung C.-I., Numerical characterization on concentration polarization of hydrogen permeation in a Pd-based membrane tube, *International Journal of Hydrogen Energy*, Vol.36 (2011), pp. 14734-14744.

Chen, W.-H., Syu, W.-Z., Hung, C.-I., Lin, Y.-L. and Yang, C.-C., A numerical approach of conjugate hydrogen permeation and polarization in a Pd membrane tube, *International Journal of Hydrogen Energy*, Vol. 37(2012), pp. 12666-12679.

Chen, W.-H., Syu, W.-Z., Hung, C.-I., Lin, Y.-L., Yang, C.-C., Influence of geometry and flow pattern on hydrogen separation in a Pd-based membrane tube, *International Journal of Hydrogen Energy*, Vol. 38 (2013), pp. 1145-1156.

Collins, J.P. and Way, J.D., Preparation and characterization of a composite palladium-ceramic membrane, *Ind. Eng. Chem. Res.*, Vol. 32 (1993) 2006.

Davieau D.D., Erickson P.A., The effect of geometry on reactor performance in the steam-reformation process, *International Journal of Hydrogen Energy*, Vol.32(2007), pp.1192–1200.

Dicks, A.L., Hydrogen generation from natural gas for the fuel cell systems of tomorrow, *Journal of Power Sources*, Vol. 61 (1996), pp. 113-124.

Emonts, B., Bogild Hansen, J., Loegsgaard Jorgensen, S., Hohlein, B. and Peters, R., Compact Methanol Reformer Test for Fuel-cell Powered Light-duty Vehicles, *Journal of Power Sources,* Vol.71(1998), pp. 288-293.

Faizal, H.M., Kuwabara, M., Kizu, R., Yokomori, T. and Ueda, T., Experimental Study on a Compact Methanol Steam Reformer with Pd/Ag Membrane, *Journal of Thermal Science and Technology*, Vol. 7, No. 1(2012), pp. 135-150.

Faizal, H.M., Kizu, R., Kawamura, Y., Yokomori, T. and Ueda, T., Effect of Feed

Flow Rate of Hydrogen Mixture on Hydrogen Permeation for Flat Sheet Pd/Ag Membrane with Stagnating Flow, *Journal of Thermal Science and Technology*, Vol. 8, No. 1 (2013), pp. 120-135.

Federico, G., Erik, E.E. and Ma Y.H., Effects of surface activity, defects and mass transfer on hydrogen permeance and n-value in composite palladium-porous stainless steel membrane, *Catalysis Today*, Vol. 118 (2006), pp.24-31.

Fujimoto, S., Ishihara, H. and Tsuruno, S., A Study on a Steam Reformer for Methanol, *JSME International Journal*, Vol. 30, No. 267(1987), pp. 1437-1442.

Gaohong, H., Yongli, M., Po Lock, Y., and Guohua C., Theoretical study on concentration polarization in gas separation membrane processes, *Journal of Membrane Science*, Vol. 153(1999), pp.243-258.

Gepert, V., Kilgus, M., Schiestel, T., Brunner, H., Eigenberger, G. and Merten, C., Ceramic Supported Capillary Pd Membranes for Hydrogen Separation: Potential and Present Limitations, *Fuel Cells*, Vol.06, No.6(2006), pp. 472-481.

Grashoff, G.J., Pilkington, C.E. and Corti, C.W., The Purification of Hydrogen-A Review of the Technology Emphasising the Current Status of Palladium Membrane Diffusion, Platinum Metals Rev., Vol. 27(1983), No.(4), pp.157-169.

Hara, S., Sasaki, K. and Itoh, N., Decline in hydrogen permeation due to concentration polarization and CO hindrance in a palladium membrane reactor, *Ind. Eng. Chem. Res.*, Vol. 38(1999), pp. 4913-4918.

He, G., Mi, Y., Lock Yue, P. and Chen, G., Theoretical study on concentration polarization in gas separation membrane processes, *Journal of Membrane Science*, Vol. 153(1999), pp. 243-258.

Hohlein, B., Boe, M., Bogild-Hansen, J., Brockerhoff, P., Colsman, G., Emonts, B., Menzer, R. and Riedel, E., Hydrogen from methanol for fuel cells in mobile system: development of a compact reformer, *Journal of Power Sources*, Vol. 61 (1996), pp. 143-147.

Hou, K. and Hughes, R., The effect of external mass transfer, competitive adsorption and coking on hydrogen permeation through thin Pd/Ag membranes, *Journal of Membrane Science*, Vol. 206 (2002), pp. 119-130.

Huang, C.-Y., Sun, Y.-M., Chou, C.-Y. and Su, C.-C., Performance of Catalysts CuO-ZnO-Al_2O_3, CuO-ZnO-Al_2O_3-Pt-Rh and Pt-Rh in a Small Reformer for Hydrogen Generation, *Journal of Power Sources*, Vol. 166(2007), pp. 450-457.

H. Israni, S. and P. Harold, M., Methanol Steam Reforming in Single-fiber Packed Bed Pd-Ag Membrane Reactor: Experiments and Modeling, *Journal of Membrane Science*, Vol.369 (2011), pp. 375-387.

Israni, S.H. and Harold, M.P., Methanol Steam Reforming in Pd-Ag Membrane Reactors: Effects of Reaction System Species on Transmembrane Hydrogen Flux, *Ind. Eng. Chem. Res.*, Vol. 49 (2010), pp. 10242-10250.

Iulianelli, A., Longo, T. and Basile, A., Methanol Steam Reforming Reaction in a Pd-Ag Membrane Reactor for CO-free Hydrogen Production, *International Journal of Hydrogen Energy*, Vol. 33(2008), pp. 5583-5588.

Jae-Young, L., Jiyong, J., Jae Kwang, L., Sunghyun, U., Eon Soo, L., Jae Hyuk, J., Nam-Ki, K., Yong-Chul, L. and Jaeyoung, L., Effect of Hydrogen Partial Pressure on a Polymer Electrolyte Fuel Cell Performance, *Korean J. Chem. Eng.*, Vol. 27, No.3 (2010), pp. 843-847.

Katsuki, K., Membrane Separation for Hydrogen Utilization (in Japanese), *Membrane* Vol.30, No.1 (2005),pp. 2-6. (In Japanese)

Li, A., Liang, W. and Hughes, R., The effect of carbon monoxide and steam on the hydrogen permeability of a Pd/stainless steel membrane, Journal of Membrane Science, Vol. 165(2000), pp. 135.

Liang, W. and Hughes, R., The effect of diffusion direction on the permeation rate of hydrogen in palladium composite membranes, *Chemical Engineering Journal*, Vol. 112(2005), pp. 81-86.

Lin, Y., Separation of hydrogen from the gas mixture out of catalytic reformer by using supported palladium membrane, Separation and Purification Technology, Vol. 25 (2001), pp. 87-95.

Liwei, P., Changjun, N., Xuebin, Z., Zhongshan, Y, Chunxi, Z. and Shudong, W., Study on a Compact Methanol Reformer for a Miniature Fuel Cell, *International Journal of Hydrogen Energy*, Vol.36(2011), pp. 319-325.

Ludtke O, Behling RD and Ohlrogge K., Concentration polarization in gas permeation, *Journal of Membrane Science*, Vol.146 (1998), pp. 145-157.

L. Holleck, G., Diffusion and Solubility of Hydrogen in Palladium and Palladium-Silver Alloys, *The Journal of Physical Chemistry*, Vol.74, No.3 (1970), pp. 503-511.

L. Ward, T. and Dao, T., Model of hydrogen permeation behavior in palladium membranes, *Journal of Membrane Science*, Vol. 153 (1999), pp. 211-231.

Ma, Y.H., Hydrogen separation membranes, in Advanced Membrane Technology and Applications (eds N.N. Li, A.G. Fane, W.S.W. Ho, and T. Matsuura), John Wiley & Sons, Inc., Hoboken, NJ, pp. 451, 2008.

Miguel, C.V., Mendes, A., Tosti, S. and Madeira. L.M., Effect of CO and CO_2 on H_2 permeation through finger-like Pd-Ag membranes, *International Journal of Hydrogen Energy*, Vol. 37 (2012), pp. 12680-12687.

Mourgues, A., and Sanchez, J., Theoretical analysis of concentration polarization in membrane modules for gas separation with feed inside the hollow-fibers, *Journal of Membrane Science*, Vol. 252(2005), pp. 133-144.

Nagy, E., Coupled effect of the membrane properties and concentration polarization in pervaporation: Unified mass transport model, *Sep. Purif. Technol.*, Vol.73 (2010), pp. 194−201.

Nagy, E., Basic equation of mass transport through a membrane layer, Elsevier, London (2012) pp 121−126.

Nagy, E., Nagy, R. and Dudas, J., Separate Expression of Polarization Modulus and Enrichment by Mass Transport Parameters for Membrane Gas Separation, *Industrial and Engineering Chemistry Research*, (2013), **DOI:** 10.1021/ie302264j

Narusawa, K., Hayashida, M., Kurashima, D., Wakabayashi, K. and Kamiya, Y., Analyses on Declining Performance of PEMFC with Fuel Containing Impurities (Proposal of Analytical Methods Adopting Poisoning Prediction Formulas and Poisoning Estimation Coefficient), *JSME International Journal, Series B*, Vol. 46, No. 4 (2003), pp. 643-649.

Narusawa, K.[(ii)], Hayashida, M., Kurashima, D., Murooka, K., Wakabayashi, K. and Kamiya, Y., Analyses on a Declining Performance of PEMFC with Fuel Containing Impurities (2nd Report, Characteristic Evaluation of Methanol Reforming Type Fuel Cells), *Transactions of the Japan Society of Mechanical Engineers, Series B*, Vol. 69, No. 687 (2003), pp. 2553-2559. (In Japanese)

Nguyen, T.H., Mori and Suzuki, M., Hydrogen permeance and the effect of H_2O and CO on the permeability of Pd0.75Ag0.25 membranes under gas-driven permeation and plasma-driven permeation, *Chem. Eng. J.*, Vol. 155(2009), pp.55-61.

Nishimura, C., Komaki, M., Hwang, S. and Amano, M., V-Ni Alloy Membranes for Hydrogen Purification, *Journal of Alloys and Compounds*, Vol. 330-332 (2002),pp. 902-906.

Phair J.W., Donelson, R., Developments and design of novel (non-palladium-based) metal membranes for hydrogen separation, *Industrial and Engineering Chemistry Research*, Vol. 45(2006), pp.5657-5674.

Pizzi D, Worth R, Baschetti MG, Sarti GC, Noda KI. Hydrogen permeability of 2.5μm palladium-silver membranes deposited on ceramic supports. *Journal of Membrane Science*, Vol. 325 (2008), pp. 446-453.

Saika, T., Nakamura, M., Nohara, T. and Ishimatsu, S., Study of Hydrogen Supply System with Ammonia Fuel, *JSME International Journal, Series B*, Vol. 49, No. 1 (2006), pp. 78-83.

Sato, T., Hamada, A. and Kitamura, K. “A Feasibility Study of Conceptual Design for International Clean Energy Network Using Hydrogen Conversion Technology”. WE-NET Annual Reports. (online), available from <http://www.enaa.or.jp/WE-NET/ronbun/1998/04/0498.htm>, (accessed 2011-09-28).

Sieverts, A. and Zapf, G. : Die Loslichkeit von Deuterium und Wasserstoff in festem Palladium, pp.359-364, vol.174, Z. phys. Ch. (1935).

Su, J., Development of a novel compact reformer for PEMFC, Ph.D thesis, University of Florida (2009).

S. Damle, A., Hydrogen Production by Reforming of Liquid Hydrocarbons in a Membrane Reactor for Portable Power Generation-Experimental Studies, *Journal of Power Sources*, Vol. 186 (2009), pp. 167-177.

S. Rao, S., Applied Numerical Methods for Engineers and Scientists, Prentice Hall, 2002.

Tong, J., Su, L., Haraya, K. and Suda, H., Thin Pd Membrane on a α-Al_2O_3 Hollow Fiber Substrate without any Interlayer by Electroless Plating Combined with Embedding Pd Catalyst in Polymer Template, *Journal of Membrane Science*, Vol. 310 (2008), pp. 93-101.

Ueda, T. and Mizomoto, M., Aerodynamic structure of a flat plate laminar boundary layer with diffusion flame, *Computational Mechanics*, Vol.5(1989), pp. 263-272.

Uemiya, S., Sato, N., Ando, H., Kude, Y., Matsuda, T. and Kikuchi, E., Separation of hydrogen through palladium thin film supported on a porous glass tube, *Journal of Membrane Science*, Vol. 56 (1991), pp. 303-313.

Uemiya, S. [(ii)], Matsuda, T., and Kikuchi, E., Hydrogen permeable palladium-silver alloy membrane supported on porous ceramics, *Journal of Membrane Science*, Vol.56 (1991), pp. 315-325.

Unemoto, A., Kaimai, A., Sato, K., Otake, T., Yashiro, K., Mizusaki, J., Kawada, T., Tsuneki, T., Shirasaki, Y. And Yasuda, I., The effect of co-existing gases from the process of steam reforming reaction on hydrogen permeability of palladium alloy membrane at high temperatures, *International Journal of Hydrogen Energy*, Vol. 32 (2007), pp. 2881-2887.

Vadrucci, M., Borgognoni, F., Moriani, A., Santucci, A. and Tosti, S., Hydrogen permeation through Pd-Ag membranes: Surface effects and Sieverts' Law, *International Journal of Hydrogen Energy*, Vol. 38 (2013), pp. 4144-4152.

Williams FA. Combustion theory. 2nd ed. Menlo Park, California: Benjamin/Cummings;1985.

Xie, D., Lu, N., Wang, F. and Fan, S., Calculation of the hydrogen production rate by a palladium membrane separator: Theoretical approach, *International Journal of Hydrogen Energy* (2013), http://dx.doi.org/10.1016/j.ijhydene.2013.01.18.

Yan, S., Maeda, H., Kusakabe, K., Morooka, S., Thin palladium membrane formed in support pores by metal-organic chemical vapor deposition method and application to hydrogen separation, *Ind. Eng. Chem. Res.*, 33 (1994) 616.

Yoon C.Y., Otero J., Erickson P.A., Reactor design limitations for the steam reforming of methanol. *Applied Catalysis B: Environmental*, Vol. 75(2007), pp. 264–271.

Zhang, J., Liu, D., He, M., Xu, H. and Li, W., Experimental and simulation studies on concentration polarization in H_2 enrichment by highly permeable and selective Pd membranes, *Journal of Membrane Scienc*e, Vol. 274(2006), pp. 83-91.

Appendix A: Derivation of Sieverts' Equation

Based on Fick's First Law, hydrogen permeation through a small area of membrane during a small time interval is given as follows:

$$f = -D\frac{dC_{H_2}}{dx} \tag{A.1}$$

where f is hydrogen permeation mole flux, D is diffusion coefficient or diffusivity, C_{H_2} is hydrogen mole concentration and x is length towards the direction of membrane thickness. Therefore, $\frac{dC_{H_2}}{dx}$ is the hydrogen concentration gradient for the length x of membrane.

Then, based on Sieverts' Law, hydrogen concentration at the membrane surface of upstream side ($C_{H_2,1}$) and downstream ($C_{H_2,2}$) are defined by Eq.(A.2) and (A.3), respectively.

$$C_{H_2,1} = K\sqrt{P_{H_2,1}} \tag{A.2}$$

$$C_{H_2,2} = K\sqrt{P_{H_2,2}} \tag{A.3}$$

where K is solubility, $P_{H_2,1}$ and $P_{H_2,2}$ are hydrogen partial pressure at membrane surface of upstream side and downstream side, respectively. Then, by substituting Eq.(A.2) and (A.3) into Eq.(A.1), the following Eq.(A.4) is obtained.

$$f = \frac{DK}{d}\left(\sqrt{P_{H_2,1}} - \sqrt{P_{H_2,2}}\right) \tag{A.4}$$

In this case, $dx = d$ where d is membrane thickness. Then, the multiplication of D and K gives q (hydrogen permeance coefficient). Finally, Eq.(A.4) can be modified to Eq.(A.5), that is Eq.(1.3) in Chapter 1.

$$f = \frac{q}{d}\left(\sqrt{P_{H_2,1}} - \sqrt{P_{H_2,2}}\right) \tag{A.5}$$